Physics Department. Annual progress report 1 January - 31 December 1978

Risø National Laboratory, Roskilde

Publication date:
1978

Document Version
Publisher's PDF, also known as Version of record

Risø-R-393

RISØ

Risø-R-393

Physics Department Annual Progress Report

1 January – 31 December 1978

Risø National Laboratory, DK-4000 Roskilde, Denmark
December 1978

Risø-R-393

PHYSICS DEPARTMENT ANNUAL PROGRESS REPORT

1 January - 31 December 1978

edited by H. Bjerrum Møller and B. Lebech

UDC 53

December 1978
Risø National Laboratory, DK 4000 Roskilde, Denmark

This report contains unpublished results and should not be quoted without permission from the authors

ISBN 87-550-0578-0
ISSN 0418-6443

Risø repro 1979

PREFACE

Research in the Physics Department at Risø covers three main fields:

Solid-state physics
Plasma physics
Meteorology

The principal activities in these fields are presented in this report that covers the period from 1 January to 31 December 1978. Introductions to the work in each of the main fields are given in the respective sections of the report.

CONTENTS

1. SOLID STATE PHYSICS

The purpose of the work in solid state physics is to contribute to the fundamental understanding of the physical properties of condensed matter. Neutron beams have properties that make them a unique tool for studies of solids and liquids on the microscopic level. Hence, the experimental work in the solid state physics section is primarily concerned with the use of the DR3 reactor for a wide variety of neutron scattering experiments and most of the sections theoretical effort is also related to neutron scattering experiments. This year a new experimental technique was added to the activity, namely X-ray scattering.

The instruments available at the horizontal neutron beams of the DR3 reactor are one double-axis and five triple-axis spectrometers. In three of the four tangential through-tubes of the reactor, water scatterers placed close to the reactor core scatter beams of thermal neutrons out through the tube to the spectrometers. The thermal flux in the centre of the beam tube is about $2 \cdot 10^{14}$ neutrons/cm^2/s. A liquid hydrogen cold source was installed in the fourth tangential tube in the spring of 1975. The source provides two of the spectrometers in the reactor hall with beams of cold neutrons. A curved neutron-conducting tube leading from the cold neutron beam to an experimental hall provide one more triple-axis spectrometer in the experimental hall at the end of the flight tube with cold neutrons. The low extrinsic background of less than one count per ten minutes makes this instrument an excellent tool for studies requiring high resolution and sensitivity. One further cold source is being installed in the tube next to the present source.

The new X-ray facility is a highly automised high resolution X-ray spectrometer to be used in conjunction with either X-rays produced by a 12 kW rotating anode X-ray generator or X-rays produced by a synchrotron. This spectrometer was constructed and installed during 1978 in the experimental hall at the DR3 reactor (1.33-1.34) as a joint project between Risø National Laboratory and the University of Copenhagen supported by the Danish Natural Science Research Council.

The experimental and theoretical work fall into four categories: namely studies of magnetic materials (1.1-1.14), phase transitions (1.15-1.12), molecular systems and liquids (1.22-1.28), and ionic and low dimensional conductors (1.29-1.39).

Neutron scattering is well suited for studies of magnetic materials and a majority of the experiments fall in this category. The magnetic ordering in materials like CeSb, CeSe, and CeTe was studied in detail as well as the more unusual magnetic transition in oxygen monolayers adsorbed on graphite. Magnetic excitations were characterized in several materials ranging from the spin waves in $ErFe_2$ and Ho_2Co_{17} to the more exciton-like modes in TbP and the pure crystal field transitions in dilute Er-Mg alloys. This last experiment was carried out at the new triple axis spectrometer situated at the end of the neutron guide and the extremely low background of this facility was essential for the outcome. Among the first experiments performed on the new X-ray facility was a study of Nd, which showed that only Bragg reflections originating from the double hexagonal close packed lattice are observed in an X-ray scattering experiment. Hence, there is no direc experimental evidence for the existence of the "triple-$\vec{q}$" magnetic structure in Nd metal.

The the theoretical work related to magnetism considered the influence by the conduction electrons on the exitation spectra of Pr. The interactions between the exitations were studied both within the context of the non-linear spin wave theory and by developing a Greens function theory which includes the effects of fluctuations. The origin of the large magnetic anisotropy in the rare earth-Co compounds, when compared to pure Co, was proposed to be caused by the variation of the c/a ratio.

Magnetic modes are normally linear corresponding to harmonic oscillations but it was recently proposed that certain magnetic materials with strong coupling in only one crystal direction would sustain non-linear modes of oscillation. Scattering from such soliton modes was observed for the first time in $CsNiF_3$ at Risø in collaboration with the Hahn-Meitner Institute in Berlin.

The effort to characterize phase transitions in magnetic system was continued by studies of the actinide compound UTe which shows interesting anomalous critical scattering. Another type of research

related to the actinides was band structure calculations which explain the ground state properties for the first ten metals in the series. Furthermore, the calculations predict an isostructural phase transition in Am resulting in an 8% change of the lattice parameter.

The experiments on adsorbed monolayers addressed questions like the melting of a 2-dimensional solid and details of the commonsurable to incommensurable transition for D_2 and H_2 on graphite.

A study of the phonon spectrum in deuterium under high pressure was carried out in collaboration with the University of Delaware, U.S.A. This study showed the importance of anharmonic and quantum effects in such solids. Another project dealing with molecular solids, namely the study of DCN, was brought to an end. Here the main result was a detailed description of the phonon spectrum which can be accounted for by a simple nearest heighbour model.

Measurements on liquids He and N_2 and on one dimensional conductors have been carried out in collaboration with the University of Copenhagen and study of the ionic conductors CaF_2 and $SrCl_2$ was made in collaboration with a group from AERE, Harwell, U.K.

1.1 Magnetic excitations in Pr metal

(J.G. Houmann, J. Jensen*, A.R. Mackintosh* (*University of Copenhagen), B.D. Rainford (Imperial College, London, U.K.), O.D. McMasters+, and K.A. Gschneider, Jr.+ (+Ames Laboratory-DoE, Iowa State University, USA))

The magnetic excitations in a single crystal of dhcp Pr were studied by inelastic neutron scattering. The excitations on the hexagonal sites and their dependence on magnetic fields up to 4.3 T applied in the basal plane were analysed in terms of a Hamiltonian in which exchange, crystal field and magnetoelastic interactions are included. The exchange is found to be strongly anisotropic, and this anisotropy is revealed directly as a splitting of most branches of the dispersion relations. By considering a variety of magnetic properties, we were able to determine the crystal field level-scheme for the hexagonal sites fairly unambiguously. The first excited level is 3.5 meV above the ground state. The value of the magnetoelastic coup-

ling deduced from the excitations is in good agreement with those obtained from other measurements. A field-dependent interaction with the phonons was observed, and a pronounced broadening of the acoustic excitations of long wavelength is ascribed to the influence of the conduction electrons. The first excited state on the cubic ions is about 8.3 meV above the ground state. The corresponding excitations show a pronounced dispersion, but the exchange anisotropy is of less importance than for the hexagonal sites.

1.2 First principles calculation of the damping and quasielastic mode of dhcp Pr

(D. Yang and P.-A. Lindgård)

Starting with the interaction between the conduction- and the 4f-electrons and taking the single-ion levels of Pr to be a singlet and a doublet, we have derived the dynamical susceptibility for dhcp Pr using Mori's memory function formalism. The dynamics of the electron hole relaxation reflects itself in the damping mechanism of the magnetic excitations and leads to the quasielastic mode at finite wave vector q, in contrast to the situation in ferromagnetic systems where the paramagnons contribute to the quasielastic mode at q = 0. The finite q response is caused by the nesting properties of the Fermi surface. Preliminary results of first principles calculations using the relativistic augmented plane wave (APW) energy bands are compared with the experimental observations of Houmann et al. (1977). It is concluded that the contribution from the considered mechanism is too small to account for the observed phenomena. Presumably effects from magnetic impurities play the dominant role.

1.3 Fluctuation corrections to the excitation spectra and to the thermodynamic properties of crystal field systems

(P.-A. Lindgård and D. Yang)

Static and dynamic phenomena in magnetic systems with large magnetic anisotropy (crystal fields) have generally been treated by mean field theories. Of particular importance has been the random phase approximation of the standard basis operator

theory (Haley and Erdös 1972) which provides a good qualitative picture of the magnetic properties at all temperatures. However, in this theory the influence of fluctuations is neglected. Consequently no damping of the excitations is obtained and the thermodynamic properties may be significantly quantitatively incorrect.

We have developed a theory which includes the effect of fluctuations. For the free energy the exact correction to the mean field free energy has the following form

F(exact) = F(meanfield)

$$- \sum_q J_q \langle \delta\vec{S}_q \cdot \delta\vec{S}_{-q} \rangle - \frac{1}{kT} \sum_q J_q \langle [\delta\vec{S}_q \cdot \delta\vec{S}_{-q}, H_o] \rangle ,$$

where $\delta\vec{S} = \vec{S} - \langle \vec{S}_z \rangle$, J_q is the exchange interaction and H_o is the single ion Hamiltonian (a general crystal field plus the mean field). A computer program was developed which evaluates the correlation functions using the random-phase approximation (RPA) and computes the free energy and the magnetization. A considerable reduction of the transition temperature T_c relative to the mean field T_c^{MF} is found by using the susceptibility $\chi(q,\omega)$ calculated in the random-phase approximation. However, a more accurate calculation of $\chi(q,\omega)$ is desirable. Here we have followed two paths: Firstly, by considering a generalization of the mean field expressions for the wave vector dependent static susceptibility χ_q, we derive the following self-consistent equation (here given for a Heisenberg system only).

$$(\chi_q)^{-1} = (\chi_q(RPA))^{-1} - J_q^2 \sum_k \{\chi_k - [(\chi_k(RPA))^{-1} + J_k]^{-1}\}$$

This simple equation contains several features obtained by the renormalization group theories such as the correct dependence of lattice dimensionality d (i.e., mean field behaviour for d > 4, no ordering for d = 1, etc.). Secondly, we have considered extending the random-phase approximation theory for $\chi(q,\omega)$ to include the effect of renormalization and damping of the excitations due to mutual interactions. Here we have used Mori's memory function

technique (Mori 1958, 1959 and Kawasaki 1968) and constructed an interpolation formula that reduces to the correct limits for T going to infinity and which should be quite reliable near T_c.

1.4. X-ray and neutron scattering studies of Nd metal

(B. Lebech, P. Bak (Nordita, Copenhagen), J. Als-Nielsen, and K.A. McEwen (University of Salford, U.K.))

The magnetic structure of the rare earth metal Nd (dhcp) has remained a mystery for more than a decade. Neutron diffraction results have been available, but none of the models proposed were able to fit the data satisfactorily. Recently, Bak and Lebech (1978) derived a model that seemed to agree with the available neutron data. In this model (the "triple-$\vec{q}$" structure), the spins form a two-dimensionally modulated pattern below the Néel temperature, T_N = (19.9±0.1) K. The magnetic ordering is

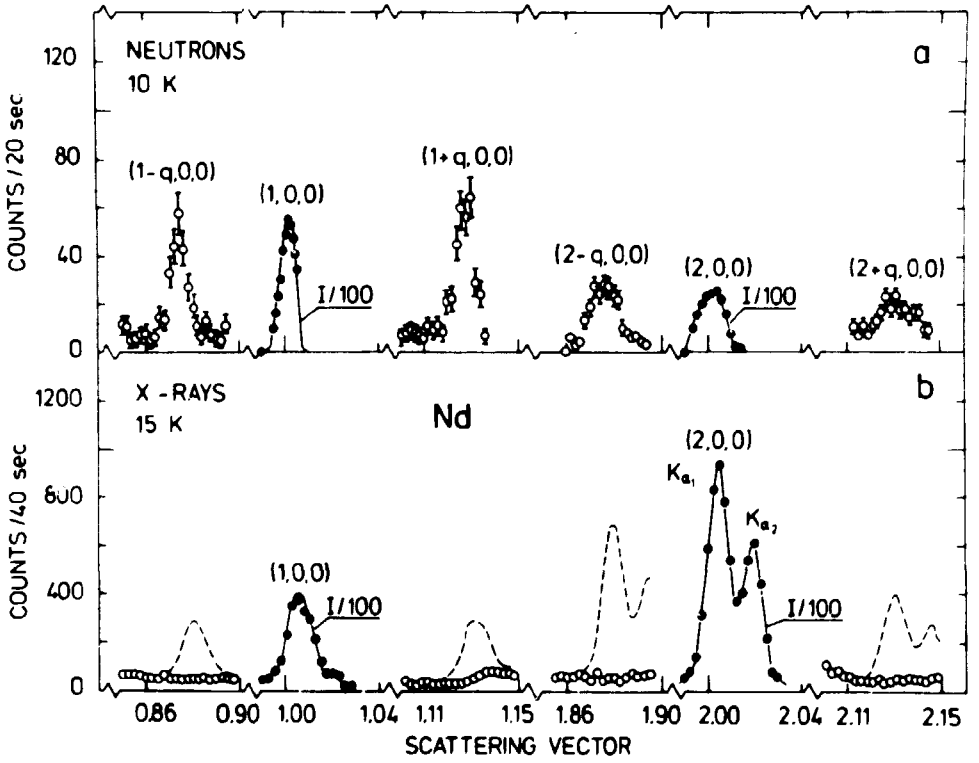

Fig. 1 Neutron (a) and X-ray (b) diffraction patterns of an Nd single crystal plate. The dashed lines in (b) show the X-ray intensity to be expected if the h±q,0,0 satellites that are observed by neutrons (a) originate from lattice distortions. (a) [1$\bar{2}$0] axis vertical and (b) [001] axis vertical.

accompanied by a similarly modulated lattice distortion (internal rearrangement mode). The spin pattern gives rise to magnetic satellites in the neutron diffraction spectrum and the lattice distortion gives rise to lattice satellites that generally coincide with the magnetic satellites. However, at particular Bragg points ({h±q,0,0}) the magnetic satellites vanish because they are forbidden due to the dipolar interaction between neutrons and magnetic moments, while the corresponding lattice satellites are allowed. Below T_N, the neutron diffraction data showed Bragg peaks at the magnetically forbidden satellite positions. These peaks were interpreted as lattice satellites and taken (Bak and Lebech 1978) as direct evidence of the "triple-$\vec{q}$" structure.

As lattice satellites should also be observable in an X-ray scattering experiment, such a search was made. The X-ray experiment was done using Mo-K_α X-rays from a rotating anode generator and the new X-ray spectrometer (1.33). The sample was a specially prepared Nd single-crystal plate (4×4×0.5 mm) with a highly posished shiny surface. The X-ray experiment was performed with both a [1$\bar{2}$0] axis vertical and a [001] axis vertical (Fig. 1b). The bragg peaks originating from the dhcp-lattice were easily observed (Fig. 1b), however, no trace of scattering appeared at the positions where the neutron scattering data (Fig. 1a) showed the magnetically forbidden reflections. An additional experiment using the X-ray spectrometer in the energy-dispersive mode yielded the same negative result. Thus the model interpreting the {h±q,0,0} as arising from a lattice distortion is in correct and further neutron diffraction studies are necessary.

A neutron diffraction investigation of the Nd single crystal plate showed {h±q,0,0} satellites below T_N in agreement with the results obtained previously on several other Nd crystals (Moon et al. 1964, S.A. Shapiro, and S. Sinha (private communication 1977), and Bak and Lebech 1978). Further investigations of these satellites revealed that the satellites are split in the basal plane perpendicular to equivalent <100> directions. Thus, instead of six satellites displaced by $\pm\vec{q}_i$, i = 1,2,3 from each dhcp-lattice point, the diffraction pattern shows twelve satel-

lites displaced by $\pm\vec{q}_i' = \pm(\vec{q}_i \pm \vec{\delta}_i)$, i = 1,2,3, where the $\vec{q}_i$'s are parallel to equivalent <100> directions and the $\vec{\delta}_i$'s parallel to equivalent $<1\bar{2}0>$ directions. At 11.5 K, $q_i \sim 0.133$ and $\delta_i \sim 0.05\ q_i$.

Thus, the magnetic structure is somewhat more complicated than previously assumed, and additional experimental information is necessary.

1.5. Magnon lifetimes in Tb at low temperatures

(H Bjerrum Møller and A.R. Mackintosh (University of Copenhagen))

The lifetimes of magnons propagating in the c-direction of Tb at 4.2 K were measured by inelastic neutron scattering. In contrast to the behaviour at higher temperatures, where magnon-magnon scattering predominates, the broadening of the magnons increases towards the boundary of the single Brillouin zone, in both the acoustic and optical branches (Fig. 2). This suggests that the

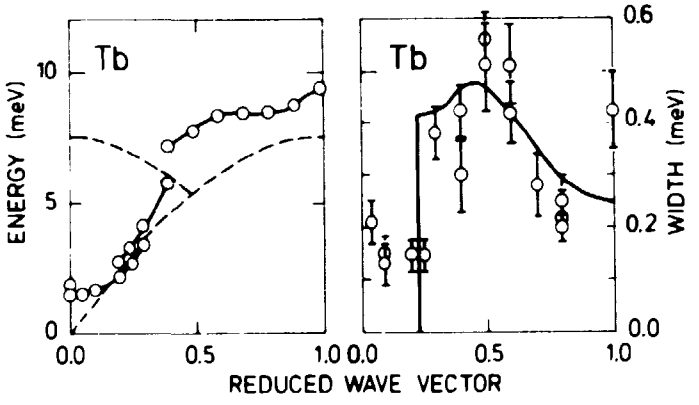

Fig. 2 Dispersion relation and energy widths of magnons propagating in the c-direction in Tb at 4.2 K. A reduced wave vector of 1.0 corresponds to the double zone boundary at 1.10 $Å^{-1}$. The breaks in the dispersion relation are caused by the magnon-phonon interaction. The solid curve for the width is calculated by Hessel Andersen and Smith (1979) assuming a spherical Fermi surface, and using a value for the exchange interaction between the 4f moments and the conduction electrons deduced from their studies of the low temperature resistivity of Tb.

scattering of the magnons by conduction electrons is important. The observed lifetimes are consistent with a recent estimate (Hessel Andersen and Smith 1979) of the magnitude of this effect. The acoustic magnons of very long wavelength behave anomalously, presumably because of dipolar interactions.

1.6 Exact spin-wave renormalization

(E. Rastelli[+] (University of Parma, Italy) and P.-A. Lindgård)

An exact pertubation expansion was derived for the Heisenberg ferromagnet to the order $1/S^2$. The equivalence for the Dyson-Maleev, the Holstein-Primakoff and the matching-of-matrix-element transformation were proved. They all give identical $T^{5/2}$ and T^4 coefficients for the low temperature behaviour of the spin wave renormalization and magnetization, respectively. For the planar ferromagnet an exact expansion in the ratio of the anisotropy to the exchange field proves the equivalence of the Holstein-Primakoff and the matching-of-matrix-element transformations.

1.7. Magnetic excitations in TbP

(J.K. Kjems, A Loidl* and H. Knorr* (*University of Mainz, F.R.G.) and B. Lüthi (University of Frankfurt, F.R.G.))

TbP is a singlet ground-state system with induced antiferromagnetic ordering below 7.35 K. The magnetic structure is type II with the moments along the propagation vector. The transition to the ordered state is of first order. The excitation spectrum in the paramagnetic phase was determined by inelastic neutron scattering using a cold source triple-axis spectrometer. Both the singlet-triplet modes and the transitions between the first two excited triplets are observed. Considerable splittings of the singlet-triplet modes are found along [110] but not along [111]. The excitation at $\frac{1}{2},\frac{1}{2},\frac{1}{2}$ shows a pronounced softening as T_N is approached from above. The results were analysed using a generalized random-phase approximation formalism with anisotropic bilinear exchange interactions. The temperature dependence of the soft mode and of the zero frequency response is well described by this model.

1.8 Crystal field transitions in Mg-0.25% Er

(J.K. Kjems and P. Touborg (University of Odense))

Crystal field transitions in a single crystal of Mg-0.25% Er was studied using the cold source triple-axis spectrometer, TAS7

[+]Supported in part by Nato Grant No. 217.9

(Fig. 15), which is situated at the end of the neutron guidetube. The low extrinsic background of less than 1 count/10 minutes made observations of very weak transitions possible. An example of the observed spectra is shown in Fig. 3.

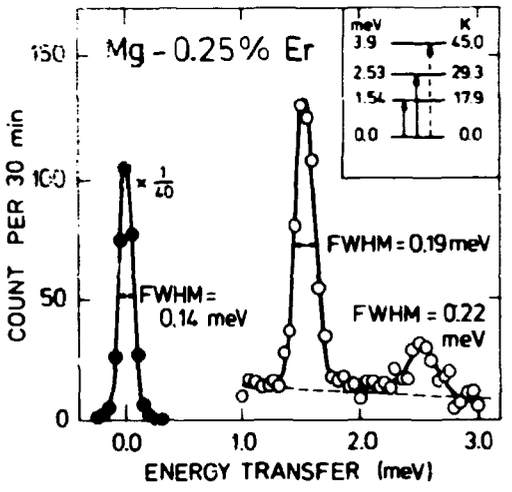

Fig. 3 Crystal field transitions at 5 K and $\vec{q}$ = 0.4,0,0 in a single crystal of Mg-0.25% Er. Note the low background which is characteristic at the TAS7 spectrometer (Fig. 15) situated at the end of the cold neutron guide tube.

The intensity variation with direction in the crystal allows for a unique determination of the matrix elements of the operators S^z, and $S^{\pm}$, respectively. The resulting crystal field level scheme and wave functions correlated well with the measurements of the susceptibility. It is noteworthy that the intrinsic linewidth of the transitions is less than 0.1 meV, i.e. considerably smaller than found for other dilute rare earth in various other host metals (La, Y, $LaSn_3$, $LaPb_3$).

1.9 Spin waves in $ErFe_2$

(J.J. Rhyne (National Bureau of Standards, Washington, D.C., USA), K. Clausen, and B. Lebech)

The rare earth - transition metal compound $ErFe_2$ crystallizes in the closely packed Laves phase structure. Below the Curie temperature (574 K), the Fe-moments are ferromagnetically aligned and antiparallel to the Er moments. Recently, Rhyne and Koon (1978) studied the spin waves of a single crystal of $ErFe_2$ at 4.2 K and 295 K by inelastic neutron scattering. At 295 K they observed three spin-wave branches; (1) an acoustic mode with almost no anisotropy energy gap, (2) a dispersionless optic mode

at ~ 5.1 meV degenerate with the acoustic mode at the zone boundary, and (3) a highly dispersive optic mode with a gap of ~ 8.75 meV at q = 0. At 4.2 K the spectra are essentially unchanged except for an anisotropy energy gap at q = 0 of ~ 8.3 meV.

Using the same crystal of $ErFe_2$, we studied the temperature dependence of the two optic modes from room temperature to just below T_c (295 K to 554 K). In a simple model neglecting anisotropy and crystal field terms the energies at q = 0 of these two modes should renormalize as

$$\omega_1^{op}(T) = 24\, J_{Er\text{-}Fe} \langle S_{Fe}^2(T) \rangle, \text{ and} \quad (1)$$

$$\omega_2^{op}(T) = 12\, J_{Er\text{-}Fe} (\langle S_{Er}^2(T) \rangle - 2\langle S_{Fe}^2(T) \rangle) \quad (2)$$

Using the sublattice magnetizations determined by Rhyne et al. (1978) we find that the upper mode renormalize as described by equation (2), but that the lower mode renormalizes faster than predicted by equation (1). Although the spin-wave peaks corresponding to the lower mode were well resolved at 295 K (FWHM ~ 3 meV) they broadened considerably (FWHM ~ 6 meV) near T_c and were barely observable at T = 551 K.

1.10 Spin waves in Ho_2Co_{17}

(K. Clausen and A. Nørlund Christensen (University of Aarhus))

Ho_2Co_{17} crystallises in the hexagonal Th_2Ni_{17} structure (Ostertag and Strnat 1966) with 38 atoms per unit cell. There are two rare earth sites and four Co sites. The magnetic structure is ferrimagnetic with an easy basal plane. All the Ho and all the Co moments, respectively, are ferromagnetically aligned, and the Ho and the Co moments are antiferromagnetically coupled. The ordered moment is 7.8 μ_B per formula unit with a Curie temperature of 1180 K (Wallace 1973 and references herein).

We have studied a large single crystal Ho_2Co_{17} by inelastic neutron scattering. The crystal (~ 1 cm^3) contains one large and several smaller grains, with an overall mosaic of ~ 40'. The shape is cylindrical with the c-axis approximately along the cylinder axis. Preliminary results of scans around the 1,1,0 and the 1,0,0 reciprocal lattice points are shown in Fig. 4.

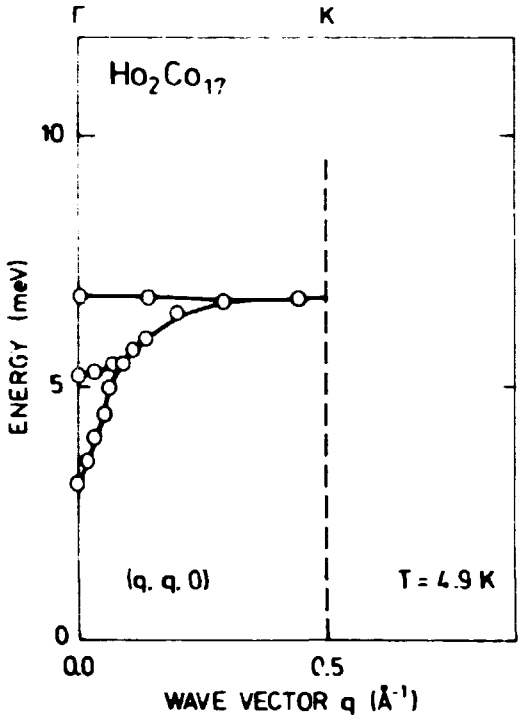

Fig. 4 Dispersion relation in the ΓK ([q,q,0]) direction of Ho_2Co_{17}. The solid curves are guides for the eye.

Furthermore, we made preliminary calculations within the linear spin-wave model. The Hamiltonian for the i'th atom was taken to be

$$H_i = -2 \sum_j J_{ij} \vec{J}_i \cdot \vec{J}_j + H_{CFi},$$

where the summation is taken only over nearest neighbours on each of the other sites and the exchange constants takes one of the three values J_{Ho-Ho}, J_{Ho-Co}, J_{Co-Co}. The crystal field term was approximated by $H_{CFi} = g\mu_B \vec{B}_i \cdot \vec{J}_i$ for the rare earth sites, and by $H_{CFi} = 0$ for the Co sites. The value for $g\mu_B B_i$ was taken from a point charge calculation of the crystal field splitting on the rare earth sites, and the exchange constants used in this preliminary calculations were the same as those of Rhyne and Koon (1978) for $HoFe_2$. The results of these calculations are in qualitative agreement with the data displayed in Fig. 4 and indicate that five of the 38 branches of the spin wave dispersion relations lie below $\sim$ 30 meV at least in a part of the zone. Two of these modes are dispersionless because $J_{Ho-Ho} \sim 0$, two have a slight dispersion determined by J_{Ho-Co}. Furthermore, these modes

should be doubly degenerate at the zone boundary. The last of the five modes below 30 meV is highly dispersive because of the large J_{Co-Co}. The remaining 33 modes have energies above 100 meV.

1.11 On the origin of the large magnetic anisotropy of rare earth-Co compounds

(B. Szpunar (Academy of Mining and Metallurgy, Cracow, Poland) and P.-A. Lindgård)

Experimental data on the magnetocrystalline anisotropy in Co, YCo_5, $GdCo_5$, $SmCo_5$, and Y_2Co_{17} were analyzed using a single ion crystal field and isotropic exchange interactions. It was found that the large magnetic anisotropy at high temperatures in the alloys is due to significant deviations of the ratio c/a of the alloy lattices from the ideal value of $\sqrt{8/3}$. A comparison between the model calculation and the available experimental data is shown in Fig. 5.

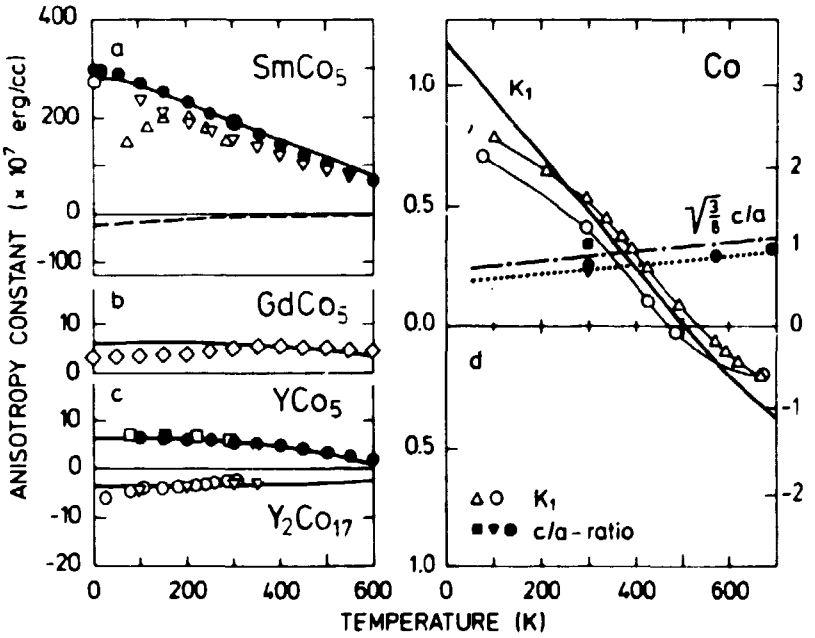

Fig. 5 Temperature dependence of the magnetocrystalline anisotropy in Co and rare-earth-Co compounds. Complete references to the experimental data shown in this figure are given by Szpunar and Lindgård (1979). (a-c) Comparison between the calculated (bold full curves) and the measured anisotropy constants K_1 (and K_2) for $SmCo_5$, $GdCo_5$, YCo_5, and Y_2Co_{17}. (d) For pure Co an assumed linear (dot dashed line) temperature dependence of the c/a-ratio is used in the calculation of K_1 (bold full curve). A satisfactory agreement is obtained between the calculated and measured K_1.

1.12 Evidence of soliton modes in the one-dimensional ferromagnet $CsNiF_3$

(J.K. Kjems and M. Steiner (Hahn Meitner Institute, Berlin))

Evidence of solitons moving along the ferromagnetic chains in $CSNiF_3$ was obtained by inelastic neutron scattering. As predicted by Mikeska (1978), the scattering is found at low a, around zero energy. The soliton activation energy, 8m, is determined from the temperature and field dependence of the intensities. At H = 0.5 T we find $8m/k_B$ = 27 K in reasonable agreement with the predicted value, as is the energy width at q = 0.1. Our results indicate that the soliton modes are an essential aspect of the spin dynamics in $CsNiF_3$. An inelastic spectrum obtained at H = 0.5 T, T = 9.3 K, and q = 0,0,1.9 is shown in Fig. 6.

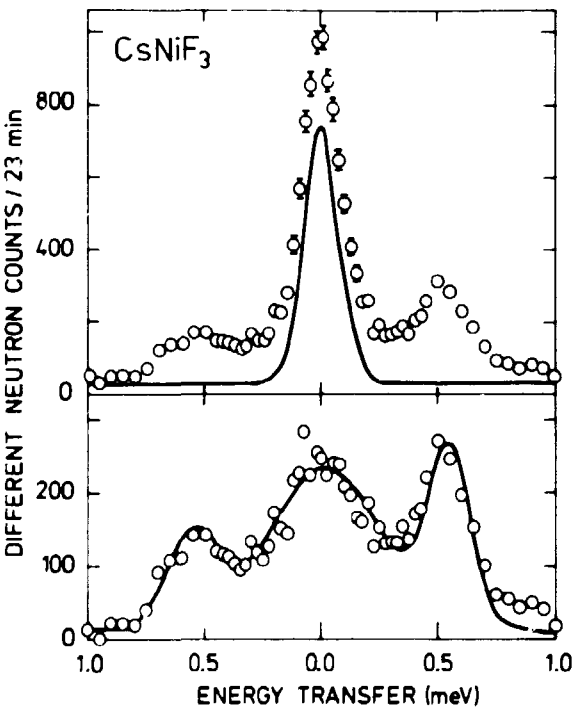

Fig. 6 Inelastic spectrum of $CsNiF_3$ at H = 0.5 T, T = 9.3 K, and $\vec{q}$ = 0,0,1.9, (a) shows the raw data with the experimentally determined incoherent background indicated by the solid curve. (b) shows the difference spectrum. The peaks at $\pm$0.5 meV correspond to spin wave excitations and the quasielastic contribution is associated with solitons moving along the magnetic chains.

1.13 Phonons in δ-NbN

(A. Nørlund Christensen (University of Aarhus), O.W. Dietrich, W. Kress (Max-Planch Institute, Stuttgart, F.R.G.), W.D. Teuchert (Technical University of Munich, F.R.G.), and R. Currat (ILL, Grenoble, France)

The carbides and nitrides of the transition metals from groups

IV to VI are hard, metallic materials with appreciable electrical conductivity. The compounds with nine and ten valence electrons become superconductors with high transition temperatures in contrast to those with eight valence electrons. The nine valence electron compounds have soft modes in the longitudinal acoustic parts of the phonon dispersion curves at 0.6 <q< 0.65 along [001] (Δ), at 0.55 <q< 0.60 along [110], (Σ), and at q = 0.5 along [111] (Λ) in the first Brillouin zone. Recently it was found (Rödhammer et al. 1978) that the phonon dispersion curves of VN with ten valence electrons are different from those of the nine valence electron compounds. A soft mode was observed near the X-point, at q = 1 as opposed to the q-values found for the nine valence electron compounds.

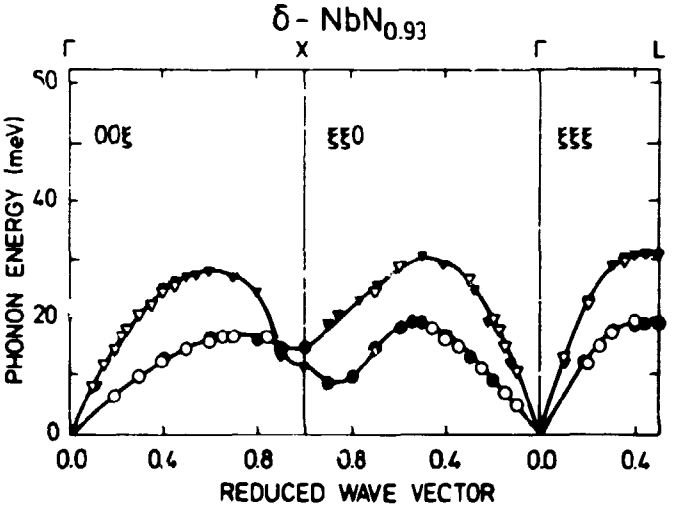

Fig. 7 Phonon dispersion relation of δ-$NbN_{0.39}$. The triangles correspond to longitudinal phonons and the circles to transverse phonons. The filled symbols indicate phonons measured at ILL, using three single crystals aligned after a common [110] axis. The unfilled symbols are phonons measured at Risø using only one crystal.

Measurements of the phonon dispersion relations of another ten valence electron compound δ-NbN are shown in Fig. 7. The transverse acoustic branch along [100] could be followed to the zone boundary. Both branches indicate a softening at the X-point similar to that found for VN. Above 25 meV the phonon groups broaden and decrease in intensity.

1.14 Bulk properties of 3d-monoxides, 4f-, and 5f-metals

(H.L. Skriver, B. Johansson (FOA, Stockholm, Sweden), O.K. Andersen (Max Planck Institute, Stuttgart, F.R.G.))

The linear methods of band structure calculations (Andersen 1975) have at present reached a stage where self-consistent calculations on elemental metals and ordered alloys are extremely fast and efficient. Using modern one-electron theories it is therefore possible to describe and predict accurately the bulk properties of a wide range of materials.

One interesting physical effect which was not treated by these methods before is the lattice constant variation found in the actinide series (Fig. 8), in the 3d-metal monoxides, and in the

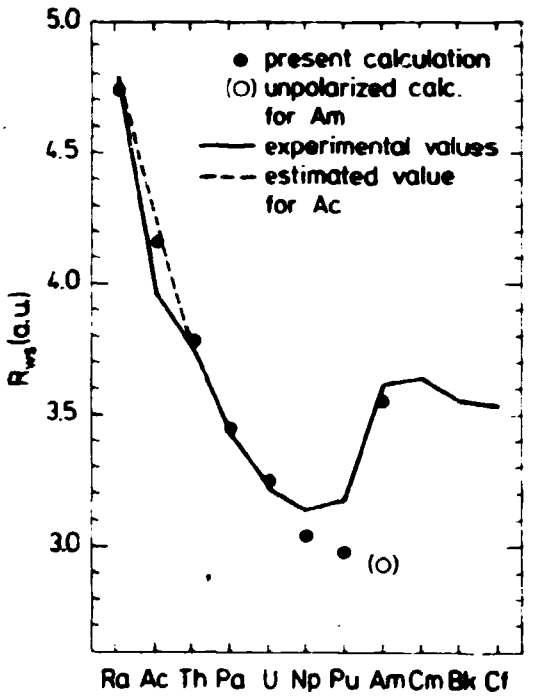

Fig. 8 Comparison between the experimental and the calculated atomic Wigner-Seitz radius, R_{ws}, for the actinide metals. The dashed line corresponds to an estimated value for Ac derived by Zachariasen (1961).

γ to α transition in Ce. While the monoxides beyond MnO are insulators the earlier oxides are metallic. Furthermore, careful examination of the experimental cohesive energies (Johansson 1974, 1975, and Johansson, and Rosengren 1975) show that in α-Ce and in earlier actinides (<Am, the 4f and 5f states respectively, contribute to the binding. Therefore, these materials should be described in a band picture where the 3d, 4f, or 5f states are treated similarly to those of the s and p electrons.

By performing spin-polarized calculations along a series of materials one may find that at a given atomic number spin-polarization sets in and this then marks the onset of localization. We have therefore made spin-polarized, self-consistent band calculations for actinides, lanthanides and 3d-monoxides, and thereby determined the lattice parameter through these series. The results for the earlier actinides are shown in Fig. 8 and they clearly demonstrate that when spin-polarization sets in (in Am) the 5f states become essentially non-bonding and thereby cause a jump in the lattice spacing.

Spin-polarized calculations in Ce and in the 3d-monoxides show a similar effect. We therefore argue that the abrupt change in the lattice parameter in all three groups of materials are caused by a localization of the 3d, 4f, and 5f states respectively. In the monoxides the localization is accompanied by a metal to insulator transition since the 3d electrons alone are responsible for electric conduction while Ce and Am remain metals because the s and d states are still delocalized.

1.15 Investigation of critical fluctuations near T_c in ferromagnetic UTe

(H. Bjerrum Møller, G.H. Lander (Argonne National Laboratory, USA), and O. Vogt (ETH, Zürich, Switzerland))

Measurements of the long-range magnetic fluctuations in the actinide antiferromagnets USb and UN have shown that the interactions are highly anisotropic. In an attempt to examine these properties in ferromagnetic systems we have measured the spatial and temporal dependence of the fluctuations in UTe, an actinide ferromagnet with NaCl crystal structure, and with a = 6.155 Å, and T_c ~ 103 K. The experiment consists of measuring the weak critical scattering around the 1,1,1 reciprocal lattice point above T_c.

The critical scattering above T_c was fitted to a spherically symmetric Lorentzian function $(d\sigma/d\Omega) \propto S/(\kappa^2 + q^2)$. The inverse correlation range, κ, varies from 0.006 to 0.150 $Å^{-1}$ over a decade of reduced temperature $\kappa \propto t^{\nu}$ with $\nu = 8.84 \pm 0.05$, which is greater than expected from simple theory ($\nu = 0.64$). Careful

scans failed to detect any energy dependence in the fluctuations or anisotropy between the transverse and longitudinal components.

1.16 Magnetic ordering in Ce-monochalcogenides: Test case for n = 4 ε-expansions

(H.R. Ott*, J.K. Kjems, and F. Hullinger* (*ETH, Zurich, Switzerland))

CeSe and CeTe were found by neutron diffraction to be type II antiferromagnets with the moment along the propagation vector and with continuous phase transitions. The critical exponent for the magnetization is $\beta = 0.36 \pm 0.02$. This constitutes a violation of the ε-expansion predictions by Bak, Krinsky, and Mukamel (1976) which hitherto have been successfully applied to a number of $n \geq 4$ systems and according to which the transitions should be of first order.

1.17 Magnetic phase diagram of the anomalous antiferromagnet CeSb

(B. Lebech, K. Clausen, and O. Vogt (ETH, Zurich, Switzerland))

The anomalous antiferromagnet CeSb is rather unique within the large class of rare-earth monopnictides that have a simple NaCl structure. The magnetic phase diagram (Rossat-Mignod et al. 1977, Fischer et al. 1978, Meier et al. 1978) shows a large number of phase transitions. In zero field all phase transitions are of first order. However, the experimental results of Meir et al. (1978) indicated that at higher fields the transition from the paramagnetic state to the magnetically ordered state was not first order. Therefore, the existence of a tricritical point was anticipated.

The results of a detailed study of the low-field high-temperature part of the phase diagram are shown in Fig. 9. Each region of the phase diagram corresponds to an antiferromagnetic or metamagnetic structure that may formally be represented by a finite Fourier series with Fourier components of wave vectors $n\vec{q}(H,T)$ parallel to the <100> axes. Each Fourier component $n\vec{q}(H,T)$ gives rise to magnetic Bragg peaks (satellites) displaced $\pm n\vec{q}(H,T)$ from a reciprocal lattice point. The datapoints in Fig. 9 show the

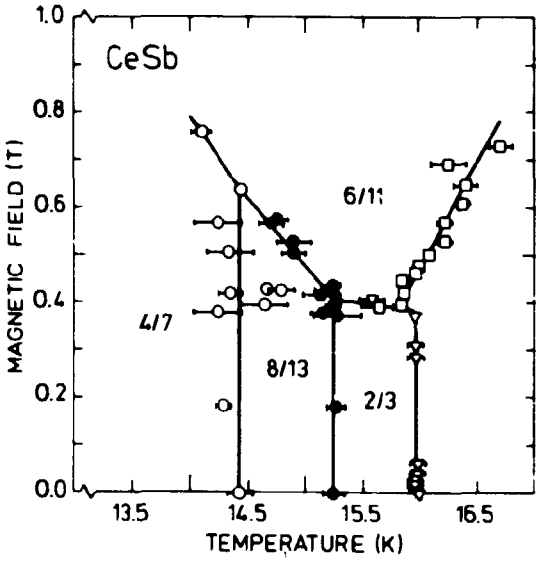

Fig. 9 High temperature region of the magnetic phase diagram of CeSb. The magnetic order are antiferromagnetic of metamagnetic structures that may be represented by finite Fourier series with components of wave vectors nq, where q = 2/3, 2/13, 2/7, and 2/11. The fractions quoted in the diagram correspond to nq for the strongest Fourier components.

transition temperature from one magnetic state to another. These transition temperatures are derived from neutron diffraction scans at various temperatures and a constant magnetic field through the $2,q_o,0$ or $2,0,q_o$ satellites, where q_o is the wave vector corresponding to the strongest Fourier component at the particular field and temperature.

All transitions, including the ones from the paramagnetic to the antiferromagnetic (q_o = 2/3) or to the metamagnetic (q_o = 6/11) state are of first order. Furthermore, within the experimental error, we did not observe any field dependence of the first order jump. Thus, below 0.8 T, there is no experimental evidence of a tricritival point in CeSb. However, a region of instability was observed at fields $\sim$ 0.4 T. In this field region a slight fluctuation in temperature could cause abrupt structural changes from q_o = 2/3 to q_o = 6/11 and back to q_o = 2/3. Likewise, the q_o = 8/13 structure appears to be absent at H $\sim$ 0.4 T, although the phase transitions from q_o = 8/13 to q_o = 2/3, from q_o = 8/13 to q_o = 6/11, and from q_o = 8/13 to q_o = 4/7 structures were well defined both above and below $\sim$ 0.4 T.

1.18 Transition temperature in Pr_3Tl under change in volume

(D. Yang and P.-A. Lindgård)

The shift of the transition temperature $T_c(V)$ of Pr_3Tl under

change in volume V was calculated using a 1/z expansion of the standard-basis operator theory (z is the number of neighbours). Good agreement with $T_c(V)$ is obtained using the parameters deduced from the dispersion relations. A simple linearized volume dependence on both the position of the first excited triplet and the exchange interaction is found to account for the effect of pressure and dilution. Both parameters are found to increase strongly with increasing pressure.

1.19 A study of the Jahn-Teller transition in $TbVO_4$, $DyVO_4$ and $DyAsO_4$

(K. Møllenbach and J.K. Kjems)

In the continued study of cooperative Jahn-Teller transitions the temperature dependence of the strain-order parameter in $TbVO_4$ (T_D = 33.4 K), $DyVO_4$ (T_D = 14.4 K) and $DyAsO_4$ (T_D = 11.2 K) was

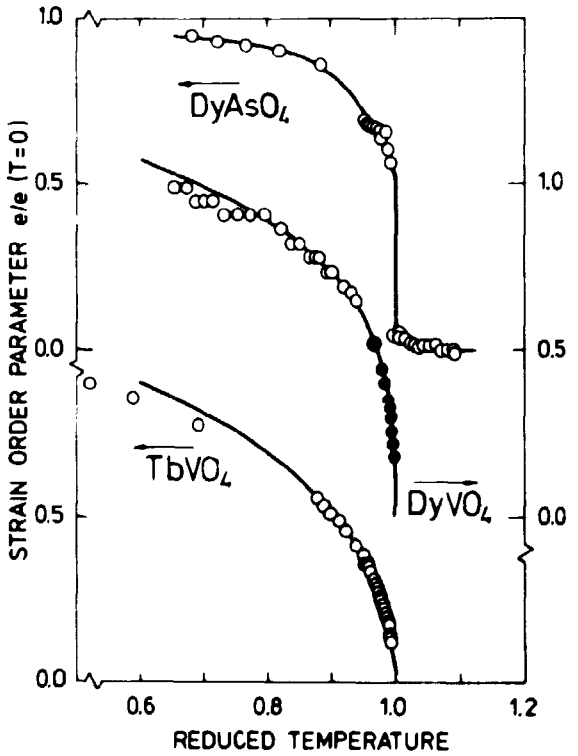

Fig. 10 The strain order parameter in $TbVO_4$ (T_D = 33.4 K), $DyVO_4$ (T_D = 14.4 K), and $DyAsO_4$ (T_D = 11.2 K) as a function of reduced temperature. The open points are the neutron scattering data (1.19). The full points are data obtained by Harley and Mc Farlane (1975).

determined by neutron- and X-ray diffraction. The results are shown in Fig. 10 and confirm the birefringence results of Harley et al. (1975). In $TbVO_4$ we find excellent quantitative agreement between a simple mean field theory and the experimental results. The results for $DyVO_4$ appear to give a non-classical order parameter exponent over a wide temperature range. The transition in in $DyAsO_4$ is first order.

The experimental results for the Dy-compounds disagree with the predictions by the microscopic theory of Elliott et al. (1972). As an alternative we analyze the data with a phenomenological Landau theory. This leads to a picture of the rare-earth zircons as a family of compounds exhibiting a tricritical behaviour with respect to the Jahn-Teller transition. $TbVO_4$ is far away from the tricritical point on the second order side. $DyVO_4$ is close to the tritical point but still on the second order side. The behaviour of the order parameter, as shown in Fig. 10, is dominated by the sixth order term in the expansion of the free energy rather than by the small quartic term. $DyAsO_4$ is beyond the tricritical point on the first order side as a result of a negative quartic term in the free energy expansion.

The validity of this simple theoretical approach is given by the renormalization group analysis of Cowley (1976). He states that in the symmetry group to which the rare-earth zircons belong the marginal dimensionality is lowered to $d^* = 2$ and thus if a compound exhibits a second order transition this transition will be described by classical exponents.

Without speculating on the possible microscopic mechanisms driving the tricritical behaviour, the behaviour is not surprising as a tricritical point was established in the rare-earth zircons with respect to the magnetic phase transitions.

1.20 The magnetic phase transition in adsorbed O_2 layers

(M. Nielsen and J.P. McTague (University of California, Los Angeles, USA)

O_2 layers adsorbed on (0,0,2) surfaces of graphite have three distinct ordered phases which are all incommensurable with the

substrate (Nielsen et al. 1978). One of these, the α phase, has an antiferromagnetic ordering and an accompanying magnetostrictive distortion of the two-dimensional crystal structure at temperatures below 11.9 K. The nature of the phase transition was studied near T_c = 11.9 K by measuring the magnetostrictive distortion as function of temperature by neutron diffraction. It is found that the transition is continous and that the exponent for the ordered magnetic moment, β, is smaller than 0.25.

1.21 Commensurable to incommensurable phase transition in adsorbed H_2 layers on graphite

(M. Nielsen, J.P. McTague (University of California, Los Angeles, USA), and J.K. Kjems)

The phase diagram of adsorbed layers of H_2 and D_2 on (0,0,2) graphite surfaces were established previously (Nielsen et al. 1978). By both elastic and inelastic neutron scattering techniques we have studied the nature of the incommensurable structures which are only slightly more dense than the commensurable √3-structure. The adsorbed monolayers of the hydrogens on graphite substrates constitute very adequate model systems for checking recent theories of commensurable to incommensurable phase transitions (Villian 1978 and Halperin and Nelson 1978).

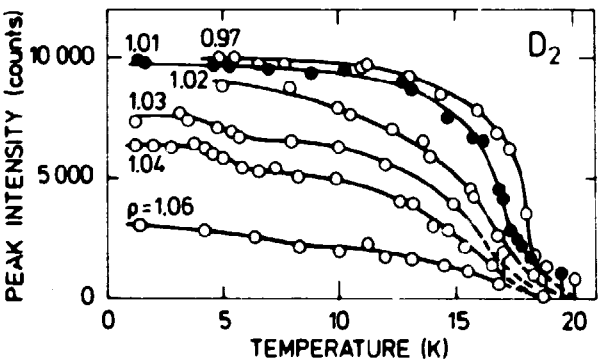

Fig. 11 Melting curves of D_2 layers adsorbed on (0,0,2) surfaces of graphite. The curves show the peak intensities of the 1,0 Bragg peak as function of temperauure. The numbers in the figure give the densities (ρ) of the adsorbed layers in units of the density of the completed √3 phase.

Our conclusion is that the melting transition changes character rather abruptly in going from the commensurable to the incommensurable structures (Fig. 11); and the dynamic response describing the motion of the adsorbed particles parallel to the adsorbing surfaces changes from that of a simple Einstein oscillator to a more complicated behaviour (Fig. 12). At the same time the 1,0

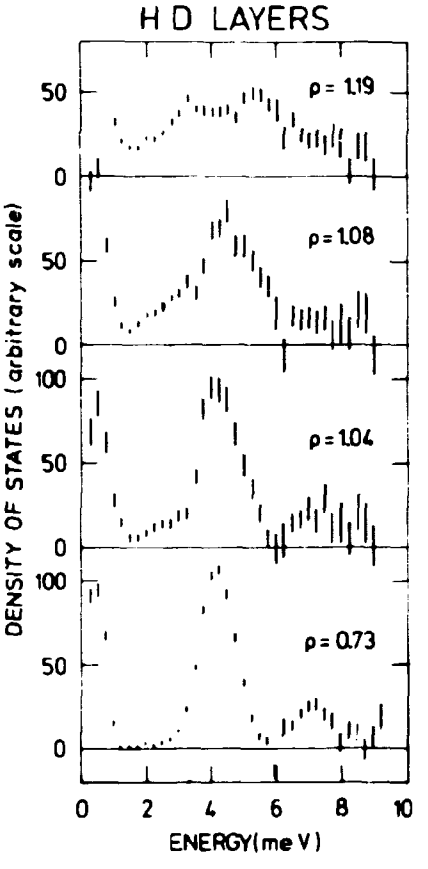

Fig. 12 Inelastic incoherent neutron scattering groups observed from HD layers adsorbed on (0,0,2) surfaces of graphite. The intensities are corrected so as to show the phonon density of states. The numbers in the figure give the densities (ρ) of the adsorbed layers in units of the density of the completed √3 phase.

Bragg peak of the hexagonal two-dimensional structure changes at not too low temperatures from a single peak characteristic of the ideal √3 phase into a structured neutron scattering group. The interpretation of these groups in terms of modulated structures or coexisting phases still remain and need further investigations.

1.22 Phonons in solid D_2

(J.W. Schmidt, M. Nielsen, and W.B. Daniels (University of Delaware, USA))

The phonon dispersion relations in solid D_2 were measured by inelastic neutron scattering as functions of temperature and

density. The single crystalline samples were grown in a pressure cell and the highest density crystal was grown at 4.5 kbar. The data were fitted to a third nearest neighbour Born von Karman tensor force model appropriate to an hcp structure, from which the density of states and the Debye temperatures were calculated. The dispersion curves for the [001] longitudinal phonons are displayed in Fig. 13a. The solid and the dot-dashed curves represent the Born-von Kármán fit to crystals grown at 2.9 kbar, and at 4.5 kbar, respectively. The dashed curve (0 kbar) is shown for comparison. The Gruneisen parameters $\Gamma_i = -\frac{d\ell n\omega}{d\ell nv}i$ were calculated and found to vary from about 1.6 for the higher density to about 2.2 for the lower densities. The line widths of the phonon scattering groups were studied for selected wave vectors as functions of density and temperature. The results for the transverse acoustic [100] basal plane phonon ($T_{\perp}A$) are shown in Fig. 13b, for the D_2 crystal grown at the pressure 2.9 kbar which give a molar volume of 15.8 cm^3.

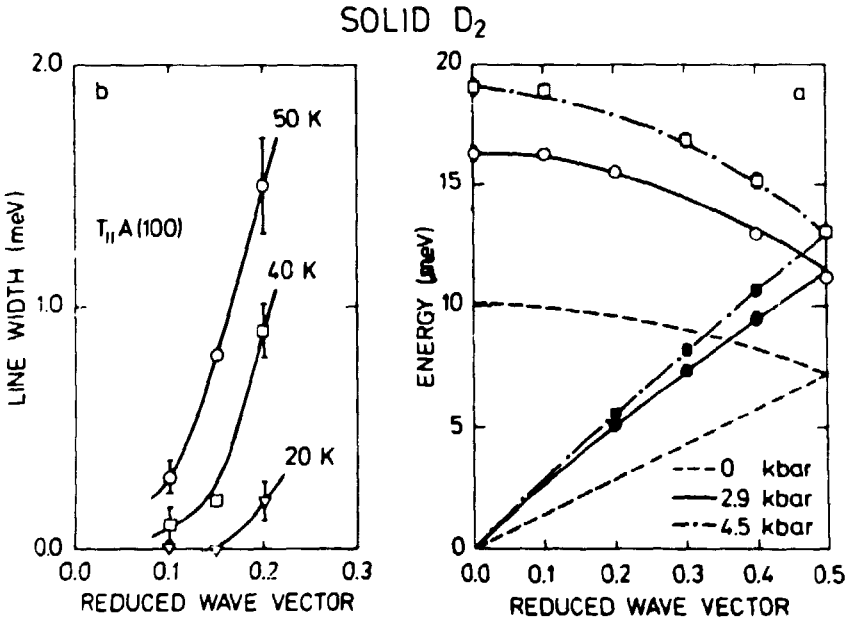

Fig. 13 a) Dispersion relations for the [001] longitudinal phonons in solid D_2. The curves are the calculated dispersions relations using a third nearest neighbour Born-von Kármán tensor force model. b) Phonon line widths for the $T_{\perp}A$ (100) phonon, for the D_2 crystal grown at 2.9 kbar having the molar volume 15.8 cm^3.

1.23 A neutron scattering study of DCN

(G.A. Mackenzie and G.S. Pawley (University of Edingburgh, Scotland))

Solid hydrogen cyanide, HCN, is a relatively simple molecular crystal which exhibits a structural phase transition from a high temperature tetragonal to a low temperature orthorhombic form at 170 K. Both structures have one molecule in the primitive unit cell. In both forms the molecule is linear and aligned along the c axis of the body centred unit cell. The simplicity of the molecular and crystal structures and the existence of a structural phase transition makes HCN unique amongst the molecular crystals, both theoretically and experimentally. Lattice dynamics calculations based on a theoretically derived intermolecular potential (Rae 1972) gave good agreement with the then available experimental data; it predicted that the phase transition was of second order and associated with the instability of the transverse acoustic mode along [110] polarised in the ab plane ($TA_{\perp}$ [110]).

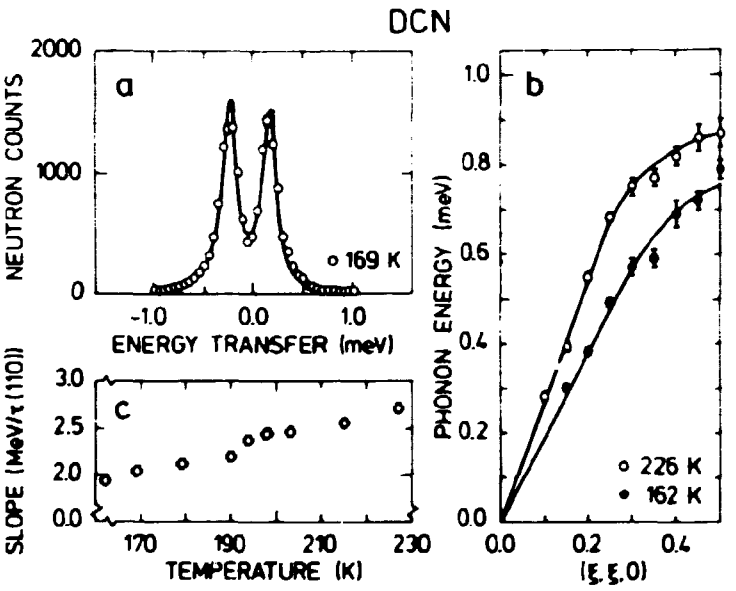

Fig. 14 Summary of the inelastic neutron scattering results for the $TA_{\perp}$ [110] mode in single crystal DCN. (a) The neutron distribution at reduced wave vector q = (0.1,0.1,0). The scans show peaks due both to neutron energy gain and loss processes. The solid curve is the result of a fit to asymmetric Lorentzians. (b) Phonon dispersion curve for the $TA_{\perp}$ [110]. The solid curves are guides for the eye. (c) The temperature dependence of the slope of the $TA_{\perp}$ [110] phonon branch.

A preliminary neutron scattering study of DCN showed that the transition is first order and that the predicted mode shows some softening as the transition at 160 K is approached from above (Dietrich et al. 1977). The crystals used in that study were, however, of insufficient size and quality to permit a detailed study of the soft phonon branch or of the other modes of vibration in the system.

Recently, we succeeded in growing a relatively large single crystal (~ 2 g) with a mosaic spread less than 1^{o}. The crystal was grown inside a cryostat from the melt by slowly lowering the temperature through the freezing point at 259 K. Using this crystal we measured the acoustic modes with propagation and polarisation directions within the ab plane of the tetragonal phase. The measurements of the LA [100], $TA_{\perp}$ [100], and LA [110] branches agree to within 10% with the theoretically based lattice dynamics calculation of Rae (1972) and show no anomalous temperature dependence.

The $TA_{\perp}$ [110] branch is an order of magnitude lower in frequency than the other acoustic modes in the system, reaching only 1 meV at the Brillouin zone boundary. High resolution measurements of this branch at temperatures between 225 and 162 K were made using 5 meV incident neutrons. A typical constant-q scan showing neutron energy gain and loss peaks is shown in Fig. 14a. Figure 14b shows the dispersion curves for the $TA_{\perp}$ [110] branch at the two extreme temperatures. The slope of the linear part of the branch is plotted versus temperature in Fig. 14c. This low frequency branch does not form part of a low frequency surface, but is at the bottom of a steep valley. The shape of this valley was determined by performing constant energy scans across it.

The measured phonon frequencies were fitted using a simple nearest-neighbours force model. The agreement was within the experimental uncertainty indicating that, as far as translational motion of the molecules in the ab plane is concerned, the dynamics of DCN is dominated by nearest-neighbour interactions.

1.24 The crystal structure of $((CH_3)_4N)_2PtCl_6$

(G.A. Mackenzie and R.W. Berg (Technical University of Denmark))

Recently, tetramethylammonium hexachloroplatinate $((CH_3)_4N)_2PtCl_6$, and a number of closely related compounds were studied by Raman and infrared spectroscopy (Berg et al. 1977, Berg 1979) and evidence of phase transitions, probably involving methyl group rotations, was found. As part of this study the crystal structure of the $((CH_3)_4N)_2PtCl_6$ at room temperature was investigated by single crystal X-ray diffraction (Berg and Søtofte 1978). The crystal structure was refined assuming the space group Fm3m with a cubic unit cell parameter of 12.72 Å. Although the data showed evidence of a slightly distorted structure with a larger unit cell the X-ray measurements were inadequate to allow a complete structure determination because of the strong scattering power of Pt and a probable multiple twinned super-structure.

The neutron powder diffraction patterns of a deuterated sample were measured at temperatures above and below the phase transition at 190 K. In the room temperature pattern super-lattice reflections were found, and these could be indexed according to the space group Fd3c with a unit cell parameter of 25.44 Å. The pattern was fitted by profile refinement first using the Fm3m structure as determined by X-rays leading to a profile R-factor of about 20%. The structure was then allowed to distort while preserving the Fd3c symmetry with the unit cell parameter doubled. This led to a significant improvement in the fit with an R-factor of 13%. Although the data analysis is not yet complete we conclude that at room temperature the structure belongs to the Fd3c space group with a unit cell parameter of 25.44 Å. The low temperature data has not yet been analysed.

1.25 The structure of $C_{16}D_{10}$ at high pressure

(G.A. Mackenzie, B. Buras, and G.S. Pawley (University of Edinburgh, Scotland))

The study of the structure of $C_{16}D_{10}$ (pyrene) by neutron powder diffraction (Mackenzie et al. 1978), was continued. Diffraction patterns measured at 6 kbar at room temperature using a large

volume high-pressure cell (Buras et al. 1977) showed considerable deviation from the pattern measured at atmospheric pressure. The 6 kbar pattern was found to change over a period of a few days, indicating that the material was slowly undergoing a change in structure. A small section of the pattern was measured repeatedly for seven days after which no further change was observed. A full diffraction pattern was then measured in the hope that it would correspond entirely to the high pressure phase (Phase II). Recently a structure for Phase II was suggested by Jones et al. (1978) who used unit cell parameters of the low-temperature phase obtained by electron diffraction and found the crystal structure which minimised the calculated lattice energy. This suggested structure was used as the starting point in the profile refinement program, but no fit was obtained. We did, however, find that a number of the measured peaks correspond to peaks calculated in phase II, while others corresponded roughly in position and relative intensity to Phase I peaks. We conclude therefore that at 6 kbar both Phase I and Phase II coexist in the sample. Phase II is probably similar to that suggested by Jones et al. (1978).

In an attempt to obtain a "pure" Phase II pattern the pattern was measured again 23 days after pressurising the cell to 6 kbar. Some change of the pattern was observed, but the Phase I peaks were still present. Increasing the pressure to 7 kbar produced no further change. We plan to fit the measured "mixed phase" patterns using the Phase I and II structures simultaneously with the recently developed profile refinement program EDINP (Pawley et al. 1977).

1.26 Neutron powder diffraction from molecular systems under pressure

(E. Baharie*, G.A. Makenzie, B. Buras, and G.S. Pawley* (*University of Edingburgh, Scotland))

A large number of molecular crystals exhibit one or more structural phase transitions with change of temperature at atmospheric pressure. In the present experiment we studied structural phase transitions with changes of pressure at room temperature in several molecular systems. The systems were perfluorbiphenyl ($C_{12}F_{10}$), fluoranil (C_6F_4O), and benzoic acid ($C_7D_5O_2H$). We

measured neutron powder diffraction patterns at various pressures (up to 8 kbar) using monchromatic neutrons and a triple-axis spectrometer in the elastic mode. The samples were contained in a large volume high-pressure pistol cell (Buras et al. 1977) and the data were analyzed using the constrained profile-refinement program EDINP (Pawley et al. 1977).

The crystal structure $D_{12}F_{10}$ at atmospheric pressure was first reported by Neronova (1968) in a single crystal X-ray study. Neutron powder diffraction (Mackenzie and Pawley 1975) and X-ray (Gleason and Britton 1976) measurements give essentially the same result as those of Neronova. The structure of $C_{12}F_{10}$ is orthorhombic, Fdd2, with eight molecules in the unit cell at room temperature and atmospheric pressure. Recently evidence of a reversible transition accompanied by loss of crystallinity at 2.5 kbars was found in a high-pressure Raman study by Adams (private communication). Our neutron powder diffraction patterns at atmospheric and 2, 4, 6 and 7 kbars pressure show evidence of at least two phase transitions. No evidence was found pertaining to the reversible transition reported by Adams, however. Attempts are being made to index the patterns of the new phases, preliminary results indicate that the high pressure structure at 6 kbars could be monoclinic, $P2_1/c$ with 4 molecules in the unit cell.

Among the first organic crystal structures to be examined by X-rays (Bragg 1921) was $C_7D_5O_2H$, but a detailed study of the crystal and molecular structure was not made until 1955 (Sim et al. 1955). The structure of $C_7H_6O_2$ is monoclinic, $P2_1/c$, with 4 molecules in the unit cell at room temperature and atmospheric pressure. The molecules are nearly planar, centrosymmetrical dimers, with hydrogen bonds between the adjacent carboxyl groups. A phase transition in this hydrogen-bonded system was reported by Bridgman (1916) but a detailed study of the new solid phase at high pressures has not been made. The sample was fully deuterated except for the hydrogen atom active in the hydrogen bonding. A powder diffraction pattern at atmospheric pressure was obtained but it proved impossible to obtain a high-pressure pattern. This failure was solely attributed to the nature of the material itself. The sample was very compressible and showed a tendency to flow out of the pressure cell following the application of only slight pressure.

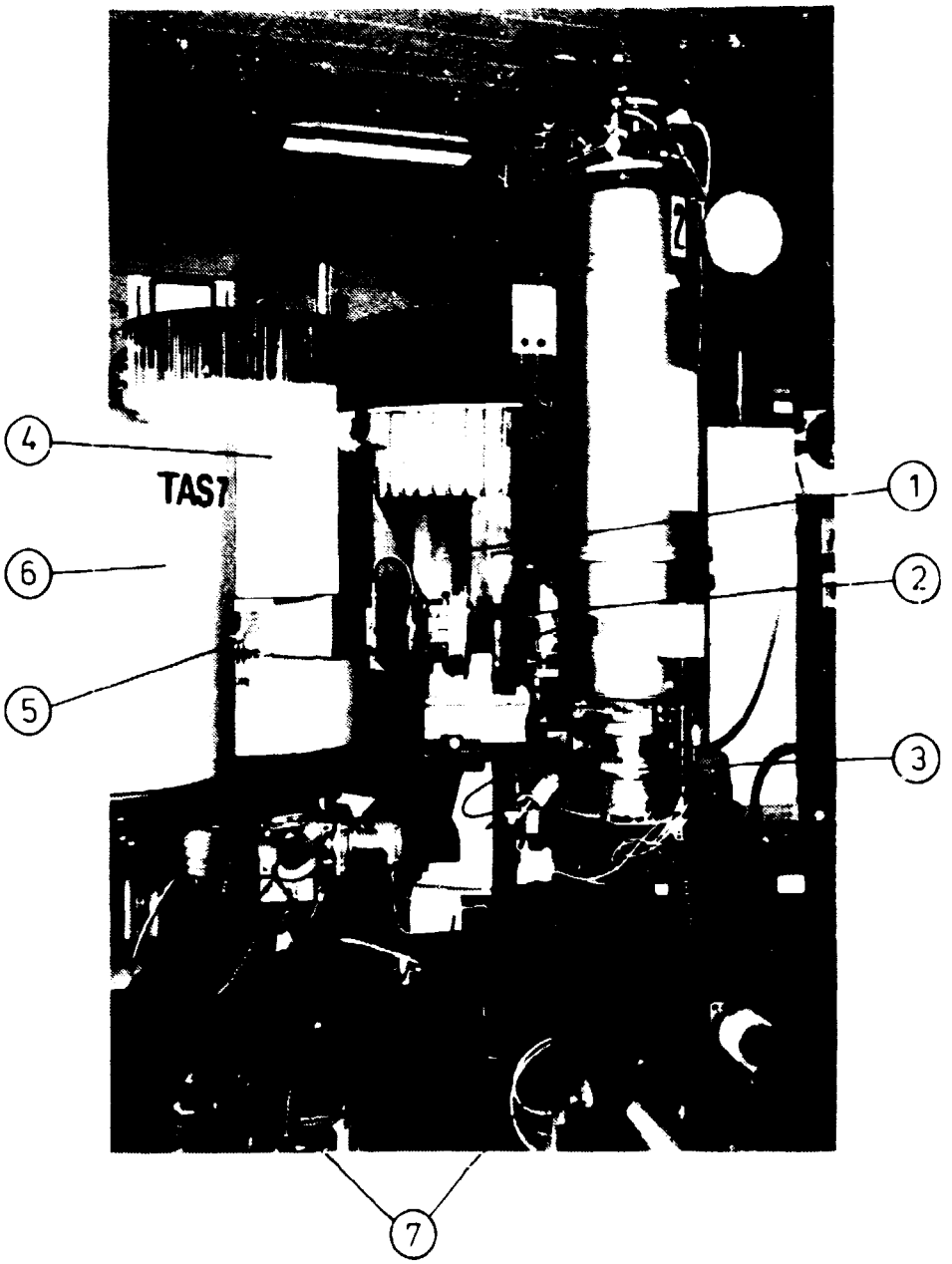

Fig. 15 The TAS7 cold neutron triple-axis spectrometer installed in the experimental hall at the end of the neutron conducting tube guiding cold neutrons from the DR3 reactor. 1) Monochromator shield. 2) Gd foil collimator for the incident monochromatic neutrons. 3) Sample turn table with goniometer and a 5 T superconducting split coil magnet. 4) Analyser shield. 5) Analyser turn table with goniometer and a pyrolytic graphite analyser crystal. 6) Detector shield. 7) Air-cushion supports.

The crystal and molecular structure of $C_6F_4O_2$ at room temperature was reported by Meresse et al. (1974) in a 3-D single crystal X-ray structural analysis. The crystal is monoclinic, $P2_1/c$, with two symmetry related molecules in the unit cell. The interest in $C_6F_4O_2$ arises from its isomorphous form with the molecular crystal $C_6Cl_4O_2$ that exhibits a phase transition which was shown to be continuous in behaviour (Ellenson and Kjems 1977). Powder diffraction patterns of $C_6F_4O_2$ were measured at various pressures up to 7.5 kbars and no evidence of a phase transition was found in contrast to the results for $C_6Cl_4O_2$.

1.27 Studies of simple histone-complexes

(R.D. Carlsson*, T. Kelley* (*Brookhaven National Laboratory, New York, USA), and K. Møllenbach[+])

It is of current interest in molecular biology to find structural information on the so-called ν-bodies, the object responsible for the bead-structure of streched chromosomes. From biochemical analysis it is known that the ν-bodies consist of eight small protein-units, twice the four histones H2a, H2b, H3, and H4.

Probably the only way to find the position of these units relative to one another is by a triangulation technique using small-angle neutron scattering from ν-bodies in an aquaous solution in connection with deuteration of units. Initially it is necessary to find the radius of gyration and the average scattering-length density of the pure histones, histone dimers, and histone tetramers. The histones from chicken eurythrocytes were purified and the complexes H2a/H2b and H3/H4 were synthesized. For both complexes the average scattering length density was found to be approximately that of a mixture of 40% D_2O in H_2O. The measurements of radius of gyration were more uncertain probably due to agregation of the histone-dimers. This problem will have to be solved before specific numbers can be given.

[+] Work done at Brookhaven National Laboratory and supported by the WHO fellowship programme.

1.28 Neutron scattering studies of liquids

(K. Carneiro, K. Schou Pedersen, and F. Yssing Hansen (Technical University of Denmark))

Diffraction from the liquids N_2 and O_2 was measured in order to establish how accurately intramolecular parameters of liquids can be determined with thermal neutrons, and to study angular correlations in diatomic liquids. The conclusion from the study was that bond lengths are well measured by diffraction experiments at wave vector transfers less than 12 $Å^{-1}$. Furthermore our analyses indicate that liquid N_2 has a tendency to perpendicular orientation of the molecules as in contrast to liquid O_2 which shows parallel orientation. This observation is what one would expect for these molecules by analogy to the low-temperature solid phases, and reflects the well known dominance of quadropolar and dipolar interactions of the N_2 and O_2 molecules respectively.

1.29 One-dimensional conductors

(K. Carneiro)

The study of phonon dispersion relations in one-dimensional conductors was continued on $K_2[Pt(CN)_4]Br_{0.3}3.2H_2O$, KCP(Br), and $(NH_4)_2[Pt(CN)_4]Cl_{0.42}3H_2O$. The two compounds are isomorphous, and it was found that their acoustic phonons $\omega(q)$ are quite similar. However, the electronic band fillings, and hence the Fermi vectors k_F, differ in the two compounds. This accounts for the major part of the differences in the electron-phonon coupling constant:

$$\lambda = g^2 N(\varepsilon_F)/\hbar\omega(2k_F),$$

Here g is the electron energy gain per ion displacement, and $N(\varepsilon_F)$ the electron density of states at the Fermi surface. The difference in λ has a rather pronounced effect on the electrical properties of the two compounds.

All six elastic constants were measured in the tetragonal KCP(Br) and compared to results of ultrasonic measurements (Takahashi et al. 1977). In particular c_{44} is of interest as it vanishes in the

ultrasonic low frequency region at temperatures around 50 K. No anomaly is observed, however, in the neutron (high frequency) region. This is the first experimental evidence of electron phonon coupling in one-dimensional conductors at small wave vectors ($q \approx 0$), and points towards the analogy between the Peierls instability and the Jahn-Teller effect.

1.30 Fast ionic conductors with fluorite structure

(J.K. Kjems, M. Dickens* and M.T. Hutchings* (*AERE, Harwell, U.K.))

An isotopically enriched crystal of $^{35}SrCl_2$ was studied in the high conductivity phase above 1023 K. Quasielastic scattering was

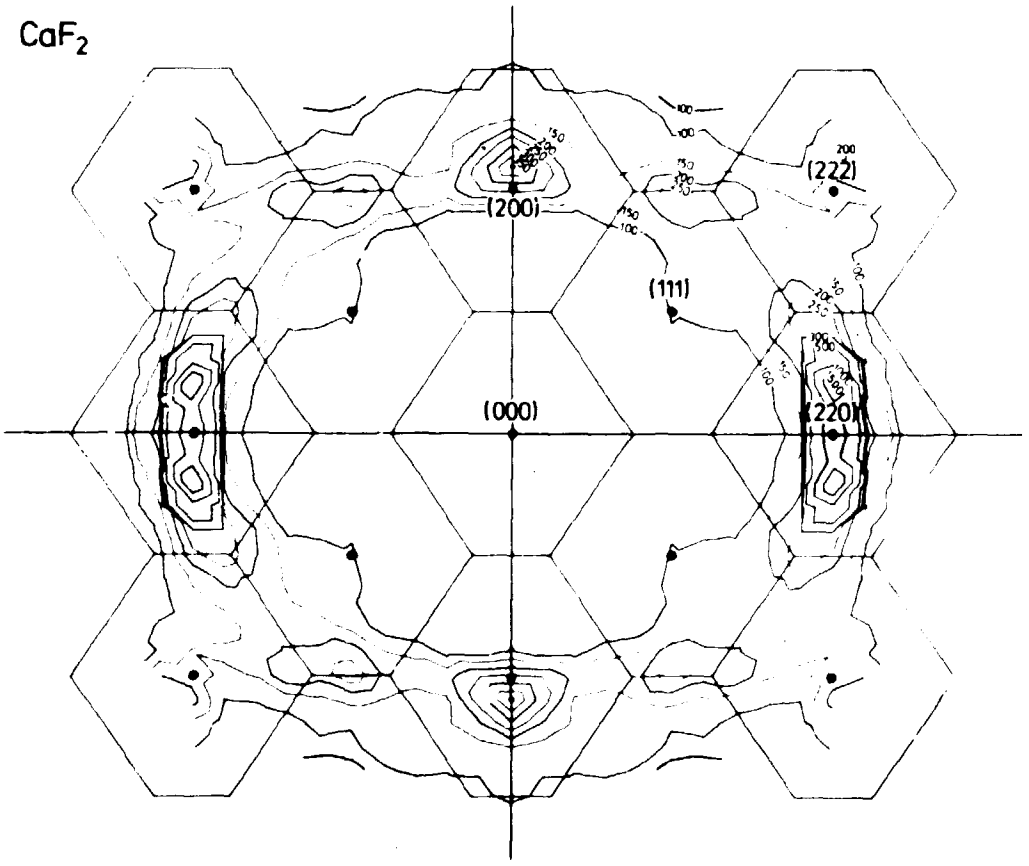

Fig. 16 Contour map of the integrated intensity of quasielastic scattering in CaF_2 at 1473 K. The scattering appears in the phase with high F^-conductivity and it indicates that a high degree of non-crystalline disorder is associated with the diffusion process. The intense scattering near the (2,2,0) lattice point is predominately due to phonons.

found with similar characteristics to that of the previously studied natural sample but with increased relative intensity compared to the phonon scattering. This proves that the quasielastic scattering is coherent. It originates from disordered diffusing Cl^- ions. The measurements were performed using the triple-axis spectrometer, TAS7, (Fig. 15) situated at the end of the neutron guide tube where the low background made higher resolution studies feasible. These studies revealed an increase of the energy width of the quasielastic scattering with temperature through the transition.

Similar studies were made on a CaF_2 single crystal around the transition at 1423 K. The same kind of quasielastic scattering as was seen in $SrCl_2$ was found above 1423 K but with an increased intensity and a typical energy width (FWHM) of about 2 meV as compared to 0.3 meV for $SrCl_2$. Pronounced variations of the energy width and of the total intensity were observed as functions of both $\vec{q}$ and temperature. A contour map of the integrated intensities in the (0,1,1) plane is shown in Fig. 16. The results are being analysed by comparison to computer simulations.

1.31 Catalysis

(K. Carneiro, M. Nielsen, and H. Topsøe (Haldor Topsøe A/S))

Neutron scattering investigations of catalytic systems were initiated with the aim of contributing to the microscopic characterization of such materials. The first system to be studied was the hydrogen-desulferisation catalyst: Mo with a few per cent of Co. Either γ-alumina or grafoil were used as supporter for the catalyst. With the latter supporter it was possible to observe diffraction peaks from MoS_2 which is formed during desulferization.

1.32 Polarized neutron triple-axis spectrometer

(J.K. Kjems and R.J. Pynn (ILL, Grenoble, France))

An experimental set-up to provide for polarization analysis was tested at the TAS 6 spectrometer. The key components are two Heussler-alloy polarizing crystals which were purchased from

Crystal Tec. Grenoble, France. An overall poparization better than 95% was achieved with a 2 cm^2 beam. The mosaic structure was not ideal and further improvement is expected after a careful selection of the Heussler alloy crystals. This will be attempted in collaboration with Crystal Tec and ILL, Grenoble, France.

1.33 High-intensity X-ray spectrometer

(J. Als Nielsen and B. Buras)

In the autumn of 1977 an application from Physics Laboratory II, University of Copenhagen and Risø to the Danish Natural Science Research Council concerning a high intensity X-ray spectrometer was approved. The application included a 12 kW X-ray generator (RIGAKU) with a rotating anode of Cu or Mo and a general-purpose triple-axis crystal spectrometer to be used at the rotating anode, and at a later stage at the storage ring DORIS at HASYLAB in Hamburg, F.R.G. The instrument was built during 1978 and installed in the guide-tube laboratory at Risø. Risø paid the installation expenses and contributed substantial manpower for the construction and manufacturing of the instrument. Some parts were manufactured at the machine shop at the H.C. Ørsted Institute of the University of Copenhagen.

The spectrometer is shown in Fig. 17. Each turnable can be set reproducibly with an accuracy of 0.001° and the distances between the monochromator, sample and analyzer can be varied. The spectrometer arms are supported by air-cushions to provide an axial load only on the turntables.

The electronics consist of a PDP11/34 computer with 2 floppy discs, interfaced to stepping motors, a digital voltmeter, and a scaler by means of the CAMAC system. The CAMAC motor drives were designed at Risø to provide options like built-in registers to keep track of the angle of each axis, three-speed manual motor settings, and suitable acceleration, and deceleration driving modes.

The programs used to control the spectrometer are written in BASIC so the user can readily modefy the programs to fit a particular purpose.

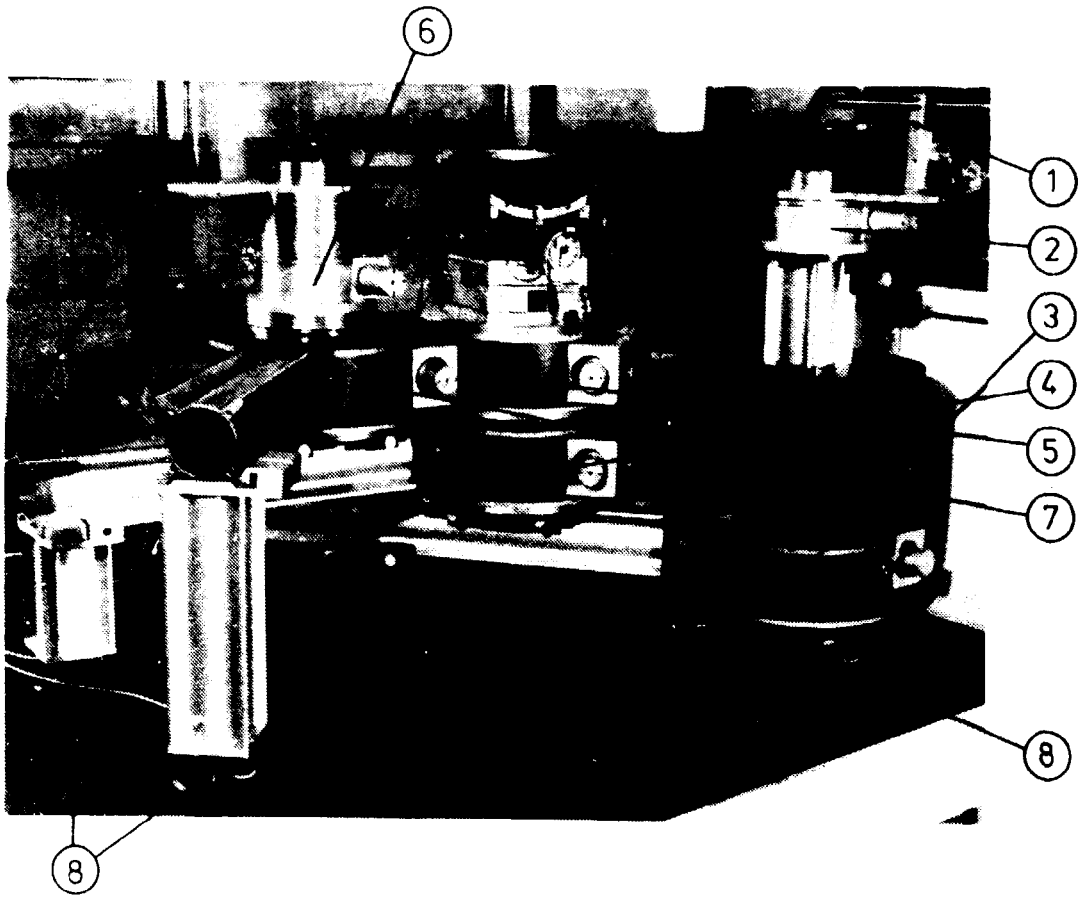

Fig. 17 The X-ray spectrometer. 1) Beam from X-ray generator. 2) Monochromator turn table with goniometer. 3) Monochromator arm with turn table. 4) Sample arm with turn table. 5) Sample turn table with goniometer and X-Y translation. 6) Analyser turntable with goniometer. 7) Detector arm with turn table. 8) Air-cushion supports.

The instrument became operational during the autumn of 1978. It has so far been used to study of the smectic A phase of liquid crystals as well as the behaviour of the rare earth element Nd at low temperatures (15 K) as described in section 1.4.

1.34 Quantitative structural studies by means of the energy-dispersive method and X-rays from a storage ring

(B. Buras, L. Gerward (Technical University of Denmark), A.M. Glazer*, M. Hidaka* (*Oxford University, U.K.), and J. Staun Olsen (University of Copenhagen))

As shown by Uno and Ishigaki (1975) using powdered samples and

by Buras et al. (1975) using single crystals, structure factors may be deduced from diffraction patterns obtained by the energy-dispersive method at conventional X-ray sources. However, lack of precise knowledge of the incident spectrum and its polarization limits the precision of these structure factors.

These difficulties are removed when synchrontron radiation from a storage ring is substituted for conventional X-rays. The spectral distribution of the incident beam (polarized almost completely in the electron orbit plane) calculated from the machine parameters is in good agreement with the spectrum derived from the diffraction patterns of known structures such as Si or Fe. Therefore, the calculated spectral distribution of the incident beam can be used for structural studies by means of the energy-dispersive method. We have used the calculated spectral distribution as input in a modified Rietveld profile refinement program to analyze diffraction patterns of urea (H_2N-CO-NH_2) and naphthalene ($C_{10}H_8$) obtained at the storage ring DORIS in Hamburg, F.R.G. As seen from the example shown in Fig. 18 the fit is satisfactory.

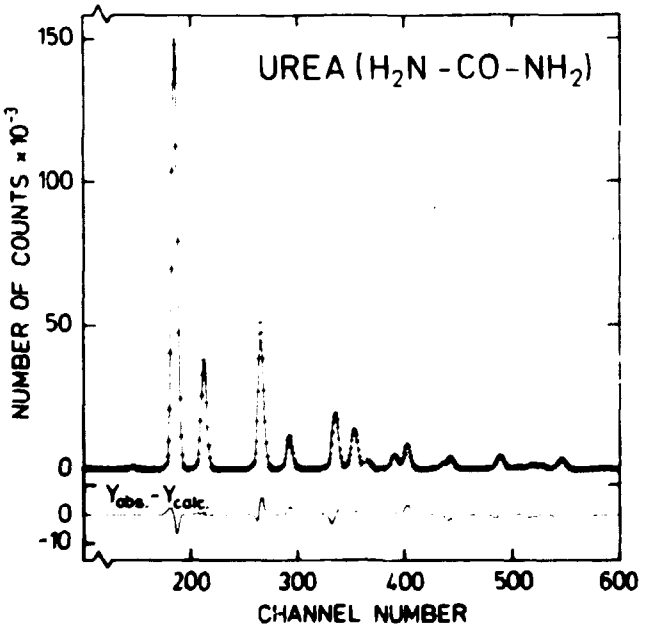

Fig. 18 Diffraction pattern of urea obtained by the energy dispersive method ($2\theta_o$ = 16.3°) and X-rays from the storage ring DORIS, Hamburg, F.R.G. The crosses are the experimental points and the full curve the results of the structure refinement. The difference spectrum is shown as the lower curve ($Y_{obs}-Y_{calc}$).

In the same series of measurements we found that the stability and time structure of the beam is sufficient to give reproducible diffraction patterns in very short times, e.g. a powder pattern from a 0.2 mm^3 sample of $BaTiO_3$ is obtained in one second with a structure factor reliability of 3.8%. These results indicate that using the energy-dispersive method at a storage ring it should be possible to refine atomic positions and to observe structural changes induced semi-continuously by changing sample environments.

1.35 References to section 1

ANDERSEN, O.K. (1975). Phys. Rev. B12, 3060-3083.

BAK, P., KRINSKY, S., and MUKAMEL, D. (1976). Phys. Rev. Lett. 36, 52-55.

BAK, P. and LEBECH, B. (1978). Phys. Rev. Lett. 40, 800-803.

BECKER, K.W., FULDE, P., and KELLER, P. (1977). Z. Phys. B28, 9-18.

BERG, R.W. (1978). J. Chem. Phys. 69, 1325-1335.

BERG, R.W. POULSEN, F.W. and BJERRUM, N.J. (1977). J. Chem. Phys. 67, 1829-1837.

BERG, R.W. and SØTOFTE, I. (1978). Acta Chem. Scand. A32, 241-244.

BRAGG, W.H. (1921). Proc. Phys. Soc. London 34, 33-50.

BURAS, B., KOFOED, W., LEBECH, B., and BÄCKSTRÖM, G. (1977). Risø Report No. 357, 32 pp.

BURAS, B., STAUN OLSEN, J., GERWARD, L., SELSMARK, B., and LINDE-GAARD ANDERSEN, A. (1975). Acta Crystallogr. A31, 327-333.

COWLEY, R.A. (1976). Phys. Rev. B13, 4877-4885.

DIETRICH, O.W., MACKENZIE, G.A., and PAWLEY, G.S. (1975). J. Phys. C: Solid State Phys. 8, L98-L102.

ELLENSON, W.D. and KJEMS, J.K. (1977). J. Chem. Phys. 67, 3619-3623.

ELLIOTT, R.J., HARLEY, R.T., HAYSE, W., and SMITH, S.R.P. (1972). Proc. Roy. Soc. London A328, 217-266.

FISCHER, P., LEBECH, B., MEIER, G., RAINFORD, B.D., and VOGT, O. (1978). J. Phys. C: Solid State Phys. 11, 345-364.

GLEASON, W.B. and BRITTON, D. (1976). Cryst. Struct. Commun. 5, 483-488.

HALPERIN, B.I. and NELSON, D.R. (1978). Phys. Rev. Lett. 41, 121-124.

HARLEY, R.T. and McFARLANE, R.M. (1975). J. Phys. C: Solid State Phys. 8, L451-L455.

HALEY, S.B. and ERDÖS, P. (1972). Phys. Rev. B5, 1106-1119.

HESSEL ANDERSEN, N. and SMITH, H. (1979). Accepted for publication in Phys. Rev.

HOUMANN, J.G., LEBECH, B., MACKINTOSH, A.R., BUYERS, W.J.L., McMASTERS, O.D., and GSCHNEIDNER, K.A. Jr. (1977). Physica B+C 86-88, 1156-1157.

JOHANSSON, B. (1974). Philos. Mag. 30, 469-482.

JOHANSSON, B. (1975). Phys. Rev. B11, 2740-2743.

JOHANSSON, B. and ROSENGREN, A. (1975). Phys. Rev. B11, 1307-1373.

JONES, W., RAMDAS, S., and THOMAS, J.M. (1978). Chem. Phys. Lett. 54, 490-493.

KAWASAKI, K. (1968). Progr. Theor. Phys. 40, 11-35.

MACKENZIE, G.A. and PAWLEY, G.S. (1975). Acta Crystallogr. A31, 851-852.

MACKENZIE, G.A., BURAS, B., and BERG, R. (1977). Risø Report No. 374, 39-41.

MEIER, G., FISCHER, P., HÄLG, W., LEBECH, B., RAINFORD, B.D., and VOGT, O. (1978). J. Phys. C: Solid State Phys. 11, 1173-1186.

MERESSE, A., COURSEILLE, C., and CHANH, N.B. (1974). Acta Crystallogr. B30, 524-526.

MIKESKA, H.J. (1978). J. Phys. C: Solid State Phys. 11, L29-L32.

MOON, R.M., CABLE, J.W., and KOEHLER, W.C. (1964). J. Appl. Phys. 35, 1041-1042.

MORI, H. (1958). Phys. Rev. 112, 1829-1842.

MORI, H. (1959). Phys. Rev. 115, 298-300.

NERONOVA, N.N. (1968). J. Struct. Chem. (USSR) 9, 130-131.

NIELSEN, M., ELLENSON, W.D., and McTAGUE, J.P. (1978). In: Neutron Inelastic Scattering 1977. Proceedings of a symposium held in Vienna, 17-21 October 1977. Vol. 2 (IAEA, Vienna) 433-457.

OSTERTAG, W. and STRNAT, K.J. (1966). Acta Crystallogr. 21, 560-565.

PAWLEY, G.S., MACKENZIE, G.A., and DIETRICH, O.W. (1977). Acta Crystallogr. A33, 142-145.

RAE, A.I.M. (1972). J. Phys. C: Solid State Phys. 5, 3309-3321.

RHYNE, J.J. and KOON, N.C. (1978). J. Appl. Phys. 49, 2133-2135.

RHYNE, J.J., SANKAR, S.G., and WALLACE, W.E. (1978). In: The Rare Earths in Modern Science and Technology. Edited by G.J. McCarthy and J.J. Rhyne (Plenum, New York) 63-68.

ROSSAT-MIGNOD, J., BURLET, P., VILLAIN, J., BARTHOLIN, H., WANG TCHENG-SI, FLORENCE, D., and VOGT, O. (1977). Phys. Rev. B16, 440-461.

RÖDHAMMER, P., CHRISTENSEN, A.N., and PINTSCHOVIUS, L. (1979). Experiments Nos. 04-01-090 and 04-01-090A at ILL, Grenoble, France, (to be published).

SIM, G.A., MONTEATH ROBERTSON, J., and GOODWIN, T.H. (1955). Acta Crystallogr. 8, 157-164.

SZPUNAR, B. and LINDGÅRD, P.-A. (1979). J. Phys. F: Metal Phys. 9, L55-59.

TAKAHASHI, T., AKAGHWA, H., DOI, H., and NAGASAWA, H. (1977). Solid State Commun. 23, 809-814.

UNO, R. and ISHIGAKI, J. (1975). J. Appl. Crystallogr. 8, 578-581.

VILLAIN, J. (1978). Phys. Rev. Lett. 41, 36-39.

WALLACE, W.E. (1973). Rare Earth Intermetallics (Academic Press, London and New York), 266 pp.

ZACHARIASEN, W.H. (1961). In: The Metal Plutonium. Edited by A.S. Coffinberry and W.N. Miner (University of Chicago Press, Chicago) 99.

2. PLASMA PHYSICS

The plasma physics section works under a contract of association between Risø National Laboratory and Euratom, and staff of the section participate as members or consultants in several of the committees concerned with the Euratom fusion programme. The research activities are centered on basic plasma physics (2.1-2.6) and on technology of interest for future fusion reactors.

The activities in basic plasma physics are mainly concentrated on nonlinear wave phenomena and cover both experimental and theoretical work. The experiments are performed in a relatively cold steady state plasma produced in a Q-machine. Among the investigations were studies of strongly turbulent, gradient driven instabilities in fully or partially ionized plasma. In addition, nonlinear electron waves in a strongly magnetized plasma loaded waveguide were examined with particular attention to the propagation of solitary structures. In this study care was taken to understand the linear behaviour in order to discriminate the truly nonlinear effects. This study demonstrated that nonlinear Landau damping is of importance for the evolution of a modulated wave train in a strongly magnetized plasma.

The technological aspects of plasma physics are studied with one of the possible refuelling schemes for fusion reactors in mind. In this particular scheme the fuel will be injected as high velocity pellets of solid hydrogens. Hence the electron emission from solids were studied both theoretically and experimentally. The experiments included a study of electron emission from solid hydrogens for oblique incidence of electrons and a study of the interaction between solid hydrogens and ions. For more direct studies of pellet-plasma interaction a small gun for acceleration of D_2-pellets was built. A small Tokamak "Dante" is presently being reconstructed and tested to provide one more facility where the interactions between a Tokamak plasma and pellets of solid hydrogens can be studied.

2.1 Solitary structures in a magnetized plasma-loaded waveguide

(J.P. Lynov, P. Michelsen, H.L. Pécseli, J. Juul Rasmussen, K. Saéki (Tohoku University, Sendai, Japan), and V.A. Turikov)

Detailed experimental, analytical, and numerical investigations were made of the propagation of nonlinear electron pulses in a single-ended Q-machine. In order to ensure well-defined boundary conditions, the plasma was surrounded by a grounded cylindrical brass tube with a 4 cm inner diameter acting as a waveguide. The pulses were excited by applying a potential to a terminating brass tube of 30 cm in length.

Two different types of pulses were observed namely a compressional structure corresponding to a negative potential which was identified as a Korteweg-de Vries soliton previously observed and described by Ikezi et al. (1971) and a pulse with positive potential indicating a deficit of electrons which we refer to as an "electron hole". A computer code was developed to simulate the experiment and the results (Fig. 19) show how the phase space and potential develop in time. The KdV-soliton is identified as

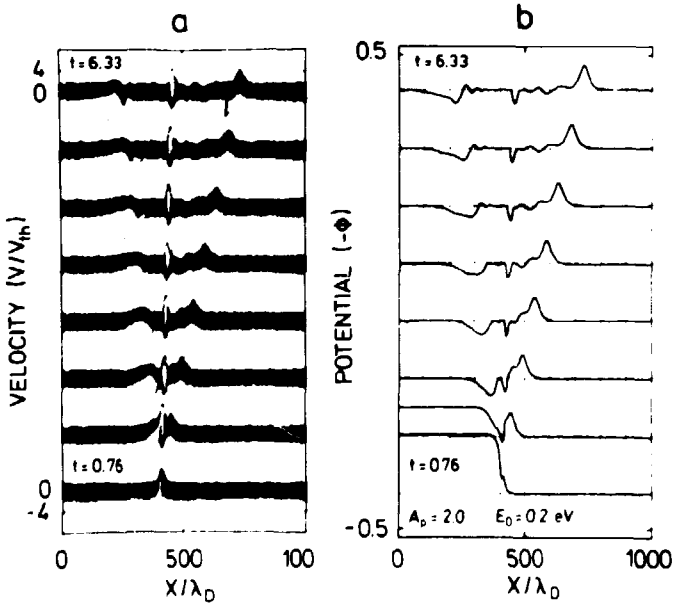

Fig. 19 Computer simulation of propagation of nonlinear electron pulses showing the development in time of the "electron hole" and the Korteweg-de Vries soliton.

a hump in phase space while the electron hole is seen to be associated with a phase space vortex.

Our main interest in the KdV-solitons was to investigate experimentally their damping by collective effects as predicted theoretically by Ott and Sudan (1969). Also the development of a potential tail trailing the soliton as predicted in a recent theory by Karpman (1979) was verified by both experiment and computer simulation (Fig. 19). The mutual interaction of the electron holes and their interaction with the KdV-solitons were investigated and a quasi-particle behaviour was observed for both properties, i.e. they preserve their identity also after collisions. If, however, the initial velocity difference between two holes close to each other were small the holes would attract each other and finally coalesce. We may therefore visualize the collision between two electron holes as a collision between two slightly sticky spheres: they stick together only in the case of small relative velocity collisions. We believe that the solitary electron hole may play a role in the case of strong coupling (Dupree 1978) similar to that of self-trapped plasma waves in the limit of weak coupling according to Langmuir turbulence theory.

2.2 Propagation of modulated electron waves in a dispersive plasma

(J.P. Lynov, P. Michelsen, H.L. Pécseli, J. Juul Rasmussen, and H. Sugai (Nagoya University, Nagoya, Japan))

Although the nonlinear behaviour of wave packets in dispersive systems were examined intensively in recent years it seems that their linear behaviour has received only superficial attention. Therefore, it is worth while to examine the linear propagation properties of amplitude-modulated waves in a strongly dispersive medium. The measurements were performed for electron plasma waves excited in a single-ended Q-machine plasma. We found that the dispersion caused a wave packet, exited at the cold end of the machine, to expand with distance as displayed in Fig. 20. The expansion can be understood by the following simple physical argument. The wave packet contains a band of frequencies around the carrier frequency ω_o. If we have dispersion, e.g.

$$(dv_g/d\omega)_{\omega=\omega_c} < 0,$$

where v_g is the group velocity, then the frequencies below ω_o will have group velocities larger than $v_g(\omega_o)$, while those above ω_o will have group velocities smaller than $v_g(\omega_o)$, and thus the wave packet will expand. The expansion rate will be determined by the dispersion term $dv_g/d\omega$. For a continuously excited amplitude-modulated wave the dispersion was found to give rise to a recurrence of the modulation which can be understood from a similar argument. Our experimental results were well explained by a simple theoretical model based on the physical argument noted above and direct numerical calculations of the wave propagation.

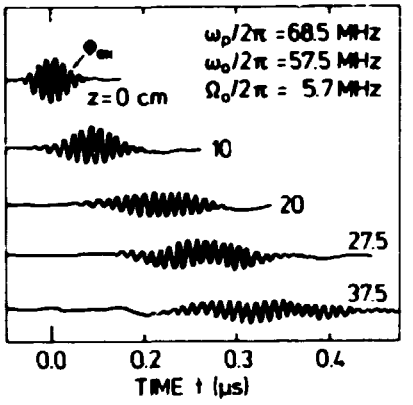

Fig. 20 The spatial evolution of a wave packet, showing the expansion along the distance from the exciter. ω_p, ω_o and Ω_o are plasma-, carrier-, and modulation-frequency, respectively.

2.3 Nonlinear wave modulation in a magnetized plasma-filled waveguide

(J.P. Lynov, P. Michelsen, H.L. Pécseli, J. Juul Rasmussen, and H. Sugai (Nagoya University, Nagoya, Japan))

The nonlinear modulation of high-frequency electron oscillations in a magnetized plasma-filled waveguide was investigated theoretically. The analysis was based upon the electron Vlasov equation and the Poisson equation in the form appropriate for the present problem. Only the lowest radial eigenmode was considered. By applying a multiple time-scale analysis the following modified nonlinear Schrödinger equation for the wave evelope was derived

$$(i\frac{\partial}{\partial t} + \frac{1}{2} v_g' \frac{\partial^2}{\partial x^2})\phi = (\alpha|\phi|^2 + \beta \int_{-\infty}^{+\infty} \frac{|\phi|^2}{x-x'}dx')\phi \qquad (1)$$

where v_g' is the k-derivative of the group velocity, v_g, and α and β are complicated functions of the plasma parameters. In deriving this equation we assumed that the phase velocity of the waves ω/k is much larger than the electron thermal velocity v_e. Therefore, linear Landau damping due to particle-wave resonance is ignored. Using the linear dispersion relation

$$\omega^2 = \omega_p^2 \cdot (ak)^2/(1-(ak)^2) + 3v_e k^2$$

it is, however, easily seen that $v_g \sim v_e$ may very well occur. Particles resonating with the wave envelope (nonlinear Landau damping) must therefore be included and their contribution gives rise to the non-local term in equation (1). Furthermore, we find that thermal effects considerably modify the coefficient α as compared with the case where the electron thermal motion is neglected (Rasmussen 1978) i.e. $v_e = 0$. An analysis of equation (1) thus shows that electron waves in the present geometry are always modulationally unstable.

An experimental investigation of the present problem is in progress. The experiment is performed in the Q-machine. Particular attention is given to competing processes, which may give rise to effects that could be misinterpreted as modulational instability. Nonlinear deformation of wave packets is also investigated. The experimental investigation is supported with numerical simulations based on a particle in cell method (Turikov 1978). Preliminary results show that under suitable conditions modulational instability and wave packet deformation as described by equation (1) can be observed.

2.4 On the origins of sideband instability

(J. Juul Rasmussen)

The so-called sideband instability is characterized by the growth of a lower sideband close to the frequency of the original wave. This instability is observed when a large amplitude electron wave is excited in a plasma. Recently, it was shown experimentally that the instability is caused by a beam arising from initially trapped

electrons which are accelerated and detrapped as the plasma wave damps (e.g. Sato et al. 1976, Franklin et al. 1978).

By making the simple assumption that all those electrons that are trapped originally are detrapped after half a bounce period, we have investigated the dependence of the growth rate γ on the initial amplitude of the electron wave ϕ_o and find $\gamma \propto \phi_o^n$ with $0.5 \lesssim n \lesssim 1.2$ in agreement with the experimental observations of van Hoven and Jahns (1975). This scaling of the growth rate and the instability of only the lower sideband clearly distinguishes the sideband instability from the modulation instability described in 2.3, where both the upper and lower sidebands grow at a rate $\gamma \propto \phi^2$.

2.5. A modified nonlinear Schrödinger equation for Langmuir waves

(K.B. Dysthe (University of Tromsø, Norway) and H.L. Pécseli)

Using the fluid description for electrons and ions in a plasma we include a simple collisional loss term, $-\nu v$, in the ion momentum equation (ν is the collision frequency). We derive the following nonlinear Schrödinger equation for the envelope, ϕ, of the modulated Langmuir wave (Dysthe and Pécseli 1977, 1978):

$$(i\frac{\partial}{\partial t} + \frac{1}{2}v_g' \frac{\partial^2}{\partial x^2})\phi = \frac{1}{2M}\omega_p T_i \{\frac{|\phi|^2}{v_g^2 - C_s^2}$$

$$+ \frac{1}{2}\nu v_g (v_g^2 - C_s^2)^{-2} \int_{-\infty}^{\infty} |\phi|^2 \exp(-\nu v_g |\frac{x'-x}{v_g^2 - C_s^2}|) dx'\} \qquad (1)$$

where v_g' is the k-derivative of the Langmuir group velocity, v_g, T_i and M are the ion temperature and mass respectively, and C_s is the ion sound speed. The last, non-local, term in equation (1) is caused by collisional losses. We note that with this term included Langmuir waves are always modulationally unstable just as in the case where a non local term accounting for nonlinear ion Landau damping is included (Dysthe and Pécseli 1977).

2.6 Strong turbulence in a low-β plasma

(T. Mikkelsen and H.L. Pécseli)

Strong turbulence in a low-β plasma was investigated and the experimental results were compared with recent theoretical investigations based on a fluid description using a cascade decomposition (Tchen et al. 1977). Here we quote only the results concerned with power spectra, G(k), of turbulent potential fluctuations. Only two subranges, denoted "production" and "coupling" subranges, were considered:

For production $$G(k) = \text{const} \cdot (T_e/eC_s)^2 \Gamma_n^2 \, k^{-3}, \qquad (1)$$

and for coupling $$G(k) = \text{const} \cdot (T_e/eC_s)^2 (\omega_o^4/\lambda_c \omega_c) \, k^{-5}, \qquad (2)$$

Where $\Gamma_n^2 = (C_s \partial \ln \bar{n}/\partial r)^2$, $C_s^2 = \kappa(T_i+T_e)/M$,

$\lambda_c = C_s^2/\omega_c$ and $\omega_o^3 = \omega_c J$,

with $J = (eC_s/T_e)^2 \int_o^\infty k^2 G(k) dk$. (An overbar denotes time average.)

These results are obtained assuming strongly $\vec{B}$-field-aligned fluctuations, but allowing for a Boltzmann distribution for the electrons. Locally homogeneous and isotropic turbulence is assumed in the plane perpendicular to $\vec{B}$.

In order to be able to rely on Taylor's hypothesis when comparing measured frequency spectra with calculations referring to wave number spectra, we carried out the experiment in a

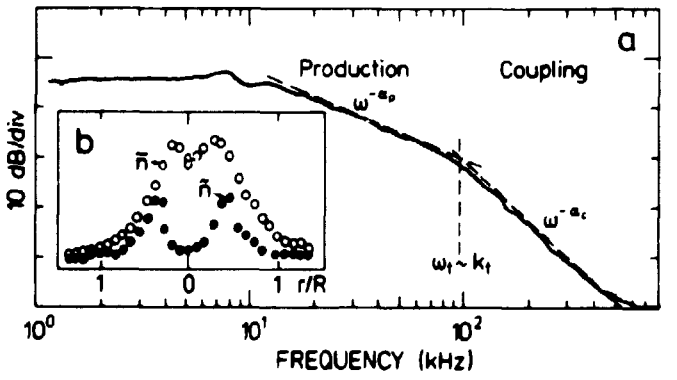

Fig. 21 (a) Spectrum of potential fluctuations. (b) Radial variation of density $\bar{n}$ and fluctuations in density $\tilde{n}$.

rapidly rotating magnetized plasma column, where a radial electric field with field strength increasing lineary with radius, produces a "solid body" $\vec{E} \times \vec{B}$ rotation. Figure 21a shows the measured d.c. radial density variation $\bar{n}$ and the observed fluctuation level, $\tilde{n}$. As expected, we find the highest fluctuation level where $\partial\bar{n}/\partial r$ is largest. Figure 21b shows an observed potential spectrum. The subranges are clearly distinguished. On the basis of $\sim$ 50 spectra we found the spectral index in the production subrange, $\alpha_p = 1.9 \pm 0.4$, and in the coupling subrange, $\alpha_c = 4.5 \pm 0.3$, to be compared with the theoretical values 3 and 5, respectively. Figure 22a shows the variation of the measured spectral coefficeint, C_m, relative to the theoretical one C_t of equation (2), for the yarying B-field (i.e. $(C_t - C_m)/C_t$ as a function of B). Similarly Fig. 22b shows the relative vari-

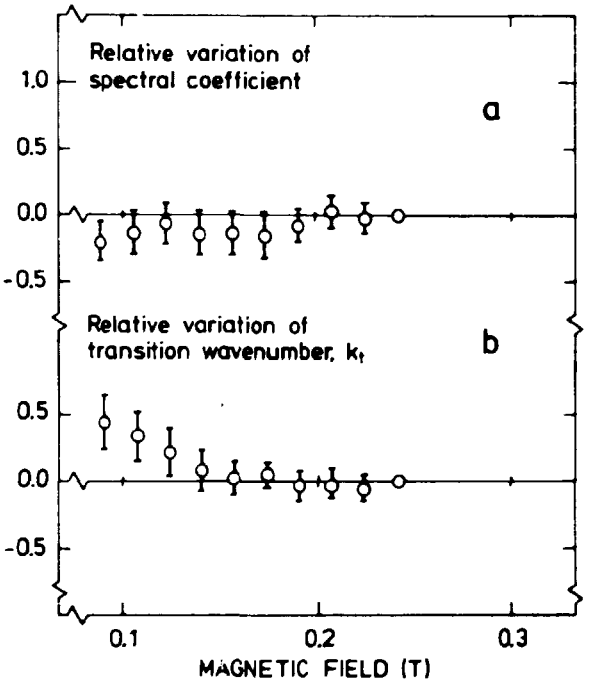

Fig. 22 (a) Variation of spectral coefficient for varying field.
(b) Transition wave number for varying field.

ation of the transition wavenumber k_t (see Fig. 21) where the theoretical value is easily deduced from equations (1) and (2). Taking into consideration the number of necessary simplifying assumptions in the theoretical analysis we find the agreement between the theoretical and experimental results to be satisfactory (Mikkelsen and Pécseli 1978).

2.7 On electron emission from solid H_2 and D_2 for oblique incidence of 1-3 keV electrons

(J. Schou and H. Sørensen)

Studies of the electron emission from solid H_2 and D_2 are of importance in understanding the interaction between pellets of H_2 or D_2 and a fusion plasma. The pellet is subject to irradiation by plasma particles with angles of incidence varying from 0° to 90°. The isotropic electron emission coefficient, i.e. the number of electrons emitted per unit flux of isotropically incident electrons, determines how a pellet will start to charge up electrically. The isotropic electron emission coefficient may be determined from an experimental study of electron emission from solid H_2 and D_2 for oblique angles of incidence. Therefore the

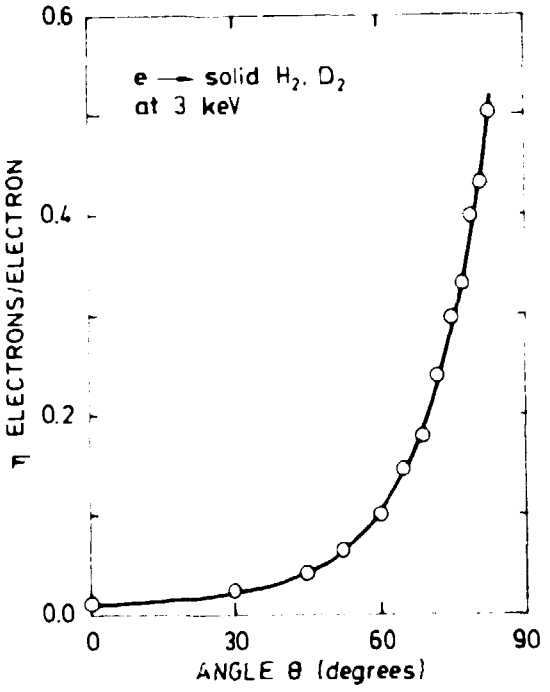

Fig. 23 The electron reflection coefficient $\eta(\theta)$ for solid H_2 and D_2 for incidence of 3 keV electrons shown as a function of the angle of incidence. The solid curve is a least squares fit.

previous studies of the electron reflection coefficient $\eta(\theta)$ and the true secondary electron emission coefficient $\delta(\theta)$ for incident electrons of 1-3 keV were extended to angles of incidence up to 83°. These measurements were possible because the experimental set-up was improved permitting the beam current to be measured independently of the target state (Sørensen and Schou 1977 and 1978b).

The electron reflection coefficient $\eta(\theta)$, which gives the number of electrons emitted between 50 eV and the energy of incidence E_o, increased strongly with the angle of incidence θ, to reach a value of 0.5 at 83^o for E_o = 3 keV. η is independent of the electron energy and target material for $\theta < 65^o$. For $\theta > 65^o$ η increases with energy, and differs for H_2 and D_2. The reflection coefficients found for H_2 are smaller than those of D_2, but the

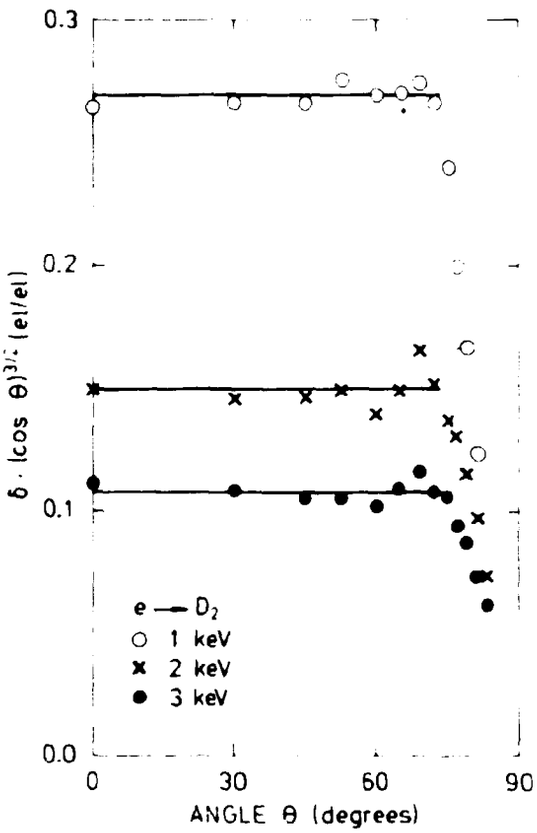

Fig. 24 The secondary electron emission coefficient $\delta(\theta)$ for oblique incidence of 1, 2 and 3 keV electrons on solid D_2. The secondary electron emission coefficients have been multiplied by $(\cos\theta)^{3/2}$.

difference is only substantial at low energies. Figure 23 shows the electron reflection coefficient for 3 keV incident electrons as a function angle of θ. The solid curve described by $\eta(\theta) = 0.879\exp(-4.30\cos\theta)$ gives an excellent fit. It is known that the variation of η with θ is stronger the lower the atomic number of the target. The results for H_2 and D_2 show stronger variation with θ than seen for Be, in good agreement with this rule.

The true secondary electrons have energies in the range 0-50 eV. Secondary electrons originate from the electrons that are released inside the target when the target atoms are ionised by

the incident and the reflected electrons. Some of the released electrons reach the surface and escape through it as secondary electrons. The released electrons lose energy inside the target material and it is only those electrons that are released in the outer layer, the escape zone, that may reach the surface with sufficient energy to escape and appear as secondary electrons. In H_2 and D_2 the electrons lose energy by exciting vibrational molecular states. The losses are largest for H_2 and the true secondary electron emission coefficient $\delta(\theta)$ is thus smallest for H_2. It was found (Sørensen 1977) that $\delta(0)$ for H_2 was 0.65 times $\delta(0)$ for D_2 for normal incidence of both electrons and hydrogen ions. For oblique incidence of electrons the number of electrons released in the escape zone will increase. In the first approximation the number will be proportional to $(\cos\theta)^{-1}$, but there will also be a contribution from the reflected electrons that pass through the escape zone. This contribution will increase very strongly with θ and the final result is that δ increases strongly with θ. We have shown (Sørensen and Schou 1977, 1978a) that

$$\delta(\theta) = \delta(0)(\cos\theta)^{-3/2}$$

for angles up to 60°. In Fig. 24 is shown $\delta(\theta)\cos\theta^{3/2}$ as a function of θ for D_2 with incident energies of 1, 2 and 3 keV. The values of $\delta(\theta)$ are derived from fits to the experimental results of δ versus E_o at different angles of incidence. It is seen that the above mentioned angular variation is valid up to an angle of $72\text{-}75^{\circ}$ and that $\delta(\theta)$ increases less fast with angle after that. Comparison to a similar set of data for H_2 shows that only at the very largest angles do the ratio between the H_2 data and the D_2 data deviate from 0.65. The qualitative behaviour of the angular dependence of the secondary electron emission coefficient is in agreement with the one reported for Be by Bronshtein and Dolinin (1968). The behaviour at the largest angles of incidence is not yet fully understood, apparently the number of electrons released within the escape zone increases less fast with angle at the largest angles.

2.8 Interaction between solid hydrogens and keV ions of N and Ne

(J. Schou and H. Sørensen)

In the studies of secondary electron emission from solid H_2 and D_2 caused by normal incidence of H and He ions only electrons were emitted, i.e. no positive particles were observed (Sørensen 1977, Sørensen and Schou 1977 and 1978a). The light H and He ions are slowed down mainly by interaction with the electrons of the target so that very little energy is transferred to the target nuclei.

Using heavier ions as projectiles a larger fraction of the particle energy will be transferred to the target nuclei, and emission of neutral and positive particles are probable. Preliminary irradiations were made with 5-10 keV N^+ and Ne^+ ions. It was found that both positive and negative particles (preferentially electrons) were emitted. The coefficients for emission of positive particles were small, of the order of 0.05 to 0.1. When surfaces of solid H_2 and D_2 are bombarded by ions sputtering may take place. Normally most of the sputtered particles are neutral, some of them will, however, be ionised. Therefore, the existence of positive emitted particles indicate that sputtering has occurred.

2.9 Theory of ion- and electron-induced secondary electron emission from solids

(J. Schou, G. Holmen*, P. Sigmund (University of Odense), and B. Svensson* (Chalmers University of Technology, Göteborg, Sweden))

On the basis of multiple-collision transport theory a framework was developed to explain important properties of both ion- and electron-induced secondary electron emission. The evaluation of the secondary electron emission yield and of the energy spectrum of the emitted electrons was made similarly to the treatment used in the theory of sputtering (Sigmund 1969, 1972). The yield dependence on the primary energy and on the atomic number of the target appears to be qualitatively correct. The main result is that the yields can be written as a product of a material

parameter, and the value at the target surface of the energy distribution representing the depth density of the kinetic energy of the slow target electrons after the slowing down of the primary particles and all fast recoil particles. Each of the two quantities may in some cases be evaluated from other existing experimental or theoretical data.

The theory concerns primary keV particles, and the aim was to investigate the yield from two metals, Al and Cu. The choice of these metals is convenient because in contrast to the case of insulating materials free conduction electrons are present and there are no thresholds for electronic excitation. The agreement with the experimental data of Holmén et al. (1977) is satisfactory.

2.10 Secondary electron emission coefficient

(C.T. Chang and P. Michelsen)

The maximum value of the secondary electron emission coefficient δ_{max} of solid D_2 was determined from a least squares fit to the experimental data of Sørensen (1977). The fit was made to the empirical formula suggested by Fuchs and Nicolai (1978) for metal surfaces. The formula relates the secondary electron emission coefficient δ to the incident energy E_o through

$$\bar{\delta} = a_1 \ln(a_2\bar{E} + 1)(1 + a_3\exp(-a_4\bar{E}))/(\bar{E} + 1)$$

where $\bar{\delta} = \delta/\delta_{max}$ and $\bar{E} = E_o/E_{max}$. δ_{max} found by the fit is $\sim$ 0.94. Good fits may be obtained for any value of E_{max} between

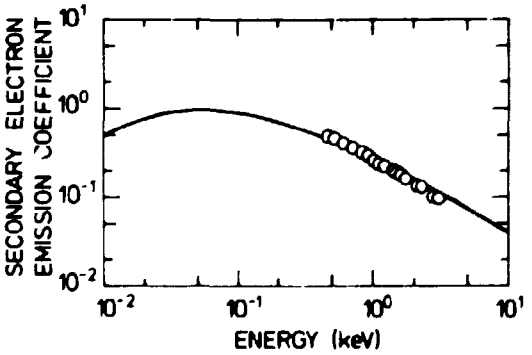

Fig. 25 The secondary electron emission coefficient versus electron energy. The solid curve is a least squares fit of the formula by Fuchs and Nicolai (1978) to the experimental results of Sørensen (1977).

10-80 ev, i.e. values of E_{max} found in the fit do not contradict the theoretically expected value of 40-80 ev (Peterson and Green, 1968). A fit is shown in Fig. 25.

2.11 Extrusion of solid D_2 and H_2 and acceleration of pellets of D_2

(A. Nordskov, H. Skovgård, H. Sørensen, and K.V. Weisberg (Department of Electronics, Risø))

The work on extrusion of filaments of solid D_2 (and H_2) (Nordskov et al. 1978) was continued. A new and improved setup for extrusion was built. The solid D_2 (or H_2) to be extruded is contained in a small cylinder mounted below the helium bath in a liquid helium cryostat. The solid D_2 is extruded through a nozzle in the cylinder by means of a piston. The extrusion process is remotely controlled and consists of several single operations such as slight heating of the solid D_2, heating of the nozzle so that the solid D_2 close to it becomes plastic, pressurising the piston, etc.

The cylinder contains so much solid D_2 that a filament of length 300 mm and 1 mm in diameter can be extruded. With solid H_2 45 succesive extrusions can be made within 32 minutes, whereas the same process takes 50 minutes with solid D_2.

A small test gun has been designed and built to attempt pneumatic acceleration of D_2 pellets made from the extruded filament. The gun is placed below the extrusion unit and a pellet made from the extruded filament is loaded into the gun. The pellet is blown out of the gun by means of H_2 gas, pressurised at the low temperature. 2.5 cm^2 of H_2 gas at normal pressure and temperature is used to fire a pellet. This is about three times the quantity of H_2 comprising the pellet.

The first tests were quite successful. An 0.8 mm diameter pellet 1.2 mm long is accelerated through a 6 cm long tube. The pellet is detected when it hits a thin (0.04 mm thick) Al plate attached to a grammophone pick-up. The pellet velocity is measured by interception of light pulses detected by a photomultiplier.

24 velocity measurements were made with pellet velocities ranging

Fig. 26 A photograph of a 0.040 mm thick and 12 mm diameter Al plate mounted on a grammophone pick up. The Al plate has been hit by 24 D_2 pellets and the dent made by these pellets is seen close to the centre of the plate.

from 69 m/s to 216 m/s. The spread in velocities is accountable mainly to the firing procedures which differed slightly, and only a few of the attempted firings were unsuccessful. At the moment the repetition rate corresponds to one firing every three minutes. So at present only D_2 pellets have been used, but it is not expected that the shooting of H_2 pellets will introduce difficulties. One would expect higher velocities for H_2 pellets because of their lower mass.

A small dent was observed where the pellets hit the Al plate. All the pellets hit within a 1 mm spot. At the distance of 25 cm from the gun nozzle to the target this corresponds to an angular spread of less than 0.2°. A photograph of the pick-up with the Al plate is shown in Fig. 22. The dent is clearly visible near the centre of the plate. When judging the size of the dent one should bear in mind that the mass of a pellet is around 0.12 mg.

Presently the pellet gun is operated manually; there are several successive steps in the operation of the gun and only a limited reproducibility can be obtained. An automatic unit for operating the gun is under construction. When this unit is ready a more thorough test will be made with respect to velocities attainable, velocity scatter, reproducibility of performance, repetition rate etc.

2.12 Injection speed requirements for pellet refuelling

(C.T. Chang)

A theoretical study of the required injection speed of a pellet to penetrate a given fraction of the minor radius of a toroidal device with assumed radial temperature and density profiles was made. It was found that in order to penetrate to a depth of 2/3 of the minor radius of a 5 GW (thermal) reactor, a speed of $\sim 10^4$ m/s is required to inject a pellet of 5 mm radius if the shielding mechanism of ablation is caused mainly by the presence of a neutral gas blanket (Parks et al. 1977).

2.13 Dante (Danish Tokamak Experiment)

(V. Andersen, P.B. Jensen, and P. Nielsen)

The experiment was shut down since midsummer in order to install a flywheel generator. In this period we made several practical changes in the Tokamak and completed the toroidal field coils. Operations should resume by the end of the year at a toroidal field strength of $\sim$ 0.8 T as originally planned.

In May the electrolytic capacitor bank was installed providing pulse durations in excess of 10 ms. At these longer pulse times the degree of control of plasma positioning increased in importance. Plasma positioning was maintained for $\sim$ 10 ms by programming the vertical field. Beyond this period programming failed; and consequently we are planning a vertical feedback system. Such a system is necessary in any case if we want to make an elongated plasma.

Part of the purpose of the experiment is to move the plasma vertically relative to a pellet. With the 5 ms duration plasma we have attempted to induce a vertical motion. A radial field

pulse of 0.2 ms duration was applied. Plasma shifts of approximately 10 cm were observed at a maximum velocity of 500 m/s. With the plasma parameters expected in Dante this should be a sufficient velocity for pellet penetration. By applying stronger radial fields, higher velocities would be obtained. No attempt was made to investigate the limit.

2.14 References to section 2

BRONSHTEIN, I.M. and DOLININ, V.A. (1968). Sov. Phys. Solid State 9, 2133-2140.

DUPREE, T.H. (1978). Bull. Am. Phys. Soc. 23, 869.

DYSTHE, K.B. and PÉCSELI, H.L. (1977). Plasma Phys. 19, 931-943.

DYSTHE, K.B. and PÉCSELI, H.L. (1978). Plasma Phys. 20, 971-989.

FRANKLIN, R.N., MACKINLAY, R.R., EDGLEY, P.D., and WALL, D.N. (1978). Proc. R. Soc. London A360, 229-242.

FUCHS, G. and NICOLAI, A. (1978). Internal Report, KFA-IPP-IB-2/78.

HOLMÉN, G. SVENSSON, B., and BURÉN, A. (1979). Proceedings of the 7th International Conference on Atomic Collisions in Solids held in Moscow, September 19-23, 1977 (to be published).

IKEZI, H., BARRETT, P.J., WHITE, R.B., and WONG, A.Y. (1971). Phys. Fluids 14, 1997-2005.

KARPMAN, V.I. (1979). Phys. Scr. (in press).

MIKKELSEN, T. and PÉCSELI, H.L. (1978). Phys. Rev. Lett. 41, 951-954.

NORDSKOV, A., SCHOU, J., SKOVGÅRD, H., and SØRENSEN, H. (1977). Risø Report No. 374, 57-58.

OTT, E. and SUDAN, R.N. (1969). Phys. Fluids 12, 2388-2394.

PARKS, P.B., TUNNBULL, R.J., and FOSTER, C.A. (1977). Nucl. Fusion 17, 539-556.

PETERSON, L.R. and GREEN, A.E.S. (1968). J. Physics B: Atomic Mol. Phys. 1, 1131-1140.

RASMUSSEN, J. JUUL (1978). Plasma Phys. 20, 997-1010.

SATO, N., POPA, G., MÄRK, E., SCHRITTWIESER, R., and MRAVLAG, E. (1976). Phys. Rev. Lett. 37, 1684-1687.

SIGMUND, P. (1969). Phys. Rev. 184, 383-416.

SIGMUND, P. (1972). Rev. Roum. Phys. 17, 1079-1106.

SØRENSEN, H. (1977). J. Appl. Phys. 48, 2244-2251.

SØRENSEN, H. and SCHOU, J. (1977). Risø Report No. 374, 52-55.

SØRENSEN, H. and SCHOU, J. (1978a). J. Nucl. Mater. 76&77, 634-635.

SØRENSEN, H. and SCHOU, J. (1978b). J. Appl. Phys. 49, 5311.

TCHEN, C.M., PÉCSELI, H.L., and LARSEN, S.E. (1977). Risø Report No. 365, 26 pp.

TURIKOV, V.A. (1978). Risø Report No. 380, 28 pp.

VAN HOVEN, G. and JAHNS, G. (1975). Phys. Fluids 18, 80-88.

3. METEOROLOGY

The meteorology section is primarily engaged in studies of the planetary boundary layer. The theoretical and experimental work can be roughly classified as follows: micrometeorological research (3.1-3.6), climatological investigations (3.7-3.8), development of meteorological instruments (3.9-3.13), and applied meteorology (3.14-3.18).

At Risø a 120 m tower is available for experimental work. Meteorological variables such as wind speed and direction, temperature and humidity are measured routinely at a number of heights. As a result of the measurements, data records containing 20 years of hourly readings are now available. These records are used extensively both by the section and by other groups.

For field experiments, there is a 50 m mobile tower, a data acquisition system installed in a van, and a telemetry system. The digital data system is capable of sampling 60 signals simultaneously at a rate of 200 per second, and the telemetry system can transmit 32 channels over essentially line-of-sight distances up to more than 50 km at a rate of 25 000 8-bit numbers per second.

Micrometeorological research aims at describing the structure of atmospheric turbulence and its dependence on external parameters, such as surface characteristics and the synoptic weather situation. An important goal is parameterization of the transport properties of atmospheric turbulence, so that the planetary boundary layer can be realistically incorporated in numerical weather prediction schemes.

The earlier investigations concerning the influence of an abrupt change in surface roughness on the flow immediately above the surface were continued at a site which exhibited a change in surface level as well as in water-land roughness. A major experiment was carried out during the summer involving more than 30 persons.

Spectral coherence is an important statistical measure with both applied and theoretical implications. Efforts were directed towards theoretical and experimental investigations of the

spectral coherence between signals from horizontally displaced anemometers. Work on numerical and physical improvements of boundary-layer models was continued. A two-dimensional numerical model of the planetary boundary layer was developed based on the anelastic system of equations and with the parameterization of the turbulent fluxes taken from a previously developed model. The model was used to simulate the dynamics of a sea breeze.

Efforts in the field of air-sea-interaction were concentrated primarily on the analysis of the data obtained during the Joint North Sea Wave Project (JONSWAP 1975) and the Joint Air-Sea Interaction experiment (JASIN -78). Climatological investigations mainly concern the analysis of data collected at Risø and other locations in Denmark.

Work was continued on the development and testing of meteorological instruments and equipment. A method was developed for correcting the output from a cup anemometer for the nonlinearity of the response in order to evaluate the total variance of the signal. Furthermore the angular response of a cup anemometer was investigated and a simple linear method of in-situ calibration of hotwires, utilizing the signal from a nearby cup anemometer, was proved useful. The design and development of a sturdy three-dimensional propeller anemometer continued. An instrument able to measure air temperature fluctuations up to 1 Hz was developed and brought into operation.

The section operates two acoustic sounders or sodars (Sound Detection and Ranging), one in a monostatic mode with Doppler-measurement of the vertical velocities, and the other in a bistatic mode. It has been attempted to run the systems continously, but at the moment this has proved unsuccessful due to frequent malfunctions of the systems. Theoretical work on acoustic sounding has lead to an expression for the time derivative of the received scattered power for short sound pulses valid for monostatic as well as bistatic configurations.

Tasks of an applied nature are taking up a large share of the section's time, because of an increase in contractual work. These tasks include: site evaluation for nuclear power stations, dispersion modelling, air pollution studies, evaluation of

dynamic effects of wind on engineering structures, development and testing of meteorological instruments, and evaluation of wind power as an alternative energy source.

The section is a member of the Gedser Test Group which is a sub-contracter to DEFU (Research Association of the Danish Electricity Supply Undertakings). The Gedser Test Group is responsible for carrying out a series of experiments on the Gedser wind turbine in order to establish a set of data for comparative analyses between this turbine and the new US models. The 200 kW Danish Gedser wind turbine is believed to be the only older large wind turbine in operation anywhere in the world.

A wind atlas of Denmark is being prepared in collaboration with the Meteorological Institute. This task was initiated at the request of the Ministry of Commerce and the Utility Companies in connection with the programme for developing large windpower plants.

The structure and statistical properties of the winds over the Great Belt were studied from measurements taken off a 70 m mast situated on a small island, Sprogø, in the middle of the Belt. A comparison with measurements simultaneously taken at the Risø tower was made. Also, climatological and experimental results from other sources were utilized in the study. This work is done under contract with the state agency responsible for the planning and the building of a bridge over the Great Belt.

With the purpose of devising an improved scheme for the forcasting of icing conditions, a model of the heat budget for the road surface was proposed. In the model the following terms are taken into account: the net radiation, the turbulent fluxes of sensible and latent heat, precipitation and phase changes, and the heat flux into the ground. The section headed a work group concerned with the implementation of automated forcasting procedures in the winter maintainence programme of the Danish roads. The work is done under contract with the Danish Administration.

In the field of atmospheric dispersion two projects were carried out. Under a contract with the Danish Defence Research Establishment a computer model for calculation of the dispersion of

effluent close to a point source was developed. The model, which is based on the advection and growth of singular puffs is able to predict time-varying concentration distributions in nonstationary wind fields.

In collaboration with the Air Pollution Laboratory and under a contract with the Danish Ministry of the Environment, atmospheric dispersion experiments for distances of 2-6 km were carried out in the Copenhagen area.

3.1 Flow over nonuniform terrain

(E.L. Petersen)

The micrometeorological models are quite advanced for locations where one-dimensional approximations are valid. However, near abrupt terrain changes one-dimensional models have been shown to be inadequate. Little is known about the development of internal boundary layer characteristics such as fluxes of momentum and heat, the structure of turbulence, relations between mean and turbulent quantities, and interactions between the surface and boundary layers. Because of the two- and, perhaps, three-dimensional nature of such terrain change problems, adequate field measurement programs require a tremendous effort. However, once a complete set of data is obtained, it may provide a test base and guidance for numerical models for years to come.

In early 1974 Risø National Laboratory and Oregon State University began a cooperative micrometeorological field study designed to investigate the effect on the wind field of sudden changes in the surface roughness. The Risø peninsula was chosen as the experimental site because a fetch of more than 3 km existed over Roskilde Fjord to the northwest of a 250×250 m grassed, level field.

Three masts along a straight line perpendicular to the coast were positioned at the coast and 50 and 175 m inland, respectively. Each mast was instrumented with sensitive cup anemometers at 1,2, 3,5,8, and 12 m, a wind vane at 13 m and Pt-resistance thermometers at 0.5 and 12.5 m. Mean wind speeds and the other meteorological varables were recorded at ten minute intervals. Almost continuous observations were made from October 1974 to September

1975 during which 28 situations occurred which were suitable for detailed studies of effects of roughness change (Peterson et al. 1976).

One of the first experimental results provided clear evidence that the sloping of the underlying terrain to 2 m above mean sea level (from the coast to 60 m inland) had a much greater effect on the mean flow than did the roughness change from sea to land. Thus, in November 1975, the experiment was moved to Bognæs at the northwestern side of Roskilde Fjord; a level site above mean sea level without any perceptiple berm at the coast.

Until March 1977 the observational system could be used only to determine the characteristics of the mean flow. The experiment was then expanded to include occasional fast recording of the cup anemometer outputs and of three light wind vanes of Risø design. During selected periode several vertically aligned hot-wires were used for recording the fine-scale structure of the horizontal wind speed.

The measurements were carried out at six heights at the transition point and at six heights at each of two positions downwind. The measurements with the hotwires in the internal boundary layer resulted in spectra of the same shape as is usually obtained over homogeneous terrain. This made it possible to make corrections to get estimates of the total variance and dissipation rates from the frequency-response-limited cup anemometer measurements. The estimated profiles of variance and dissipation rates were consistent with the results of the second-order-closure turbulence models.

In spite of the lack of stress measurements it was possible to get reasonable estimates of the profiles of the dimensionless rates of mechanical production and dissipation of turbulent kinetic energy ϕ_m and ϕ_ε. These were very similar, but showed rather large positive excursions from the upwind values just above the new equilibrium layer. The main difference between the estimates of ϕ_ε and ϕ_m was that the ϕ_m-profiles were less smooth than the ϕ_ε-profiles (Højstrup 1979).

The experience gained from the measurements at the Risø and Bognæs sites clearly indicated the necessity of being able to

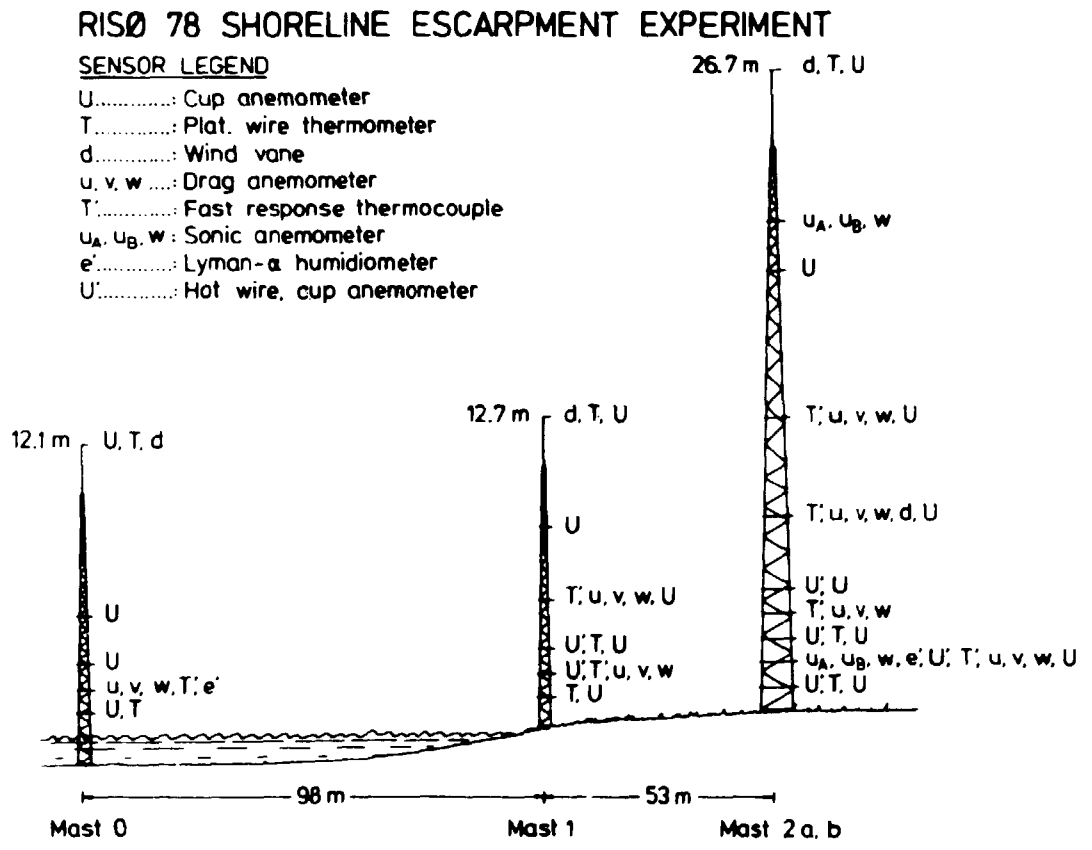

Fig. 27 Sensor array in the Risø 78 experiment. Each letter depicts one parameter measured. The mast 2 a,b is in reality two masts.

distinguish between the influences of a change in terrain height from a change in roughness. In order to pursue this goal a joint experiment, "Risø 78", was planned and executed in cooperation with Pennsylvania State University and Oregon State University.

The equipment used in the two previous studies was re-installed at the original Risø site. The major difference between this and the first experiment was that in the later study a mast was erected in the fiord, 98 m upwind from the coast line. The experimental set-up is depicted in Fig. 27. The core of the instrumentation consisted of nine drag anemometers eith thermocouples for determining the heat flux and the three components of the wind vector, eighteen cup anemometers, six hot-wire anemometers, three sonics, thermometers, wind vanes, and Lyman-α humidiometers. A total of 72 signals were recorded with sampling rates from 10-200 Hz.

An initial analysis of some of the data obtained during the experimental campaigns has shown some interesting features. The flow is retarded when approaching the escarpment so that the velocities measured at the coast are 20-40 cm/s smaller than those measured 98 m from the coastline where the influence of the escarpment must be negligible (Fig. 28). The measurements also show a more rapid growth of the internal boundary layer than could be expected from a simple roughness change.

In addition to the experiment concerning the escarpment and surface roughness change a series of more or less independent experiments were conducted. Horizontally averaged surface layer temperature profiles over the water were measured by means of a passive optical technique. The technique is based on the fact that measurements of the image distortions of a distant object can be used to calculate the temperature profile (Fraser 1977).

The tristatic calibrated Doppler sodar designed at Pennsylvania State University was installed at the site together with the Risø monostatic sodar (Sensitron) and bi-static sodar (Aerovironment). The following four particular measurements were attempted: A) Monitoring of the stability of the planetary boundary layer and tracking of persistent temperature inversion and wind shear layers; B) monitoring of the planetary boundary layer winds at selected levels to about 500 m maximum; C) monitoring (in selected conditions) of the vertical heat flux and turbulent kinetic energy dissipation rates at selected levels to

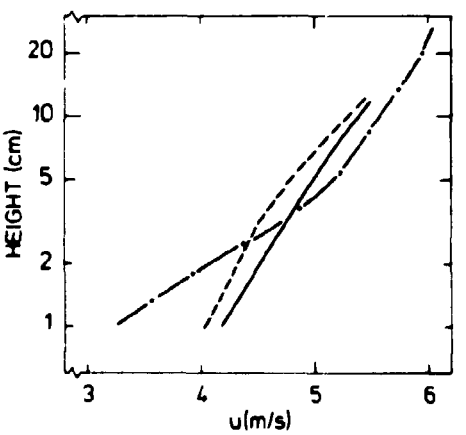

Fig. 28 Mean velocity profiles taken at the three positions shown in Fig. 27. The full line is the upstream profile taken 98 m from the coastline. The dashed line is measured on the coastline and clearly shows the retardation of the flow caused by the escarpment. The dashed-dotted line is the inland profile, indicating a retarded flow in the bottom caused by the roughness change, and accelerated flow higher up caused by the sloping terrain.

about 500 m; D) identification, if possible, of the height and time variations of the internal boundary layer downwind of the terrain transition zone.

A diffusion experiment was performed where a tracer (sulphur-hexafluoride) was released close to the mast in the water and tracer sampling-units were positioned along mast 2 (Fig. 27). This permitted a determination of the vertical shape of the tracer concentration distribution to be made. In order to establish where in the tracer plume the vertical distribution was measured sampling units were also spread out in a lateral array. A preliminary analysis indicates that the shape of the vertical tracer distribution is better described by the non-Gaussian expression $\chi = \chi_o \exp(-z^b/B)$. Here χ is the tracer concentration at height Z, and χ_o, B and b are characteristic constants. For the actual experiments b covers the range 1.2-1.8.

Apart from the Risø personnel, the experimental and planning crew constituted the following members: Dennis W. Thomsen, John M. Norman, Alistair B. Fraser, Kenneth H. Underwood, Steve G. Perry, Kathy Perry, Wilhelm H. Mach, and Robert Peters (Pennsylvania State University); Ernest W. Petersen (Oregon State University); Erik Lyck (Air Pollution Laboratory, National Agency of Environmental Protection, Denmark); Peter A. Taylor (Atmospheric Environment Service, Canada).

3.2 Spectral coherence

(L. Kristensen and J.A. Dutton)

The spectral coherence $coh_{\alpha\beta}(\omega)$ between two real time series $\alpha(t)$ and $\beta(t)$ is defined as

$$coh_{\alpha\beta}(\omega) = |\phi_{\alpha\beta}(\omega)|^2/(\phi_{\alpha\alpha}(\omega)\cdot\phi_{\beta\beta}(\omega)),$$

i.e. as the absolute square of the complex cross spectrum $\phi_{\alpha\beta}(\omega)$ between the two time series, normalized by the power spectra $\phi_{\alpha\alpha}(\omega)$ and $\phi_{\beta\beta}(\omega)$.

The coherence is important in applying knowledge about turbulence to engineering problems that involve wind loads on structures because it provides information on the simultaniety of forcing on diverse parts of the structure.

We have investigated the spectral coherence, when $\alpha(t)$ and $\beta(t)$ are signals from horizontally displaced anemometers. In this case the function $coh_{\alpha\beta}(\omega)$ is convenient in the experimental study of the space-time behaviour of turbulence because no absolute calibration of the anemometers, neither static nor dynamical, is required.

Pielke and Panofsky (1970) and Ropelewski et al. (1973) have discussed the behaviour of the coherence coh(D,n) between the signals from two anemometers with the spatial separation D as a function of the cyclic frequency $n = \omega/(2\pi)$. They argued that

$$coh(D,n) = \exp(-anD/U) \tag{1}$$

where U is the wind speed and a is a dimensionless parameter, which is independent of n, D and U, but dependent on other parameters such as the scale and the strength of the turbulence and the direction of the mean wind velocity with respect to the straight line connecting the anemometers. They found that a is of the order 10.

Recently Kristensen (1979) postulated that spectral coherence for displacements along the mean wind direction does not follow equation (1). Using an analogy between the decay of eddies and radioactive particles where eddies may decay enroute between anemometer 1 upstream and anemometer 2 downstream, and may miss anemometer 2 completely, because of sideways diffusion - and assuming that coh(D,n) is equal to the square of the probablity that an eddy recorded by anemometer 1 is also recorded by anemometer 2, the key parameter was found to be

$$\alpha = (\sigma/U)(D/\ell);$$

σ is the r.m.s. velocity and ℓ the scale of the turbulence. The expression for longitudinal coherence was

$$coh(D,n) = \exp(-2\alpha G(\frac{n\ell}{U}) \times \begin{cases} (1-\exp(-\frac{1}{2\alpha^2(\frac{n\ell}{U})^2}))^2 & \text{for } \alpha \leq 1 \\ (1-\exp(-\frac{1}{2\alpha(\frac{n\ell}{U})^2}))^2 & \text{for } \alpha \geq 1; \end{cases} \tag{2}$$

$G(ni/U)$ is a dimensionless function of the dimensionless frequency ni/U . It is necessary to assume horizontal homogeneity and local isotropy of the turbulence to derive equation 2. Additional length scales will enter the expression if the turbulence does not have these properties.

In the inertial subrange the function $G(ni/U)$ becomes $G(ni/U) = (ni/U)^{2/3}$. A modest measurement program was initiated for providing additional data for engineering applications and testing the validity of the above results.

3.3 Strain-dependent eddy viscosity for spectral modelling of turbulence

(C.M. Tchen (City University of New York, USA), S.E. Larsen, and H.L. Pécseli)

Following a kinetic theory of turbulence by Tchen (1978), an analytical expression for strain-dependent eddy viscosity is derived, and is used as a basis for formulating spectral modelling of turbulence. The application to modelling of turbulence in a neutral surface boundary layer yields a logarithmic wind profile with an estimate of the von Kármán constant. The problem of relating the wavelength, which scales the eddy viscosity, with the spatial length scale associated with the mean wind profile is resolved by Fourier transformation of the equation for the mean wind profile. The approach avoids difficulties in earlier efforts by Roth (1970), and is readily extended to non-neutral flows. It can then be expected that the Monin-Obukhov similarity functions can be analytically determined.

3.4. Numerical modelling of the planetary boundary layer

(I. Troen)

A two-dimensional numerical model of the boundary layer was developed. The model uses the dynamical equations based on the anelastic system (Ogura and Philips 1962) and the parameterization of turbulent fluxes is taken from the model of Busch et al. (1976). The model was used to simulate the dynamics of sea-breezes and Fig. 29 show the results of such a simulation.

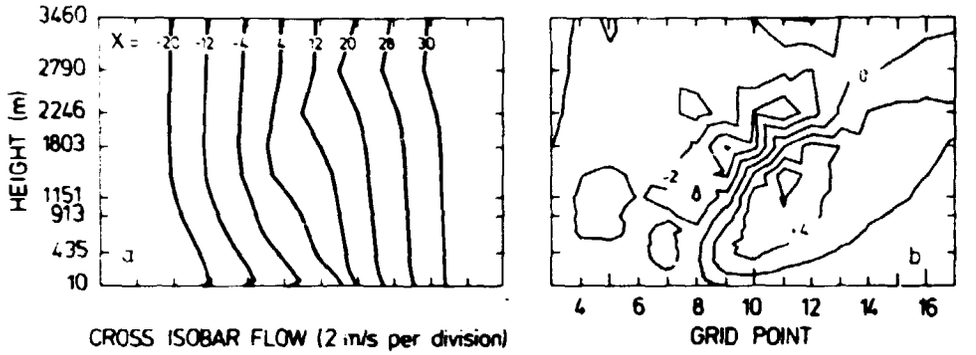

Fig. 29 (a) Vertical profiles of the cross isobar flow after 440 minutes for different distances (x) from the coast line. x is measured as positive inland from the coastline. The intergration is started with zero wind and a stratification corresponding to 1/N = 150 s, where N is the Brunt-Väisälä frequency. The flow is forced by a prescribed surface temperature variation inland taken from Neumann and Mahrer (1971). (b) Vertical velocity field. The coastline is at grid point number 8, the contour interval is 2 cm/s, and the grid distance is 4 km.

The equation for the mixing length in the Busch model has the form:

$$\frac{\partial \lambda}{\partial t} = \frac{\lambda_s - \lambda}{\lambda} \sqrt{u_*^2 + w_*^2}.$$

Where λ_s is a prescribed asymptotic value for λ, u_* is the local friction velocity and w_* is the convective velocity scale.

In the present model this is generalised merely by adding advective terms:

$$\frac{\partial \lambda}{\partial t} = - u\frac{\partial \lambda}{\partial x} - w\frac{\partial \lambda}{\partial z} + \frac{\lambda_z - \lambda}{\lambda} \sqrt{u_*^2 + w_*^2}.$$

The anelastic (non hydrostatic) system of equations allows the dynamic model to be used down to very small horizontal scales, but until now the model was only used with a horizontal grid length of 4 km. The vertical grid distance is 20 m between level 2 and 3 and exponentially increasing to give a model top at 8 km with 22 levels.

The pressure is computed by a method similar to the method used by Neumann and Mahrer (1971) except for the numerical procedure employed in the solution of the resultant Poisson-type differential equation:

$$\left(\frac{\partial^2}{\partial x^2}\pi + \frac{1}{\rho}\frac{\partial}{\partial z}\rho\frac{\partial}{\partial z}\pi\right) = D^* \equiv \frac{\partial}{\partial x}u^* + \frac{1}{\rho}\frac{\partial}{\partial z}\rho w^* \qquad (1)$$

with $\pi \equiv c_p\Theta\,(P/p)^*$. The boundary conditions are $\pi = 0$ at lateral boundaries and $\frac{\partial}{\partial z}\pi = 0$ at top and bottom.

u^*, w^* are the velocities obtained from the prognostic equations where only the hydrostatic part π_h of the total pressure is included:

$$\pi_{tot} = \pi_h + \pi$$

$$\pi_h = -\frac{\rho}{\Theta}\int_{z_T}^{z}\theta' dz.$$

z_T is the heigth of the model top, ρ is density, c_p is the specific heat at constant pressure, P and Θ are constant scales for pressure and potential temperature respectively. The equation for the pertubation pressure (1) is solved by the direct method, i.e. first a sine-transform of equation (1) is performed resulting in $(-k^2 + V)\pi_k = D_k$, where V is the finite-difference operator corresponding to the last term on the left of equation (1). This linear system of equations is then solved and π is obtained from the inverse transform of π_k.

The velocities at the next timestep are then finally obtained from

$$u^{n+1} = u^* - \frac{\partial}{\partial x}\pi \cdot 2\Delta t$$

$$w^{n+1} = w^* - \frac{\partial}{\partial z}\pi \cdot 2\Delta t.$$

3.5 Nocturnal boundary layer

(I. Troen and L. Mahrt (Oregon State University, Oregon, U.S.A.))

The mean structure of the nocturnal planetary boundary layer was studied with data from the Wangara (Clarke et al. 1971), the O'Neill (Lettau and Davidson 1957), the Haswell experiments, and from the Risø-tower.

The main conclusion is that the layer of significant turbulent fluxes extend to just below the level of maximum wind (the

"nocturnal jet") which coincides with the level of maximum gradient Richardson number. However, the inversion layer and the layer of significant cooling is often 25% higher, apparently due to clear air radiative cooling and/or shrinking of the layer of turbulence.

3.6 Air-sea interaction

(S.E. Larsen, O. Mathiassen, and N.E. Busch)

The work on Air-sea interaction was concentrated on analyses of data obtained during the JONSWAP 1975 experiment in the North Sea (Busch and Larsen 1975).

The data available from this experiment consists of turbulence data (three turbulent components of the wind velocity, temperature and humidity) measured by the Risø group and (ten minute average) profiles of velocity, temperature and humidity, measured by a group from the Meteorological Institute, University of Hamburg, F.R.G. The turbulence data were measured by means of wind vane mounted hot-wires and cold wires and a Lyman-α humidiometer.

Early in the analysis it was deduced that the pre-established sensor calibrations were almost useless because of sensor contamination over the ocean (Fig. 30). Therefore, the sensors were

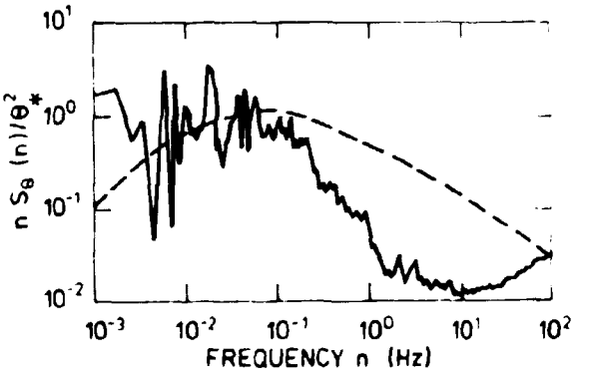

Fig. 30 The influence on cold wires of the contamination over the ocean is illustrated by comparing a measured temperature spectrum $nS_\theta(n)/\theta_*^2$, to the expected form (dashed curve). On installation this particular sensor (type 5μ W) has a cutoff frequency of ∿ 120 Hz. After a week of continuous operation the contamination has reduced the cutoff frequency by about two decades to ∿ 0.1 Hz.

"calibrated" by comparing the time variation of the ten minute averaged turbulence data with the corresponding profile data. This method was found to work for the temperature and humidity sensors but was too coarse for the velocity sensors. To improve on this we used the redundancy in the velocity system; measurements were made both with a single vertical hot wire and with a three dimensional hot-wire configuration. The two independent measures of the horizontal velocity was sufficient to establish a satisfactory calibration of the hot wires (Larsen et al. 1979). The analysis is now concentrated on two problems: Firstly, on comparing the directly measured fluxes with those which can be indirectly obtained from the profiles and secondly, on establishing the behaviour of similarity functions and spectra over water, for a comparison with measurements over land.

3.7. Observational data on surface flux scaling

(K.L. Davidson)

Preliminary and intermediate analyses were made on surface layer data obtained during the JASIN-78 (Joint Air-sea interaction) experiment. The data were obtained by Naval Postgraduate School personnel aboard the R/V Challenger from mid-August to mid-September. The data were from single-level measurements of mean and turbulent wind, temperature and humidity and of aerosol size distributions, 0.1 to 30 pm. These data will be interpreted relative to the surface flux scaling of the marine atmospheric mixed layer and aerosol size distributions. The nature and scope of present scaling procedures were described by Tennekes (1973) and Toba (1965) for the mixed layer and aerosol distributions, respectively.

Objective computational procedures were developed to estimate the surface fluxes from the mean and turbulence data and to estimate specific mixed layer parameters. Surface flux estimates were obtained for two ten day periods in JASIN. Large variations in surface momentum and total heat flux occurred during the periods. These variations will each be combined with mixed layer parameters as the potential temperature increases across the inversion and the lapse rate in the warm air. Objective methods for estimating the latter parameters were applied to radio-sonde data obtained

in conjunction with a Shipboard sodar in the east Pacific. They appear to be well suited when the surface layer is moderately unstable and the inversion base is below 400 m.

3.6 Paleo-climatological models

(S.E. Larsen and E.L. Petersen)

Recently Petersen and Larsen (1978) discussed a statistical climate model based on the auto-correlation of a 700 000 years series of the O^{18}/O^{16} ratio. The conclusion was that within the general framework of Auto Regressive Integrated Moving Average (ARIMA) processes the most satisfactory model is a third order autoregressive process. However, this process had the drawback that it did not explain the semi-periodic character of the series with periodicity around 20 000, 40 000 and 90 000 years.

These periods seem to relate to the insolation variation caused by changes in the earth's orbital elements. Therefore efforts are made to extend the established model to a forced model, with the forcing being a simple function of the insolation. It is tentatively concluded that a simple linear expression of the insolation is insufficient to generate the rather strong 90 000 year period evident in this and other climate series. Hence, various simple non-linear models are currently being studied.

As a spin from the climate studies a composite spectrum of temperature variations was generated. The different parts of the spectrum shown in Fig. 31. are obtained as follows. The turbulent part, 10^{-4}-10^{3} Hz, summarize the knowledge about such spectra in the atmospheric surface boundary layer. These spectra are shown for thermally unstable ($Z/L \simeq -0.5$), neutral ($Z/L \simeq 0$), and stable situations ($Z/L \simeq 0.5$).

The period range from 10 years to 1 hour is covered by the 20 years of temperature measurements at the Risø tower (7 m above terrain). For periods ranging from 1000 to 1 year the spectrum is based on a O^{18}/O^{16} series from Greenland calibrated against several European 100-200 years temperature series.

The low frequency part of the spectrum (periods longer than 1000 years) is based on several series of O^{18}/O^{16}, such as the Camp

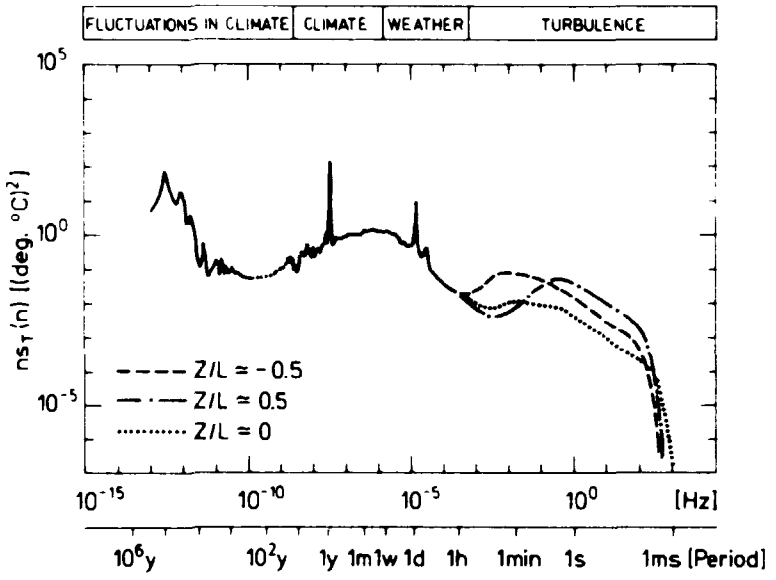

Fig. 31 Composite spectrum of the temperature variation at latitude close to the ground. The spectrum ranges from the turbulent dissipation range at frequencies around 1 kHz to the ice age cycles corresponding to periods of about 100 000 years. The origin of the different parts of the spectrum is described in section 3.8.

Century series (Johnson et al. 1972) and the series used by Petersen and Larsen (1978). The calibration is done by matching the spectra from the low frequency part with the spectra which cover periods up to 1000 years. The three low frequency peaks shown in the spectrum correspond to the 90 000, 40 000, and 20 000 years periodicities described above.

3.9 Cup anemometer dynamics and angular response

(L. Kristensen, J. Højstrup, and N.E. Busch)

Cup anemometers are widely used because they are simple, sturdy and reliable instruments that generally require a minimal maintenance. A further major advantage from an operational point of view is that there is no need for alignment into the wind direction. Therefore, the cup anemometer is ideal for making continuous measurements.

When the instruments are used to measure rapid wind speed changes, such as gusts in airports, knowledge of their dynamic behaviour

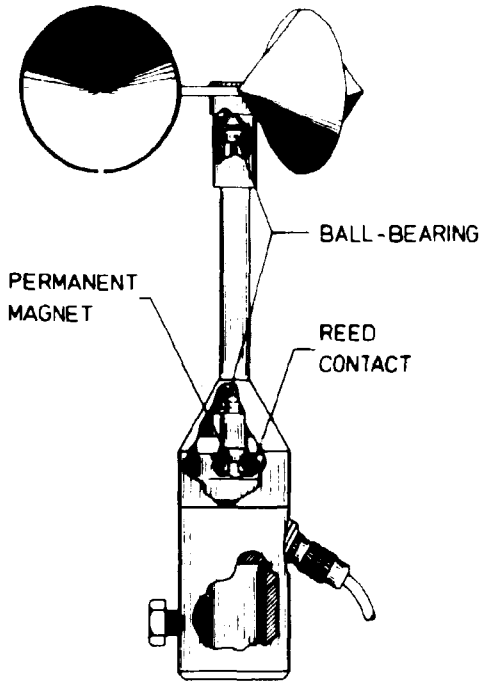

Fig. 32 The Risø cup anemometer in which electric pulses are created by means of a stationary reed contact and a permanent magnet mounted on the rotating shaft. The height of the anemometer measured along the axis is 260 mm. Cup diameter and radius, defined as the distance from the instrument axis to the centre of a cup, are 70 mm and 58 mm, respectively. The cups are made of carbon-reinforced plastic and the weight of the cup wheel, including the arms, is approximately 40 g. The calibration of this instrument is given by $U = U_s + L\Omega$, where $U_s \sim 0.2$ m, $L \sim 0.2$ m, and Ω is the angular velocity in rad/s. The apparent starting speed U_s and L vary for different anemometers of the same type.

is necessary. Simple considerations based on for example a geometrical model by Busch (1965) lead to the conclusion that for not too rapid or large changes of wind speed the cup anemometer reacts as a first-order linear filter with time constant τ_o given by

$$\tau_o = \ell/U_o,$$

where U_o is the mean wind speed and ℓ is the so-called distance constant. It can be shown from most dynamical models that ℓ is independent of wind speed, if the angular velocity of the cup wheel is proportional to U_o for all wind speeds. Because this

is a rather good approximation for most cup anemometers, when U_o is greater than a few meters per second ℓ is the parameter which in most situations contains the necessary information for describing the dynamic behaviour.

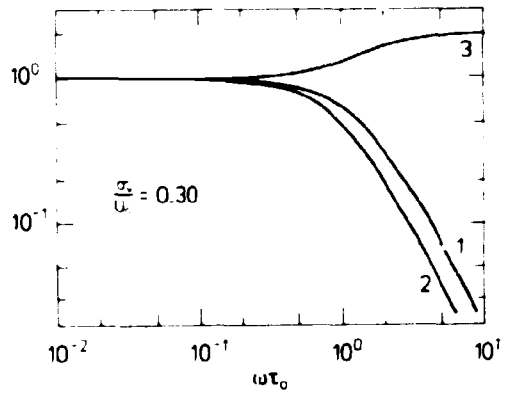

Fig. 33 Theoretical response of a cup anemometer. (2) is the first order approximation to the power transfer function. (1) is the pseudo-transfer function obtained as the ratio between the measured spectrum (including distortion) and the true spectrum. (3) is the ratio between curves (1) and (2). $\tau_o = \ell/U_o$, The turbulence intensity is 30%.

The dynamical response of the Risø cup anemometer shown in Fig. 32 was investigated. The distance constant turned out to be about 2 m, but a careful analysis of the dynamical model's response to rapid fluctuations shows that the non-linearity of the instrument is important in analysing the effect of fluctuations of frequency higher than $\omega_o = U_o/\ell$. This result in a slight overestimation of the mean velocity, but more important is the distortion's effect in making it practically impossible to correct the measured fluctuations for instrumental response. The assumptions involved in the calculations of the response curves shown in Fig. 33 are: (1) the horizontal velocity component is Gaussian and (2) the height of measurement Z > 1 m. Both assumptions are very well satisfied in most measuring situations.

A method for correcting the cup anemometer signal to yield the total variance was developed. The frequency range is divisible into three parts (Fig. 34): (1) a low frequency part needing no corrections, (2) a medium frequency part in which it is possible to restore the spectrum by application of the inverse transfer-function, and (3) a high frequency part in which the noise and distortion contents are severely limiting its usefulness.

The corrections to the power spectra were obtained by first applying a fast Fourier transform to the cup anemometer time

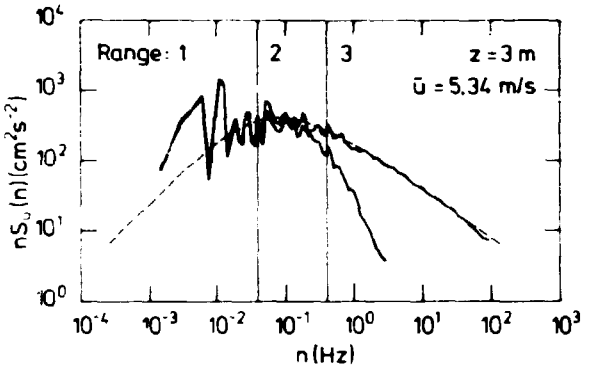

Fig. 14 Measured power spectra of hot wire and cup anemometer signals. The smooth dashed curve is the "universal" shape of the velocity spectrum. In range (1) the cup anemometer responds ideally to fluctuations. In range (2) it is possible to correct the cup anemometer spectrum by use of the first order transfer function. In range (3) correction is not possible because of the noise and distortion content.

series. The corrections then proceeded in four steps:

A) Frequency ranges (1) and (3) were deleted from the spectrum.

B) Frequency range (2) was corrected with the proper first-order transfer function.

C) A spectrum of the proper "universal" shape was fitted to the corrected spectrum in range (2). The fit was performed so that the total variances in frequency range (2) were the same for the fitted spectrum as for the measured corrected spectrum.

D) The total variance was integrated. In range (1) the measured variance was used. In range (2) the measured corrected spectrum was used, and in range (3) the fitted spectrum was used.

The resulting variances were compared with those measured by nearby hot wires, and the resulting mean and standard deviation of the relative difference between the two variances were 0.007 and 0.04 respectively for the 28 cases investigated.

In light winds and on moving platforms, such as buoys, the direction of the wind $\vec{U}$ may deviate and vary significantly from the

normal $\vec{n}$ to the anemometer axis. In such situations it is useful to know the so-called angular response of the anemometer. Let the angle between $\vec{U}$ and $\vec{n}$ be ϕ, and the angular velocity of the cup wheel in this situation be $\Omega(U,\phi)$. Then the angular response $A(U,\phi)$ is defined by

$$A(U,\phi) = \frac{\Omega(U,\phi)}{\Omega(U,0)}$$

This function was derived by Busch et al. (1979) from the anemometer equation of motion given by Wyngaard et al. (1974). The ideal angular response is of course the cosine response, i.e. $A(U,\phi) = \cos\phi$. In this case the anemometer measures only the wind component perpendicular to the anemometer axis, and the interpretation of the measurement is relatively simple.

The angular response is in general dependent on U. Even when this is not the case the angular dependence is seldom ideal except for $|\phi|$ less than $\sim 10^{\circ}$.

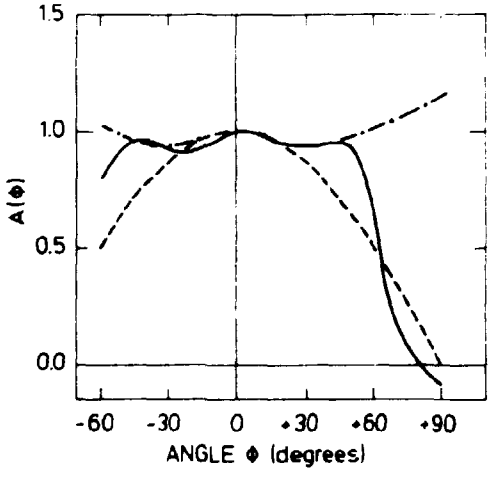

Fig. 35 Angular response of the Risø cup anemometer (full curve). Positive angles ϕ mean that the wind attacks from above (negative W). The dot-dashed curve is the calculated angular response and the dashed curve shows $\cos\phi$. Note that the anemometer rotates backwards for $\phi = 90^{\circ}$.

In order to determine $A(U,\phi)$ for the Risø cup anemometer a series of wind-tunnel experiments were performed. It was found that $A(U,\phi)$ for $|\phi| < 45^{\circ}$ is independent of U within 0.001 for 7 m/s $\leq U \leq$ 18 m/s. The angular response $A(\phi) = A(U,\phi)$ of the Risø cup anemometer is shown in Fig. 35. It appears that $A(\phi)$ agrees with the theoretical calculations based on the theory by Wyngaard et al. (1974) for positive $\phi < 45^{\circ}$. For negative values of ϕ, $A(\phi)$

falls below cosϕ down to approximately -25°, where $A(\phi)$ crosses cosϕ. This asymmetric behaviour is due to the lack of symmetry with respect to the plane normal to the axis of rotation of the cup wheel.

3.10 In-situ calibration of hot wires

(J. Højstrup)

Hot wires are fragile instruments. They are susceptible to contamination that can cause the calibration to drift and they have a non-linear voltage-velocity relationship. In order to avoid both the cumbersome laboratory calibration of each single hot wire and the problems caused by calibration drift, a method was developed by which a nearby cup anemometer was used for calibrating the hot wires continuously in-situ. The cup anemometers had earlier been wind-tunnel calibrated and their high calibration stability and simplicity in maintenance and operation made them ideally suited to this purpose.

At low frequencies ($n \ll \bar{u}/(2\pi\ell)$, where the cup anemometer distance constant $\ell \sim 2$ m) the cup anemometers are capable of responding ideally to wind fluctuations, i.e. the static calibration is valid for slow fluctuations, see Fig. 34. Thus the in-situ calibration essentially consisted in matching the averages and variances obtained by low-pass filtering (block-averaging) of both the cup anemometer and the hot-wire signals (Fig. 36). The linear calibration formula used was,

$$u_{Hw} = (v_{Hw} - \bar{v}_{Hw})\frac{\sigma_{cup,T}}{\sigma_{Hw,T}} + \bar{u}_{cup}, \qquad (1)$$

where $\sigma_{cup,T}$ is the standard deviation of the cup anemometer velocity after block averaging over time T, $\sigma_{Hw,T}$ the standard deviation of the raw hot-wire signal after block averaging over time T, $\bar{u}_{cup}$ the cup anemometer velocity averaged over one run, v_{Hw} the raw hot-wire signal, $\bar{v}_{Hw}$ the hot-wire signal averaged over one run, and u_{Hw} the calibrated hot-wire velocity.

The hot-wires were used without linearizers, so the correct calibration should be nonlinear ($u_{Hw} \simeq (aV_{Hw}^2 - b)^{2.3}$), instead of the simple form of equation (1), therefore a number of checks were made to validate the linear approximation. A special

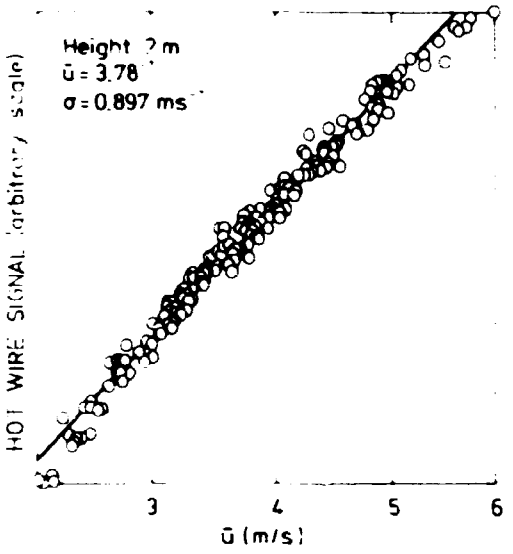

Fig. 36 Cup anemometer readings block-avaraged over 4 s plotted versus the correspondingly averaged values of the hot wire readings. The full line is the calibration line according to equation (1).

experiment was set up in which the hot-wires were equipped with analog linearizers, and the power spectra from the linearized signals were compared with the power spectra obtained from signals from the same sensors taken before the linearization. The conclusion of this experiment was that the simple linear method of calibration did not affect the power-spectra of the signal. Higher order moments of even order are only slightly influenced by the non-linearity but those of odd order are not measured correctly.

3.11 Temperature fluctuation sensor

(S.E. Gryning and D.W. Thomson (Pennsylvania State University, U.S.A.))

An instrument was developed to measure air temperature fluctuations. The air temperature fluctuations are band-pass filtered with an upper frequency limit of about 1 Hz and a lower frequency limit of about $2.2\ 10^{-4}$ Hz.

The measurements of the temperature fluctuations are obtained with a pair of copper-constantan thermocouples. One junction point is in direct contact with the air, extending 5 mm into the air stream, the other is placed in the centre of a 10 cm diameter acrylic sphere (Fig. 37). The measured temperature

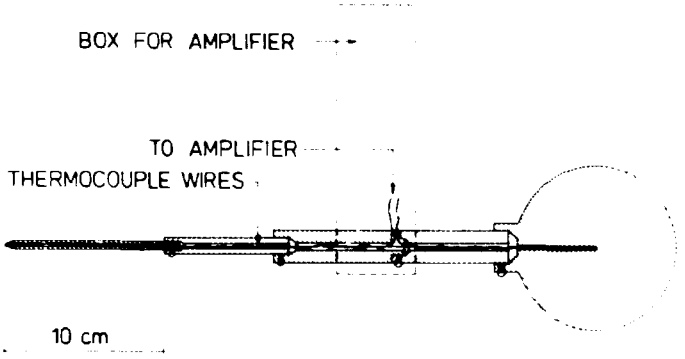

Fig. 37 Schematic drawing of the temperature fluctuation sensor. The bore in the sphere is filled with silicone oil to assure thermal contact between the thermocouple junction point in the centre and the sphere. The dashed lines indicate the box for the amplifier. The outer acrylic surface is covered with adhesive Sn-foil.

fluctuations of the wind are the temperature differences between the junction point in the centre of the sphere and the other in direct contact with the air. The copper wires in the thermocouple pair are connected to a DC-amplifier that amplifies the temperature induced voltage difference 5000 times before the electric signals are transmitted to the recording instruments.

The ability of the centre of the acrylic sphere to serve as a valid temperature reference was verified by evaluating the thermal time constant for the sphere. The time constant is equal to the time for the centre of the sphere to reach 63% of a given temperature step in the surrounding medium. The results of these calculations were tested by submerging a uniformly tempered acrylic-sphere in a well-stirred ice bath and observing the evolution of the excess temperature at the centre of the sphere in relation to the icebath temperature. The thermal time constant of the 10 cm diameter acrylic sphere turned out to be 70 minutes.

The acrylic sphere, which is only partially transparent for solar light, is completely covered with adhesive Sn-foil to minimize direct radiative heating of the interior of the sphere and the junction point in the centre. The temperature of the junction point in direct contact with the air follows the fluctuations in the passing air, with a time constant about 1 s.

In addition it is heated by solar radiation. The radiation error was determined in the laboratory by heating the instrument with light from a photolamp. At a radiation strength of 400 W/m^2, and a wind velocity of 3.5 m/s the error due to radiation was found to be $0.15^{o}C$.

3.12 Design and development of a sturdy propeller anemometer

(O. Christensen)

In the beginning of the sixties the well known and widely used Gill propeller anemometer (Gill 1975) was developed. This anemometer is a very sensitive anemometer, which can be used on a routine basis for air pollution studies in remote areas. The anemometer consists of a two- or four-bladed helicoidal propeller of nine inches diameter. The material is of foamed polystyrene giving the propeller a total weight of about 10 g. The helicoidal has a pitch yielding approximately one revolution per 20 cm of passing air. The distance constant is about 0.9 m for axial flow. The propeller was in the early design driving a miniature d.c. tachometer generator with a very low moment of inertia. The microbearings supporting the propeller shaft opposes the shaft rotation with so little friction that the threshold sensitivity of the propeller is only 0.1-0.2 m/s. The Gill propeller anemometer has actually only one disadvantage: it cannot be employed in routine climatological studies because of its rather delicate construction. Thus, measurements are limited to a maximum of 25 m/s.

We have used Gill propellers for some years. A special three-propeller anemometer designed by us has shown to be very promising for three-dimensional turbulence measurements; however, the weakness of the propellers limit the applicability of the sensor. Hence a year ago we decided to design a new propeller anemmometer with the following features:

A) Material strength to withstand windspeeds up to 60 m/s.
B) A distance constant less than or equal to the distance constant of Gill propeller.
C) A sensitivity threshold no larger than 1 m/s.

D) An internal microprocessor (or other means of on-line computation) to evaluate the three-dimensional wind vector in a cartesian coordinate system up to frequencies limited only by the distance constant of the propellers.

The design and development have followed two lines. One line is concerned with propeller geometry, the choice of materiel, and the manufacturing and testing of prototypes. The other explores the questions connected with detection and recording of the instantaneous propeller revolution speed and the on-line computations involved when instantaneous revolution speeds of three propellers are to be converted into three-dimensional wind vector components.

Figure 38 shows a prototype propeller fulfilling the above mentioned criteria. It is a four-bladed 10 cm diameter helicoid propeller composed of a composite plastic material. The theor-

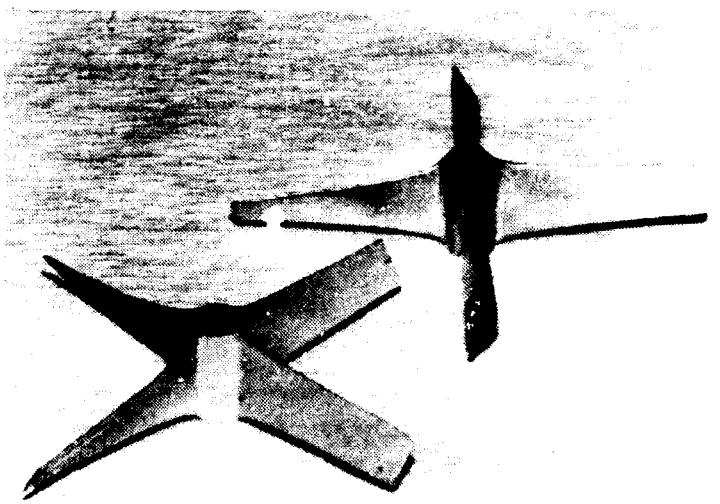

Fig. 38 Helicoid propeller. The theoretical pitch factor γ_t = 1.48, and the measured pitch factor γ_r = 1.50.

etical pitch distance $L_p = 2\pi R\gamma_t$ is equal to 46.3 cm, i.e. the propeller should theoretically make one revolution when it passes through 46.3 cm of air. The blade chord is shaped according to $a/a_R = (r/R)^{0.301}$ yielding a tipchord, which is one half the chord at the rod. The width of the rod chord is 1.0 cm. The relative blade thickness is also determined by the above formula.

The inference is that the blades are sectional airfoils with a thickness to chord ratio of 10% at all sections. The blade cross section is a plate with rounded leading and trailing edges. We have also tested a cross section following the NACA 0012 airfoil profile. However, the performance did not justify the difficulties involved in manufacturing this complicated propeller shape.

Preliminary tests in the closed circuit wind tunnel at the Danish Ship Research Laboratory indicate that the design criteria are fulfilled. The propeller sustained axial as well as non-axial wind speeds larger than 70 m/s. The distance constant was measured to be 0.4-0.5 m, well below the distance constant of the Gill propeller. The threshold speed was expected to be rather high but was found to be only 0.8 m/s. Once the propeller began to rotate, it continued until the wind speed was below 0.3 m/s. The angular response is not yet measured, but a peculiar behaviour was noticed at an angle of attack of $\sim 90^{\circ}$, probably because of a hysteresis phenomenon. More tests are needed before the final decision on the propeller shape can be made. Furthermore, we have noticed the plastic constructional material to be thermally unstable.

3.13 Acoustic sounding

(L. Kristensen)

Acoustic sounding in the atmosphere by means of sodars (Sound Detection And Ranging) has proved to be a valuable tool in the detection of the depth of ground based invensions; thermals; gravity waves; in the estimate of the depth of the mixed layer; and also in the remote determination of wind speed by means of measurements of the Doppler shift of the returned signals.

The scattering agents are turbulent "inhomogeneities" of the velocity- and temperature-fields. The theoretical basis for the interpretations of the strength of the returned, scattered sound pulse is presented and discussed in detail by Tartarskii (1971). He shows that once the acoustic antenna geometry and the strength of the velocity- and temperature-turbulence (C_V^2 and C_T^2) are known, the strength of the scattered sound pulses can be predicted. What is more interesting from a meteorological point

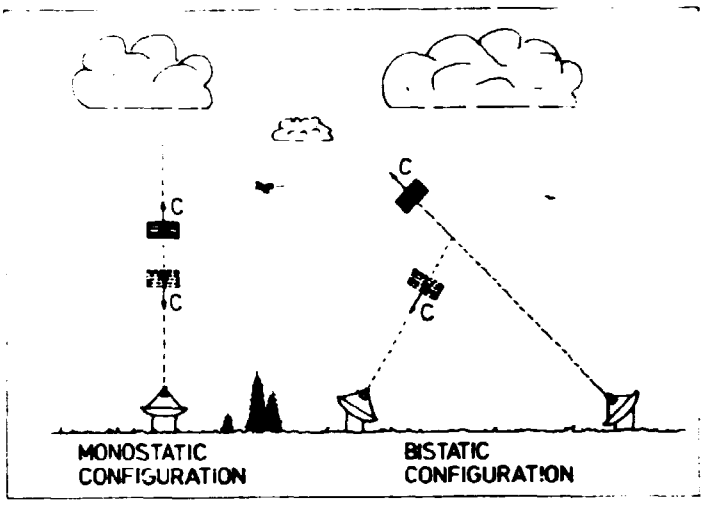

Fig. 39 Geometries of monostatic and bistatic sodars. A monostatic sodar uses the same antenna for transmission and reception. Short transmitted and scattered sound pulses are indicated.

of view is the possibility of deriving turbulent properties from the properties of the scattered sound pulses. (Thomson et al. 1978). In order to do this with high precision a detailed knowledge of the sodar geometry as well as absolute calibration with respect to transmitted and received power is essential.

Figure 39 shows the geometrical configurations of a monostatic and a bistatic sodar. From the expression for the sound scattering cross section it is possible to derive expressions for the time derivative dP/dt of the received scattered power for short sound pulses (Kristensen 1978). In the monostatic case we have

$$\frac{dP}{dt} = 0.051\ P_o\ \frac{A\sigma^2}{c_o t^2} k^{1/3} \exp(-\alpha c_o t) \left(\frac{C_T}{T_o}\right)^2 \qquad (1)$$

Here t is the time elapsed after transmission, P_o the peak power, i.e. the power per steradian transmitted along the antenna axis, σ the width of the antenna beam in radians, A the antenna area, c_o the speed of sound at the temperature T_o, and α the atmosphere's sound attenuation coefficient at wave number k.

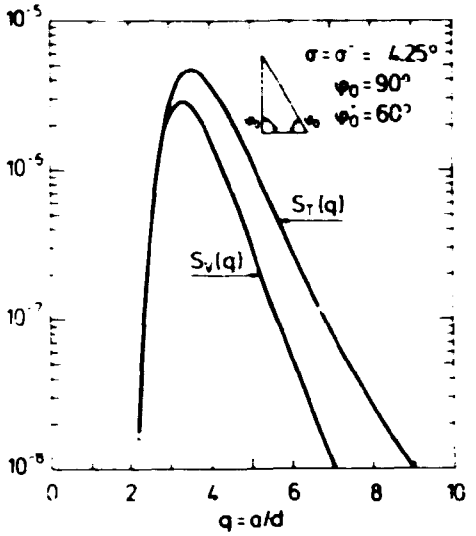

Fig. 40 The two system functions S_T and S_V in a special case. Instead of time t the dimensionless quantity $q = c_o t/(2d)$ is used as abscissa. The parameters σ and σ' are widths of the antenna beams.

For bistatic sodars the expression for dP/dt is more complicated. Here we get

$$\frac{dP}{dt} = P_o \frac{Ac_o}{2d^2} k^{1/3} \exp(-\alpha c_o T) \left\{ \left(\frac{C_T}{T_o}\right)^2 S_T(t) + \left(\frac{C_V}{c_o}\right)^2 S_V(t) \right\} \quad (2)$$

where d is the distance between the transmitter and receiver antennas, and S_T and S_V are the so-called system functions. The only parameters buried in S_T and S_V are those characterizing the geometry of the bistatic setup. The two functions are shown for a particular case in Fig. 40. In order to derive equations 1 and 2 it is necessary to assume that we have a calm isothermal atmosphere with locally homogeneous and isotropic turbulence with a constant coefficient of sound attenation α. Furthermore, we have considered only the farfields from axisymmetric antennes with Gaussian directivities and sound wave numbers k in the inertial subrange of the turbulence.

By range gating the signals from both a monostatic and a bistatic sodar it is possible to determine C_T^2 and C_V^2 at a particular height, because dP/dt in the monostatic case is independent of C_V^2 (equation 1), whereas dP/dt for the bistatic case depends on both C_T^2 and C_V^2 (equation 2). In the inertial subrange these two constants completely determine the structure functions for the fluctuating parts of the temperature and the longitudinal velocity. These constants are useful because they are related

to the rates of dissipation of both kinetic energy and temperature variance, ϵ and N through

$$\frac{C_T^2}{C_V^2} \approx \frac{4}{5}\frac{N}{\epsilon} \text{ and } C_V^2 \approx 2\epsilon^{2/3}$$

(Wyngaard et al. 1971, Tartarskii 1971, and Kristensen, 1978).

3.14 Measurements on the Gedser windmill

(C.J. Christensen, S. Frandsen, and P. Lundsager (Engineering Department, Risø))

An extensive programme aimed at studying the behaviour of the old Gedser windmill was undertaken under contract with (and partly paid by) Research Association of the Danish Electricity Supply Undertakings (DEFU) for the Danish Windpower Programme. Also the Danish Ship Research Laboratory took part in the programme.

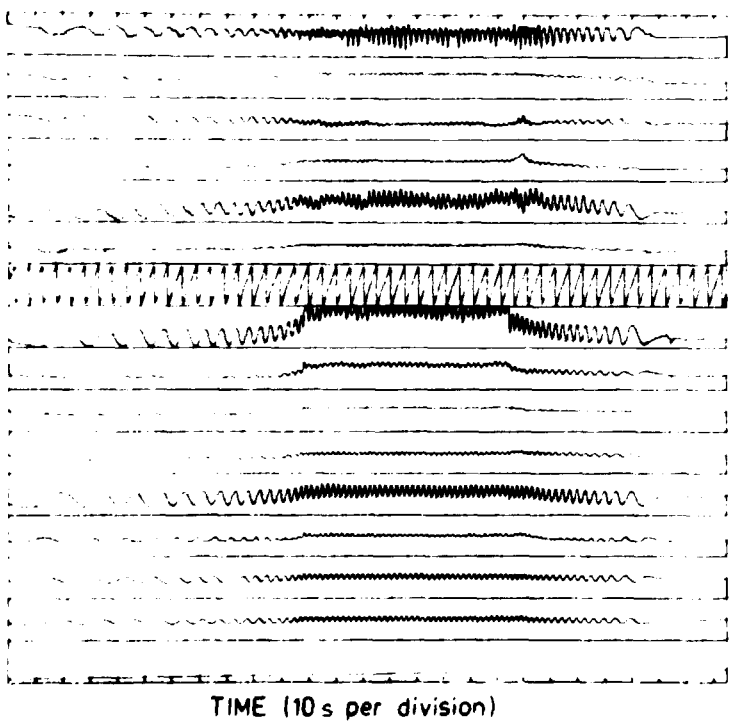

Fig. 41 Example of wing gauge data from the Gedser windmill showing the start-run-stop of the mill. The first six tracks (from the top) show flap wise bending moments and supporting stay forces counter balancing these moments. Track number seven is a time indicator, the next eight are edgewise driving moments and forces. The last track is a timer.

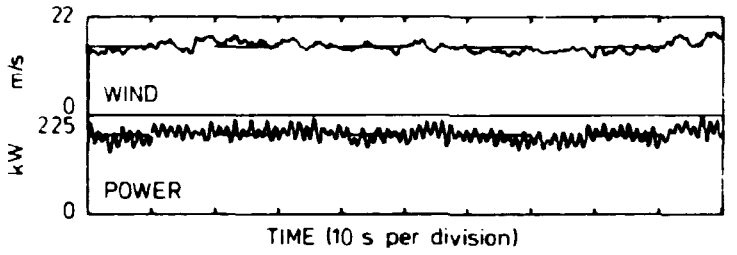

Fig. 42 Simultaneous measurements of wind speed (25 m upwind) and power from the Gedser mill. The 0.8 Hz power fluctuations are clearly seen.

The experimental setup contains some 50 sensors. Among these are strain gauges for measuring moments and forces in rotorblades with supporting stays, in the tower top, and in the generator shaft. Electric power (active and reactive), voltage, rotor and nacelle position are measured. A 40 m meteorological mast carrying five wind vanes and eight cup anemometers 35 m from the mill supplies wind data. The instruments are scanned at 50 Hz and the signals are digitized and stored on magnetic tape using both digital telemetry from the rotor (S-band link) and the data acquistion van during runs of approximately 45 minutes.

The experimental setup was completed and the major errors corrected in the winter of 1977/78. Since then a series of runs were made. An interim status report to DEFU (Christensen et al. 1978) was written.

Only a few preliminary results can be shown at this time. As an example of the data obtained Fig. 41 shows a time series of some rotor strain gauge channels. Fig. 42 illustrates the wind speed and the electric power from a typical run. As is often the case with wind-mills using induction generators, heavy power fluctuations ($\pm$ 20 kW at 200 kW) mar the power quality. Fig. 43 displays the variance- (power-) spectrum for the electric power time series of Fig. 42. The many sharp peaks in this spectrum are not yet fully understood. The simplest possible model of the power train (rotor, transmission, and generator which delivers power proportional to the slip) produces broad peaks, not the sharp ones that are seen. The 0.5 Hz peak is synchronous with the rotor rotation and is understood to be evidence of an imbalance in the

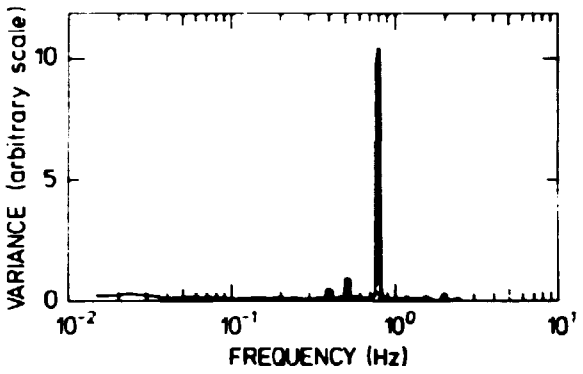

Fig. 43 Variance spectrum of the electric power from the Gedser mill.

rotor. The prominent 0.8 Hz peak is not understood. Many of the peaks are caused by nonlinear effects (mostly in the generator). Only few of the peaks contain significant variance.

Finally, in Fig. 44 wind speed is plotted versus electric power. The points represent ten minute averages. They are obtained from the part of the experiment that supplies long-term climatological data. The correlation is remarkably smooth and well defined as

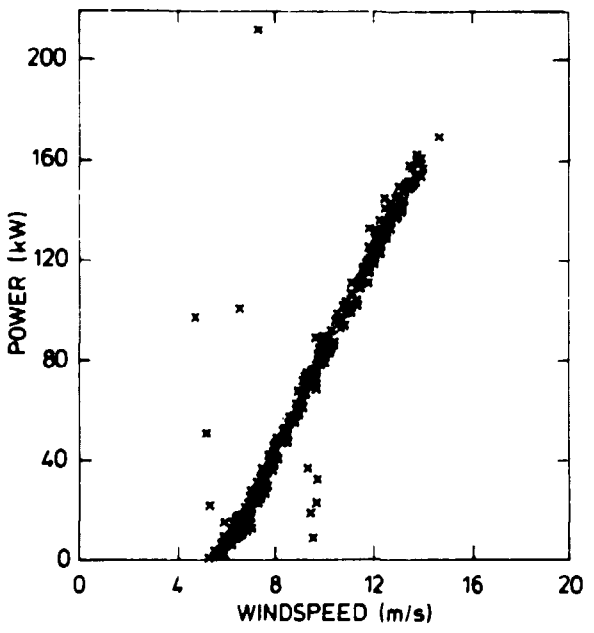

Fig. 44 Wind speed and power correlation. Measured as ten minute averages. The scattered point presumably arise from erroneous mearurements.

would be expected from 10 minute averages. The near linearity of the correlation is surprising. Unfortunately we have not yet observed the expected power saturation in stronger winds.

3.15 Wind atlas

(I. Troen, E.L. Petersen, O. Christensen, and K. Hedegaard (Danish Metereological Institute))

In order to estimate the power output from proposed wind energy generators to be placed at different locations it is necessary to know the probability distribution of wind velocities at a given site. Work to supply this kind of information was initiated as a joint project between Risø and the Danish Meteorological Institute sponsored be the Research Association of the Danish Electricity Supply Undertakings.

The plan is to use surface pressure observations from synoptic stations in Denmark and neighbouring countries to generate a time series ($\sim$ 15 years) of the surface geostrophic wind. Based on Rossby-number similarity it is then possible to obtain the actual wind velocity as a function of the surface roughness and the static stability. If one assumes that the baroclinity and the stability are unifrom over the geographically very limited Denmark, one can then establish the probability distribution by using the climatological record from the Risø tower.

3.16 Dynamic windloading

(S. Frandsen, O. Christensen, and M. Nansen-Nielsen (Vølund A/S))

The experimental part of a project concerning cross-wind excitation of steel chimneys was concluded in May 1977. The project is a joint venture between Risø, The Technical University of Denmark, and the Danish firm Vølund A/S, manufacturers of steel chimneys. The Danish Council of Technology granted financial support.

When a reasonably axisymmetric cylinder is exposed to a flow field, flow separation will take place just on the down stream side of the body. When the Reynolds number, defined with respect to the diameter of the body, exceeds a certain small value, per-

iodic vortex shedding will take place. This results in an alternating force on the body perpendicular to the mean flow direction. When the frequency of the vortex shedding, which is proportional to flow speed, coincides with an eigenfrequency of the cylinder, resonance occurs. Very often the cross flow forces are a prime-factor in the design of steel chimneys. The present Danish wind code (Dansk Standard DS 410.2 1977) as well as other national wind codes assume that the oscillating force can be replaced by an equivalent static force of magnitude

$$q = (\frac{\pi}{\delta})\ q_o\ D\ C_L,$$

where q_o is the dynamic wind pressure, D the diameter of the structure, C_L the lift coefficient and δ the logarithmic decrement. This design method indicates that the phenomena is interpreted as a deterministic problem. C_L may possibly be a function of various parameters such as the roughness length of the terrain and turbulence intensity.

The aim of the preliminary data processing was to get estimates of δ and C_L. These calculations demonstrated (Christensen and Frandsen 1977) that at least two severe problems had to be treated in more detail:

A) A re-interpretation of the results from the damping experiments (where the chimneys were manually set into motion and the decay of the oscillations recorded) had to be made. The preliminary analysis showed that the characteristics of some of the chimneys were highly anisotropic both with respect to damping and to the eigenfrequency which was dependent on direction. At least one chimney showed an irreducible coupling between the orthogonal directions. A typical example of this is shown in Fig. 45, which illustrates the planar motion of the top of a chimney during a damping experiment. These features were unexpected because of the axial symmetry of the load-bearing mantles.

B) The finite distance from the chimney to the tower, instrumented for sampling of meteorological data had to be accounted for. This distance, which varied from 75 to 200 m, makes it impossible to compare an instantaneous correlation between the wind field and the chimney deflections.

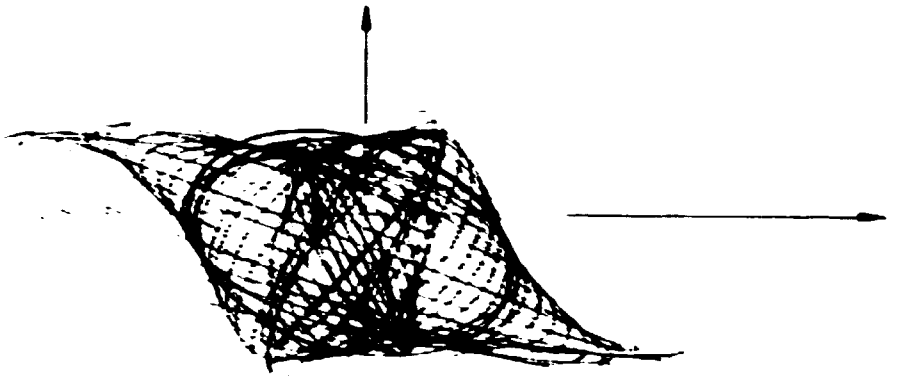

Fig. 45 Planar motion of chimney top at Brovst. The orthogonal directions are strongly coupled, as may be seen by the change of direction of the motion as the chimney oscillation decay.

In a second analysis these two subjects were examined in detail. The principal directions were found by rotating the coordinate system in which the motion of the chimney is described until the damping was at its maximum and minimum respectively along the perpendicular axes. The corresponding eigen frequencies were also determined. Once the principal directions were found, C_L was estimated by decomposing the deflections along the axes, calculating a wind speed at the chimney top (120 s average, extrapolated from the wind profile) and by assuming that the alternating vortex shedding force decomposes along the same principal exes. Fig. 46 shows an example of the data used for the determination of the lift coefficient.

The second analysis confirmed with a higher degree of significance, the results obtained by the preliminary calculations: the magnitude of the structural damping is in some cases only half of what the wind code prescribes as the lowest value that can be used for steel chimneys. Furthermore, the lift coefficient was found never to exceed half the value given in the wind code. In addition it was found that the damping for one chimney could vary by a factor of two. The magnitude of the damping depends strongly on the number of smoke pipes, the way these are supported, and perhaps most important of all on the design of the inlet of the smoke pipes into the chimney. It was also found that the equivalent lift forces depend on the amplitude of the oscillations. Hence,

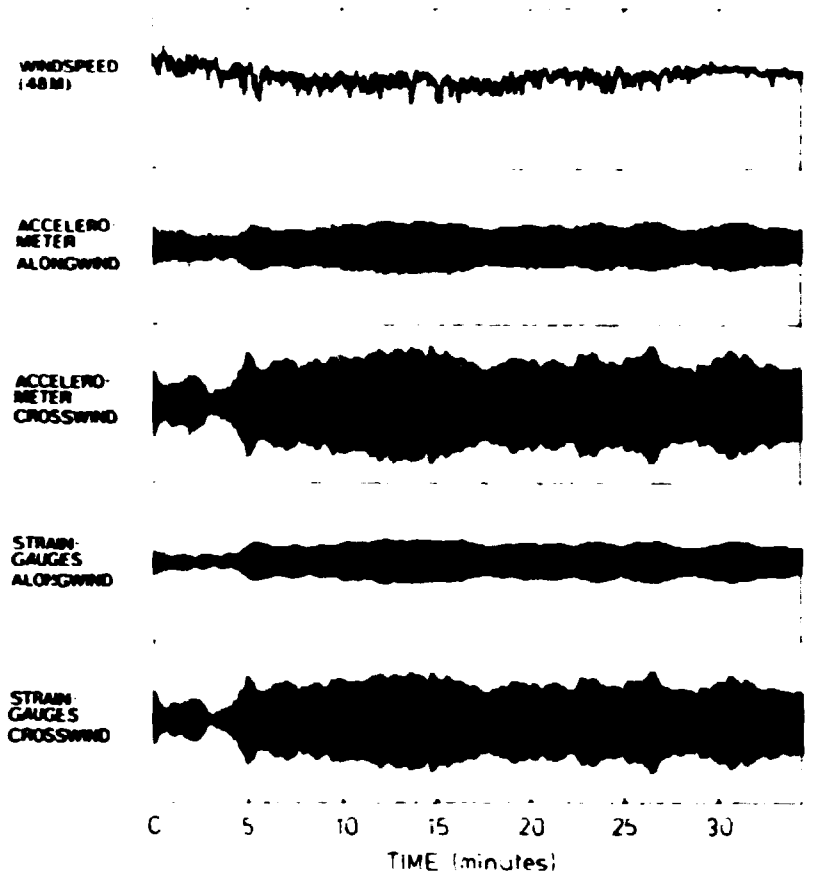

Fig. 46 Time record of strain gauges, accelerometers, and wind speed.

a large amplitude results in a large lift coefficient presumably because of larger coherence of the vortices.

3.17 Determination of atmospheric dispersion in an urban environment by means of tracers

(S.E. Gryning and E. Lyck (National Agency of Environmental Protection; Air Pollution Laboratory))

The ability of the atmosphere to disperse effluents released from a point source is dependent on a variety of local parameters, such as atmospheric stability, topography, surface roughness and release height. The influence can be estimated by carrying out diffusion experiments, and the dependence of the dispersion on local parameters may be established. Atmospheric dispersion

experiments for distances of 2-6 km are being carried out in the Copenhagen area. The purpose is to gain insight in the special features on atmospheric dispersion in an urban area. The tracer is released at a height of 115 m from the TV-tower in Gladsaxe and tracer sampling-units are positioned in 1-3 crosswind series downwind from the tower. The experiments are performed with up to 40 radio-controlled tracer sampling-units and 22 units with a more primitive controlling system. During the experiments tracer sampling units are mounted in lamppost standards at positions marked out in advance. The TV-tower is equipped with standard meteorological instruments, run by the Danish Meteorological Institute, to establish vertical profiles of wind direction, wind speed, and wind temperature. In addition, three-dimensional measurements of the fluctuating wind components are made during the experiments at the release height in the TV-tower.

Three of the experiments were partly analyzed. Fair agreement was found between the measured values of the lateral plume width and values determined from the turbulent wind fluctuations, using statistical dispersion theory. Furthermore, the lateral spread of the plume seems to be greater than the values given by the PGT-curves (Turner 1970).

3.18 Short range simulation model of smoke diffusion*

(T. Mikkelsen)

Work has started on developing a computer model for the calculation of diffusion of smoke close to the point of release. In contrast to the Gaussian plume model, which represents a statistical time-averaged concentration pattern, the puff model has proved capable of simulating updated instantaneous plume pictures by utilizing measurements of a corresponding actual wind field.

The implementation scheme used is based on wind data measurements at a single point. Hence, these single point records are required to be representative with respect to the properties of the mean wind as well as the turbulence of the range in question.
The technique in the puff-model computations is to generate puffs

---

*Supported by the Danish Defence Research Establishment

with a specified release rate in a three-dimensional grid. The individual puffs are advected by a short-term-averaged mean wind sequence: $\bar{V}_{t_{av}}$ (averaging time t_{av}), which initially is prepared from the single point measurements. Simultaneously with the puff advection the growth of the individual puffs is calculated on the basis of the meteorological input data. The puffs are hypothesised to be three-demensional isotropic Gaussian entities, the sizes of which are characterized by the standard deviation σ. As the puffs are advected in the downwind direction their growth is computed by means of the expression (Smith and Hay, 1961)

$$\sigma(X_N) = \sigma(0) + |0.22\,cor \cdot t_{av}| \sum_{n=1}^{N} i_v(n) \cdot \bar{V}_{t_{av}}(n)$$

where X_n: puff position after N advection steps.

$\sigma(0)$: initial puff size.

$i_v(n)$: lateral intensity of turbulence defined as:

$$i_v(n) = \sqrt{v'^2}/V_n^2$$

Here v'^2 is the lateral variance in the wind field and V_n the magnitude of the windvector $\bar{V}_{t_{av}}$, time-averaged over the nth time interval of length t_{av}. The correction factor (cor) accounts in

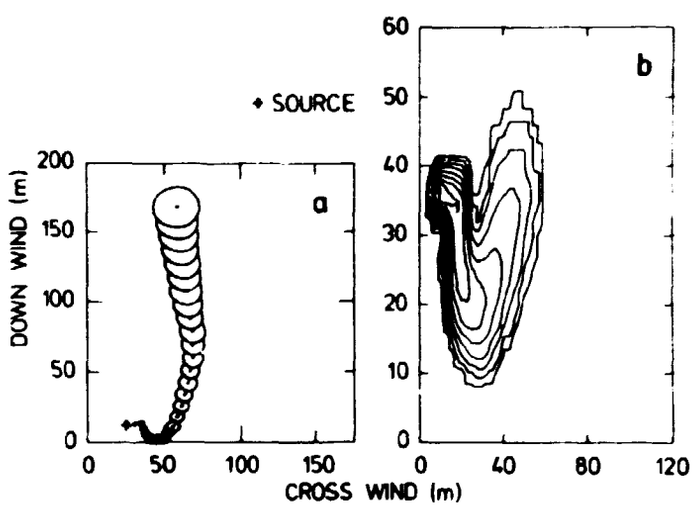

Fig. 47 (a) Top view of a puff-chain 40 s after the release of smoke. (b) Isoconcentration in the region near the smoke for advection rate = 1/s, release rate = 1 g/s, and averaging time = 2 s.

a parametic way for the stability of the atmosphere. In the case of hot effluxes, plume rise caused by buoyancy is also calculated during each advection step. Once the advection and size of all puffs are calculated, the updated grid concentrations are obtained at each grid point by summing up all the contributions from puffs in the grid.

An example of such a generated puff chain is shown in Fig. 47a. In this case the simulation shows a meandering plume. The corresponding concentration pattern at the ground level (z=0) is shown in Fig. 47b. As seen from the figures, the puff model can simulate concentration distributions in a dynamical way even at short time scales.

3.19 References

BUSCH, N.E. (1965). Risø Report No. 99, 92 pp.

BUSCH, N.E. and LARSEN, S.E. (1975). Risø Report No. 334, 68-70.

BUSCH, N.E., CHANG, S.W., and ANTHES, R.A. (1976). J. Appl. Meteorol. 15, 909-919.

BUSCH, N.E., CHRISTENSEN, O., KRISTENSEN, L., LADING, L., and LARSEN, S.E. (1979). Wind speed and direction: Cups, vanes, propellers and lasers. Accepted for publication in the proceedings of a NATO-sponsored School on Air-sea Interaction, held at Ustaoset, Norway, April 17-28, 1978.

CHRISTENSEN, C.J., FRANDSEN, S., LUNDSAGER, P. (1978). Gedser Test Group, GTG report 771.105-1.

CHRISTENSEN, O. and FRANDSEN, S. (1977). A field study of cross wind exitation of steel chimneys, Preprint of short contribution from a seminar on Safety of Structure under Dynamic Loading, held at Trondheim, Norway, June 23-July 1, 1977.

CLARKE, R.H., DYER, A.J., BROOKS, R.R., REID, D.G., and TROUP, A.J. (1971). The Wangara experiment: boundary layer data (Commonwealth Scientific and Industrial Research Organization, Aspendale, Australia)(CSIRO, Division of Meteorological Physics, Technical Paper No. 19).

FRASER, A.B. (1977). Appl. Opt. 16 (1), 160-165.

GILL, G.C. (1975). Boundary-Layer Meteorol. 8, 475-495.

HØJSTRUP, J. (1979). The structure of the atmospheric internal boundary layer developing after an abrupt change in surface roughness. Risø Report No. 397 (in preparation).

JOHNSEN, S.J., DANSGAARD, W., CLAUSEN, H.B., and LANGWAY, C.C. Jr. (1972). Nature 235, 429-434.

KRISTENSEN, L. (1978). Risø Report No. 381, 48 pp.

KRISTENSEN, L. (1979). On longitudinal spectral coherence. Accepted for publication in Boundary-layer Metereol.

LARSEN, S.E., MATHIASSEN, O., and BUSCH, N.E. (1979). Analysis of data from 3-dimensional hot wire probes using comparison with profile instrumentation for calibration. To be published in the proceedings of a meeting on Dynamic Flow Measurements, held at Marseille, France, September 11-14, 1978.

LETTAU, H.H. and DAVIDSON, B. (editors) (1957). Exploring the atmosphere's first mile. Proceedings of the Great Plains turbulence field program, held at O'Neill, Nebraska, August 1-September 8, 1953. Vol. 1-2 (Pergamon, New York) 578 pp.

NEUMANN, J. and MAHRER, Y. (1971). J. Atmos. Sci. 28, 532-542.

OGURA, Y. and PHILLIPS, N.A. (1962). J. Atmos. Sci. 19, 173-197.

PETERSEN, E.L. and LARSEN, S.E. (1978). Tellus 30, 193-200.

PETERSON, E.W., KRISTENSEN, L., and Su, C.-C. (1976). J. R. Meteorol. Soc., 102, 857-869.

PIELKE, R.A. and PANOFSKY, H.A. (1970). Boundary-Layer Meteorol. 1, 115-130.

POPELEWSKI, C.F., TENNEKES, H., and PANOFSKY, H.A. (1973). Boundary-Layer Meteorol. 5, 353-363.

ROTH, R. (1970). Boundary-Layer Meteorol. 1, 131-136.

SMITH, F.B. and HAY, J.S. (1961). Q. J. R. Meteorol. Soc. 87, 82-101.

TARTARSKII, V.I. (1971). The Effects of the Turbulent Atmosphere on Wave Propagation. (Israel Program for Scientific Translations, Jerusalem), 472 pp.

TCHEN, C.M. (1978). C.R. Hedb. seances Acad. Sci. A286, 605-607.

TENNEKES, H. (1973). J. Atmos. Sci. 30, 558-567.

THOMSON, D.W., COULTER, R.L., and WARHAFT, Z., (1978). J. Appl. Meteorol. 17, 723-734.

TOBA, Y. (1965). Tellus 17, 365-382.

TURNER, D.B. (1969). Workbook of atmospheric dispersion estimates. Rev. ed. (National Air Pollution Control Administration,

Cincinnati, Ohio) (Public Health Service Publication, 999-AP-26) 84 pp.

WYNGAARD, J.C., IZUMI, Y., and COLLINS, S.A., Jr. (1971). J. Opt. Soc. Am. 61, 1646-1640.

WYNGAARD, J.C., BAUMAN, J.T., and LYNCH, R.A. (1974). In: Flow, its measurement and control in science and industry. Proceedings of a conference held at Pittsburgh, Pa., May 10-14, 1971. Vol. 1, part 2 .Instrument Society of America, Pittsburgh, Pennsylvania) 701-708.

4. LIQUID N_2 AND He PLANT

The production of liquid N_2 and He amounted to 200 000 and 19 000 litres, respectively. Out of these amounts, 10 000 litres of liquid He were delivered to laboratories in Copenhagen, Odense and Århus.

5. EDUCATIONAL ACTIVITIES AND PUBLICATIONS

5.1. Lectures

ALS-NIELSEN, J., Mean field theory and marginal dimensionality in phase transitions. University of Copenhagen (November).

BURAS, B., Condensed matter studied by means of synchrotron radiation and pulsed neutron beams (lecture series). University of Copenhagen (spring semester).

BURAS, B., X-ray energy-dispersive diffractometry using synchrotron radiation, National Bureau of Standards, Washington D.C., USA (April).

BUSCH, N.E., Luftforurening og meteorologi, Vurdering og forolkning af luftforureningsmålinger (Air pollution and meteorology: Evaluation and interpretation of air-pollution measurements). University of Copenhagen (March).

BUSCH, N.E., Comments on a study of some of the consequences of hypothetical reactor accidents as Barsebäck. Public Hearings on the Evaluation of Nuclear power accidents and risks. Stockholm, Sweden and Copenhagen (April).

BUSCH, N.E., Observations of flow and short-range diffusion over inhomogeneous terrain.

1) Atmospheric Environment Service, Toronto, Canada (May)
2) Canadian Centre for Inland Waters, Burlington, Ontario, Canada (May).

CARNEIRO, K., Physics of one-dimensional conductors. University College of North Wales, Bangor, Gwynedd, U.K. (September).

CHANG, C.T., A bird's-eye view of the pellet refuelling problems, Ispra, Italy (January).

CHANG, C.T., Highlights of Tokamak experimental trends during the last three years.

1) Institute of Physics, Academic Sinica, Peking, People's Republic of China (June).
2) Southwestern Institute of Physics Academic Sinica, Lasshan, Szechwan, People's Republic of China (June).

DAVIDSON, K.L., Estimating surface fluxes from shipboard measurements; JASIN - 7. Royal Ducth Meteorological Institute, de Bilt, The Nederlands (November).

DAVIDSON, K.L., Small scale turbulence properties of the marine atmospheric surface layer. Chr. Michelsens Institute, Bergen, Norway (December).

DUTTON, J.A., The second fundamental theorem of atmospheric dynamics. University of Hamburg, Hamburg, F.R.G. (October).

DUTTON, J.A., Dynamics of nonlinear thermally forced dissipative flows. Six lectures given at the Danish Centre of Applied Matematics and Mechanics, Technical University of Denmark, Lyngby (October and November).

GRYNING, S.E., Medium range dispersion experiments close to a shoreline in near neutral conditions. Norwegian Institute for Air Research, Oslo, Norway (December).

JENSEN, V.O., 40 double lectures on plasma physics. Technical University of Copenhagen, Lyngby.

JENSEN, V.O., JET og europæisk fusionsforskning (JET and European fusion research). Dansk Kerneteknisk Selskab, Copenhagen (February).

JENSEN, V.O., Fusionsforskning (Fusion research). Lecture given to journalists, Århus (September).

JENSEN, V.O., Fusionsforskningens perspektiver (Perspectives for fusion research). Technical University of Denmark, Lyngby (October).

JENSEN, V.O., Om plasmafysik og fusionsforskning (On plasma physics and fusion research). Lecture given to high school teachers, Fredensborg (October).

KJEMS, J., Spin waves and soliton modes in the 1-D magnet, $CsNiF_3$.

1) Technical University of Norway, Trondheim, Norway (November).
2) University of Oslo, Norway (November).
3) University of Frankfurt, Frankfurt, F.R.G.(November).

KRISTENSEN, L., Metereological instruments (lecture series). Pensylvania State University, Pensylvania, USA (winter term).

KRISTENSEN, L., Problems in wind measurements with cup anemometers and wind vanes.

1) U.S. Naval Postgraduate School, Monterey, California, USA (March).
2) San Jose State University, San Jose, California, USA (March).

KRISTENSEN, L., Micrometeorological instrumentation, Oregon State University, Oregon, USA (April).

LINDGÅRD, P.-A., Multicritical phenomena. Hahn-Meitner Institute, Berlin (May).

MICHELSEN, P., Solitary waves in a collisionless plasma. Akademie der Wissenshaften der DDR, Berlin, G.D.R. (December).

MIKKELSEN, T., Atmospheric dispersion simulation by means of a puff-model. Studsvik Energi AB, Sweden (October).

MØLLENBACH, K. (and KJEMS, J.K.), Study of the orderparameter near the Jahn-Teller transition in $TbVO_4$, $DyVO_4$ and $DyAsO_4$. Brookhaven National Laboratory, New York, USA (November).

MØLLENBACH, K., The resolution function of a neutron diffractometer for protein crystallography. Brookhaven National Laboratory, New York, USA (December).

MØLLENBACH, K., Principles in neutron diffraction from biological substances. Naticnal Bureau of Standards, Washington D.C., USA (December).

NIELSEN, M., Monolayers of He, H_2 and O_2 adsorbed on graphite studied by neutron scattering.
1) University of Uppsala, Sweden (April).
2) Brookhaven National Laboratory, New York, USA (September).

NIELSEN, P, Fusion, fremtidens energiforsyning (Fusion - the energy supply of tomorrow).
1) H.H. Koch Auditorium, Risø (October).
2) Niels Bohr Auditorium, Risø (November).

PÉCSELI, H.L., Nonlinear waves in a Q-machine plasma. Princeton University, New Jersey, USA (October).

PÉCSELI, H.L., Strong turbulence in low β-plasma. University of Iowa, Iowa, USA (November).

RASMUSSEN, J. JUUL, Eindhoven University of Technology, The Netherlands (November).
1) Interaction between ion acoustic waves and electron plasma waves.
2) Finite amplitude electron plasma waves in a cylindrical waveguide.

SCHOU, J., Interaction between charged keV particles and solid H_2, D_2 and N_2. Max-Planck-Institute for Plasma Physics, Garching, F.R.G. (December).

5.2. Publications

ALS-NIELSEN, J. (1976)*. Experimental test of renormalization group theory on the uniaxial dipolar coupled ferromagnet $LiTbF_4$. Phys. Rev. Lett. 37, 1161-1164.

ALS-NIELSEN, J.,BIRGENEAU, R.J., KAPLAN, M., LISTER, J.D., and SAFINYA, C.R. (1977)*. High resolution X-ray study of a second-order nematic-smectic-A phase transition. Phys. Rev. Lett. 39, 352-355.

ALS-NIELSEN, J., BIRGENEAU, R.J., KAPLAN, M., LISTER, J.D., and SAFINYA, C.R. (1977)*. Experimental observation of anomalous ordering in a Landau-Peierls system. Phys. Rev. Lett. 39, 1668-1671.

ALS-NIELSEN, J., BIRGENEAU, R.J., GARCIA-GOLDING, F., KAPLAN, M., LITSTER, J.D., and SAFINYA, C.R. (1978). High resolution X-ray studies of the smectra A-nematic transition. Ann. Phys. Paris 3, 357-358.

ALS-NIELSEN, J., BJERRUM MØLLER, H., and MØLLENBACH, K. (1978). Proposal on a joint EMBO-RNL small angle neutron scattering facility for molecular biological research. Risø-M-1976, 10 pp.

ANDERSEN, V. CHANG, C.T., JØRGENSEN, L.W., NIELSEN, P., and SILLESEN, A. (1978). Pellet refueling program at Risø. Proceedings of the Fusion Fueling Workshop PPL, Princeton University, New Jersey Nos. 1-3, 1977, 114-116.

BAK, P. and LEBECH, B. (1978). "Triple-$\vec{q}$" modulated magnetic structure and critical behaviour of neodymium. Phys. Rev. Lett. 40, 800-803.

BURAS, B. (1978). Some experience with and future requirements for semiconductor detectors used for synchrotron radiation X-ray energy-dispersive diffractometry. Stanford Synchrotron Radiation Laboratory Report No. 78/04 (VIII), 124-131.

BURAS, B., NIIMURA, N., and OLSEN, J. STAUN (1978). Optimum resolution in X-ray energy-dispersive diffractometry. J. Appl. Cryst. 11, 137-140.

BURAS, B. OLSEN, J. STAUN, and GERWARD, L. (1978). White beam, X-ray, energy-dispersive diffractometry using synchrotron radiation. Nucl. Instr. Methods 152, 293-296.

CHANG, C.T. (1978). On the injection speed of a refuelling pellet. Risø Report No. 389, 17 pp.

CHANG, C.T. and PÉCSELI, H. (1978). Estimations of the effect of alpha particles on a refuelling pellet. Risø Report No. 378, 19 pp.

---

* Not included in previous Progress Reports

CHRISTENSEN, A. NØRLUND and LEBECH, B. (1978). A reinvestigation of the structure of ε-tantalum nitride. Acta Cryst. B34, 261-263.

DICKENS, M.H., HUTCHINGS, M.T., KJEMS, J.K., and LECHNER, R.E. (1978). Quasielastic neutron scattering by superionic strontium chloride. J. Phys. C: Solid State Phys. 11 L583-L588.

DUNSWORTH, A.E., JAN, J.-P., and SKRIVER, H.L. (1978). de Haas-van Alphen effect, LMTO bandstructure and Fermi surface of β-AgMg. J. Phys. F: Metal Phys. 8, 1427-1435.

DYSTHE, K.B., MJØLHUS, E., PÉCSELI, K.L., and STENFLO, L. (1978). Langmuir solitons in magnetized plasma. Plasma Phys. 20, 1087-1099.

DYSTHE, K.B. and PÉCSELI, H.L. (1978). Nonlinear Langmuir wave modulation in weakly magnetized plasmas. Plasma Phys. 20, 971-989.

FISCHER, P., LEBECH, B., MEIER, G., RAINFORD, B.D., and VOGT, O. (1978). Magnetic phase transitions of CeSb: I. Zero applied magnetic field. J. Phys. C: Solid State Phys. 11, 345-364.

GJØRUP, H.L., HEDEMANN JENSEN, P., JENSEN, N.O., PETERSEN, E.L., PEJTERSEN, V., PETERSEN, T., THYKIER-NIELSEN, S., and HEIKEL VINTHER, F. (1978). En teknisk vurdering af Jan Beyea's rapport: "A study of some of the consequences of hypothetical reactor accidents at Barsebäck". Risø-M-1997, 15 pp.

GJØRUP, H.L., HEDEMANN JENSEN, P., JENSEN, N.O., PETERSEN, E.L., PEJTERSEN, V., PETERSEN, T., THYKIER-NIELSEN, S., and HEIKEL VINTHER, F. (1978). A technical evaluation of Jan Beyea's report: "A study of some of the consequences of hypothetical reactor accidents at Barsebäck." Risø-M-2108, 20 pp.

GRYNING, S.E., LYCK, E., and HEDEGAARD, K., (1978). Short-range diffusion experiments in unstable conditions over inhomogeneous terrain. Tellus 30, 392-403.

HANSEN, P. AAROSIIN (1977). Magnetic anisotroyp and related matters studied by neutron diffraction. Risø Report No. 360, 78 pp.

JENSEN, N.O. (1978). Vindmålinger på Sprogø, 1. halvårsrapport (Wind measurements at Sprogø, 1st semi-annual progress report). Work done under contract to Statsbroen Storebælt, 82 pp.

JENSEN, N.O. (1978). Vindmålinger på Sprogø, 2. halvårsrapport (Wind measurements at Sprogø, 2nd semi-annual progress report). Work done under contract to Statsbroen Storebælt, 67 pp.

JENSEN, N.O. (1978). Notat vedrørende Danmarks klima (Note on the Danish climate). Work done under contract to Statsbroen Storebælt, 15 pp.

JENSEN, N.O. (1978). Øvre estimater på korrelations afstande i laterale retninger (Upper estimates on cross wind correlation distances). Work done under contract to Statsbroen Storebælt, 78 pp.

JENSEN, N.O. (1978). Specialundersøgelse af vindprofiler ved Sprogømasten (Special investigation of wind profiles from the Sprogø mast). Work done under contract to Statsbroen Storebælt, 110 pp.

JENSEN, N.O. (1978). Notat vedrørende koherensforhold i den naturlige vind (Note on the conditions of coherence in the natural wind). Work done under contract to Statsbroen Storebælt, 17 pp.

JENSEN, N.O. (1978). Varsling af glatføre (Forcasting of icing conditions). Work done under contract to Vejlaboratoriet, 36 pp.

JENSEN, N.O. (1978). Simultaneous measurements of turbulence over land and water. Boundary-Layer Met. 15, 95-108.

JENSEN, N.O. (1978). Change of surface roughness and the planetary boundary layer. Quart. J. Roy. Met. Soc. 104, 351-356.

JENSEN, N.O. and AGEE, E.M. (1978). Vortex cloud street during AMTEX 75. Tellus 30, 517-523.

JENSEN, N.O. and FRANDSEN, S. (1978). Atmospheric turbulence structure in relation to wind generator design. Proceedings of the 2nd International Symposium on Wind Energy Systems, BHRA-Fluid engineering, Amsterdam, The Netherlands, C1, 1-12.

JENSEN, N.O. and LENSCHOW, D.H. (1978). An observational investigation of penetrative convection. J. Atmos. Sci. 35, 1924-1933.

JENSEN, N.O. and PETERSON, E.W. (1978). On the escarpment wind profile. Quart. J. Roy. Met. Soc. 104, 719-728.

JENSEN, T.D., MICHELSEN, P., and RASMUSSEN, J. JUUL (1978). Wave propagation in an ion beam plasma system. Risø-M-2120, 24 pp.

JENSEN, V.O. and NIELSEN, P. (1978). Fusionsforskningen ind i afgørende ny fase. (Fusion research enters a new state of affairs). Ingeniøren No. 41, October 13, 12-13.

KJEMS, J.K., OTT, H.R., SHAPIRO, S.M., and ANDRES, K. (1978). Magnetic excitations and the cooperative Jahn-Teller transition in $PrCu_2$. J. Phys., Paris, 39, suppl. C6, 1010-1012.

KJEMS, J.K. and STEINER, M. (1978). Evidence for soliton modes in the 1-dimensional ferromagnet $CsNiF_3$. Phys. Rev. Lett. 41, 1137-1140.

KOFOED-HANSEN, O. (1978). Højenergi-fysikkens grundlag (Basic concepts of high-energy physics). Fysisk Tidsskrift 76, 11-39.

KOFOED-HANSEN, O. (1978). On alpha-particle heating at a thermonuclear plasma, Risø Report No. 385, 45 pp.

KOFOED-HANSEN, O. (1978). The role of mesonic degrees of freedom in scattering of hadrons on nuclei. Prog. Part. Nuc. Phys. 1, 193.

KRISTENSEN, L. (1978). On sodar techniques. Risø Report No. 381, 48 pp.

KRISTENSEN, L., UNDERWOOD, K.H., and COULTER, R.L. (1978). Sodar geometry. Proceedings of the Fourth Symposium on Meteorological Observations and Instrumentation, Denver, Colorado, USA, AMS, Boston, 391-395.

LARSEN, S.E. and RASMUSSEN, K. RØMER (1978). Comments on measurements of air velocity by means of a triple hot-wire probe. DISA-Information No. 23, September 4.

LEBECH, B. and BAK, P. (1978). Two-dimensionally-modulated, magnetic structure of neodymium metal. Risø-M-2124, 7 pp.

LINDGÅRD, P.-A. (1978). Excitations and spin waves. In: Rare Earths and Actinides, Inst. Phys. Conf. Ser. 37, 96-109.

LINDGÅRD, P.-A. (1978). Phase transitions and critical phenomena. In: Topics in Current Physics. Neutron diffraction 6, 197-241.

LINDGÅRD, P.-A. (1978). Spin waves in the heavy-rare-earth metals Gd, Tb, Dy, and Er. Phys. Rev. 17, 2348-2360.

LINDGÅRD, P.-A. (1978). Theory of anisotropic magnets. Risø Report No. 358, 83 pp.

LUNDSAGER, P., CHRISTENSEN, C.J., and FRANDSEN, S. (1978). Interim report on the measurements on the Gedser Wind Mill. GTG 771-105-1.

LYCK, E. and GRYNING, S.E. (1978). Undersøgelse af et sporstofs udbredelse fra en høj skorsten i et byområde: Standpunktsrapport pr. 1/4 1978. (Determination of atmospheric dispersion in an urban environment by means of tracers). Progress Report (1/4 1978): National Agency of Environmental Protection; Air Pollution Laboratory and Risø National Laboratory.

MACKENZIE, G.A., BURAS, B., and PAWLEY, G.S. (1978). The structure of octofluoronaphthalene at high pressure investigated by neutron diffraction. Acta Cryst. B34, 1918-1923.

MEIER, G., FISCHER, P., HÄLG, W.. LEBECH, B., RAINFORD, B.D., and VOGT, O. (1978). Magnetic phase transitions of CeSb: II. Effects of applied magnetic fields. J. Phys. C: Solid State Phys. 11, 1173-1186.

MICHELSEN, P. (1978). Euratoms langtidsplan mod en fusionsreaktor. The future plans of Euratom towards a fusion reactor), Ingeniøren No. 15, April 14, 18-19.

MICHELSEN, P., PÉCSELI, H.L., and RASMUSSEN, J. JUUL (1978). Interaction between ion acoustic waves and electron plasma waves. Plasma Physics 20, 45-57.

MIKKELSEN, T. and PÉCSELI, H.L. (1978). Investigation of strong turbulence in a low β-plasma. Phys. Rev. Lett. 41, 951-954.

NIELSEN, M. ELLENSON, W.D., and McTAGUE, J.P. (1978). The dynamics and structures of adsorbed surfaces. Proceeding of a Symposium on Neutron Inelastic Scattering, IAEA, Vienna, October 17-21 1977, 2, 433-457.

NIELSEN, M. and McTAGUE, J.P. (1978). The dynamics of physisorbed layers studied by neutron scattering. Proceeding of an International on Vibrations in Adsorbed layers, Jülich, F.R.G., June 12-14 1978, ISSN0344-5798, 37-50.

NIIMURA, N., MØLLER, H. BJERRUM, and RISTE, T. (1978). Quasielastic neutron scattering in normal and deuterated p-azoxyanisole. Physia Scripta 18, 157-160.

OLSEN, J. STAUN, BURAS, B., JENSEN, T., ALSTRUP, O., GERWARD, L., and SELSMARK, B. (1978). Influence of polarization of the integrated intensities in X-ray energy-despersive diffractometry. Acta Cryst. A34, 84-87.

OTT, H.R., KJEMS, J.K., and ANDRES, K. (1978). Crystal field transitions in $PrCu_2$ near the cooperative Jahn-Teller transition at T_D = 8 K. In: Rare Earths and Actinides, Inst. Phys. Conf. Ser 37, 149-150.

PETERSEN, E.L. and LARSEN, S.E. (1978). Stochastic model building for discrete time series applied on a paleo temperature series from the last 700 000 years. Proceeding from Nordic Symposium on Climatic Changes and Related Problems, Copenhagen, 24-28 April. Danish Meteorological Institute, Climatological Papers No. 4.

PETERSEN, E.L. and LARSEN, S.E. (1978). A statistical study of a composite isotopic paleotemperature series from the last 700 000 years. Tellus, 30, 193-200.

PETERSON, E.W., BUSCH, N.E., JENSEN, N.O., HØJSTRUP, J., KRISTENSEN, L., and PETERSEN, E.L. (1978). The effect of local terrain irregularities on the mean wind and turbulence characteristics near the ground. Proceedings of WMO Symposium on Boundary Layer Physics Applied to Specific Problems of Air Pollution, World Meteorological Organisation, Norrköping, Sweden, 45-50.

RASMUSSEN, J. JUUL (1978). Finite amplitude electron plasma waves in a cylindrical waveguide. Plasma Physics 20, 997-1010.

RASMUSSEN, J. JUUL, SANDU, D., and SCHRITTWIESER, R. (1977). Ion-acoustic instability in the presence of high frequency oscillations. Plasma Physics 19, 1139-1144.

RISTE, T., OTNES, K., and MØLLER, H. BJERRUM (1978). Hydrodynamic instabilities and neutron scattering. Proceedings of a Symposium on Inelastic Scattering of Neutrons, IAEA Vienna, October 17-21 1977 1, 511-532.

SKRIVER, H.L. and ANDERSEN, O.K. (1978). Self-consistent calculation of ground-state properties for ordered transition metal alloys. Proceedings of the International Conference on the Physics of Transition Metals, Toronto, Canada, 1977.

SKRIVER, H.L., ANDERSEN, O.K., and JOHANSSON, B. (1978). Calculated bulk properties of the actinide metals. Phys. Rev. Lett. 41, 42-45.

SKRIVER, H.L., VENEMA, W. WALKER, E., and GRIESSEN, R. (1978). Effect of hydrostatic pressure on electronic states in palladium. J. Phys. F: Metal Phys. 8, 2313-2321.

SCHOU, J. and SØRENSEN, H. (1978). The penetration depth of 0.5-3 keV electrons in solid hydrogen and deuterium. J. Appl. Phys. 49, 816-821.

SCHOU, J., SØRENSEN, H., and LITTMARK, U. (1978). Energy reflection coefficients for 5-10 keV ions incident on Au, Ag and Cu. J. Nucl. Mat. 76&77, 359-364.

SHAPIRO, S.M., MØLLER, H. BJERRUM, AXE, J.D., BIRGENEAU, R.J., and BUCHER, E. (1978). Spin dynamics and magnetic ordering in mixed valence systems. J. Appl. Phys. 49, 2101-2106.

STEENSTRUP, S. and BURAS, B. (1978). A Monte Carlo simulation of ultra cold neutron production by Bragg reflection from a moving single crystal. Nucl. Instr. Methods 154, 549-555.

STEINER, M. and KJEMS, J.K. (1978). Inelastic neutron scattering studies of solitons in $CsNiF_3$ in an external field. J. Phys. Letters 39, L493-494.

SØRENSEN, H. and SCHOU, J. (1978). Interaction between solid nitrogen and 1-3 keV electrons. J. Appl. Phys. 49, 5311-5318.

SØRENSEN, H. and SCHOU, J. (1978). On secondary electron emission from solid H_2 and D_2. J. Nucl. Mat. 76&77, 634-635.

TURIKOV, V.A. (1978). a particle simulation code for analysis of nonlinear electron oscillations in a magnetized plasma wave-guide. Risø-M-2116, 26 pp.

TURIKOV, V.A. (1978). Computer simulation of the formation of Langmuir solitons and holes in a cylindrical magnetized plasma column. Risø Report No. 380, 28 pp.

5.3 Conference contributions

ALS-NIELSEN, J., High resolution X-ray studies of the smectic A-Nematic transition. Physics and Applications of Smectic and Lyotropic Liquid Crystals, Madonna di Campiglio, Italy, January 9-13.

ALS-NIELSEN, J., Bragg profiles from the smectic A phase and relation to 2-dimensional crystals. Workshop on Phase Transitions on Surfaces, Nordita/Risø National Laboratory, March 6-8.

ALS-NIELSEN, J., Experimental observation of the Landau-Peierls instability in the smectic A phase of liquid crystals. Workshop on Properties of One- and Two-Dimensional Conductors, Nordita, Copenhagen, June 6-14.

ALS-NIELSEN, J., On the resolution X-ray studies of the liquid crystal SmA phase. Critical fluctuations in the nematic phase, and relation to superconductivity. Danish Physical Society, Spring Meeting, Elsinore, June 15-16.

ALS-NIELSEN, J., Mean field theory, the Ginzberg criterion, and marginal dimensionality of phase transitions. Eleventh International Congress of Crystallography, Warsaw, Poland, August 3-12.

ALS-NIELSEN, J., Mean field theory and marginal dimensionality of phase transitions. Fourth General Conference of the European Physical Society, U.K., September 25-29.

ANDERSEN, O.K., JOHANSSON, B., and SKRIVER, H.L., Calculated bulk properties of the actinide metals. Danish Physical Society, Spring Meeting, Elsinore, June 15-16.

BURAS, B., Konzeption und Konstruktion eines Mehrzweck-Messplatzes für Energie-dispersive Beugung und für 3-Achsen-Spektrometrie (Conception and construction of a multi purpose experimental arrangement using the energy dispersive method or triple-axis spectrometry). Arbeitstagung veranstaltet von der Kommission für Synchrotron-Strahlung der Arbeits-Gemeinschaft Kristallographie. Max-Planck-Institute of Solid State Physics, Stuttgart, F.R.G., March 10-11.

BURAS, B., Some experience with and future requirements for semiconductor detectors used for synchrotron radiation X-ray energy-dispersive diffractometry. Workshop on X-ray instrumentation for Synchrotron Radiation Research, Stanford, USA, April 3-5.

BURAS, B., X-ray structural studies using synchrontron radiation, Deutsche Physikalische Gesellschaft, 42. Physikertagung, Berlin, October 3-7.

BURAS, B., Perspectives for synchrontron radiation research, Danish Physical Society, Annual Meeting, Copenhagen, November 24.

BURAS, B., LEBECH, B., and MACKENZIE, G.A., High-pressure cells for neutron crystal spectrometry. Eleventh International Congress of Crystallography, Warsaw, Poland, August 3-12.

BURAS, B., GERWARD, L., GLAZER, A.M., HIDAKA, M., and OLSEN J. STAUN, Structural studies by means of energy-dispersive

method and X-rays from a storage ring. Fourth General Conference of the European Physical Society, York, U.K., September 25-29.

BURAS, B., OLSEN, J. STAUN, and GERWARD, L. Energy dispersive X-ray diffraction with synchrotron radiation from a storage ring. Danish Physical Society, Spring Meeting, Elsinore, June 15-16.

BUSCH, N.E., Vinden over hav, land og by (The Winds above Sea Surfaces, Land Surfaces, and Built-up Aeras). Workshop on Wind Techniques, Technical University of Denmark, Lyngby, June 12.

BUSCH, N.E., Short-range diffusion experiments over inhomogenious terrain. Workshop on Mesometeorology, Las Cruces, New Mexico, USA, September 18-22.

BUSCH, N.E., The effect of local terrain irregularities on the mean wind and turbulence characteristics near the ground. Workshop on Mesometeorology. Las Cruces, New Mexico, USA, September 18-22.

BUSCH, N.E., CHRISTENSEN, O., KRISTENSEN, L., LADING, L., and LARSEN, S.E., Wind speed and direction. Cups, vanes, propellers and lasers. Instruments and methods in air-sea interaction. NATO School on Instrumentation and Methods in Air Sea Interaction, Ustaoset, Norway, April 16-28.

BUSCH, N.E. and JENSEN, N.O., Meteorology and energy: A European perspective. Atmosphere-Ocean, 12th Annual Congress of the Canadian Meteorological and Oceanographic Society, Toronto, Ontario, Canada, May 31 - June 2.

BUSCH, N.E., LARSEN, S.E., and THOMSON, D.W., Data analysis of atmospheric measurements. Dynamic measurements in unsteady flows. Dynamic Flow Conference 1978, Marseille, France, September 11-14.

CARNEIRO, K., Adsorbed helium. Workshop on Neutrons in Helium, Institute Max von Laue-Paul Langevin, Grenoble, France, August 30.

CARNEIRO, K., Diatomic liquids. Conference on Neutron Scattering and the Liquid State, Canterbury, U.K., September 25-29.

CHANG, C.T., A bird's-eye view of the pellet refuelling problems, Plasma og Gassutladningssymposiet, Gausdal, Norway, February 5-8.

CHANG, C.T., Injection speed of a refuelling pellet. IAEA 7th International Conference on Plasma Physics and Controlled Nuclear Fusion Research, Innsbruch, Austria, August 23-30.

CHRISTENSEN, O., Statisk og dynamisk vindlast. (Static and dynamic windloading). Workshop on Wind Techniques, Technical University of Denmark, Lyngby, June 12.

CHRISTENSEN, C.J. and LUNDSAGER, P., Investigations of structural dynamics on the Gedser WTG and on new Danish wind turbines. 1st Meeting of Experts - Structural Dynamics - IEA Implementary Agreement for Cooperation on the Development of Large Scale Wind Energy Conversion Systems, Münich, F.R.G. October 12.

GLAZER, A.M., HIDAKA, M., BURAS, B., OLSEN, J. STAUN, and GERWARD, L., Energy-dispersive methods with synchrotron radiation. Eleventh International Congress of Crystallography Warsaw, Poland, August 3-12.

GLAZER, A.M., HIDAKA, K., BURAS, B., OLSEN, J. STAUN, and GERWARD, L., Energy dispersive powder diffraction with synchrotron radiation, Crystallography Group, Autumn Meeting on "New Techniques in Crystallography", London, U.K., November 16.

HINZE, E., WILL, G., BURAS, B., OLSEN, J. STAUN, and GERWARD, L., Energy-dispersive as a method for X-ray diffraction under high pressure in a diamond anvil cell. Eleventh International Congress of Crystallography, Warsaw, Poland, August 3-12.

HØJSTRUP, J., Atmospheric flow after an abrupt change in surface roughness. Colloquium on Fluid Transport and Deposition of Particles and Turbulence. University of Aarhus, September 14-15.

JENSEN, N.O., Vindens spredning af røg og partikler (Dispersion of smoke and particles by the wind). Workshop on Wind Techniques, Technical University of Denmark, Lyngby, June 12.

JENSEN, N.O. and FRANDSEN, S., Atmospheric turbulence structure in relation to wind generator design. 2nd International Symposium on Wind Energy Systems, Amsterdam, The Netherlands, October 3-6.

KJEMS, J.K., Neutron scattering from magnetic materials. Danish Physical Society, Winter School on Experimental Methods in Solid State Physics, Copenhagen, January 23-26.

KJEMS, J.K., Spin waves and soliton modes in the 1-D magnet $CsNiF_3$. Workshop on Electronic Properties of One- and Two-Dimensional Conductors, Nordita, Copenhagen, June 6-14.

KJEMS, J.K., BUYERS, W.J.L., CROW, J.E., and NIELSEN, M., Pressure dependence of the critical fluctuations in the singlet ground state system Pr_3Tl. Danish Physical Society, Spring Meeting, Elsinore, June 15-16.

KJEMS, J.K., BUYERS, W.J.L., CROW, J.E., and NIELSEN, M., Pressure dependence of the critical fluctuations into singlet ground state system Pr_3Tl. International CNRS Colloguium on "La Physique des Terres Rare a l'Etat Metallique", St. Pierre de Chartreuse, France, September 4-7.

KJEMS, J.K., OTT, H.R., SHAPIRO, S.M., and ANDRES, K., Magnetic excitations and the cooperative phase transition in $PrCu_2$. Conference on Low Temperature Physics LT-15, Grenoble, France August 23-29.

KRISTENSEN, L., UNDERWOOD, K.H., and COULTER, R.L., Sodar geometry. Forth Symposium on Meteorological Observations and Instrumentations, Denver, Colorado, USA, April 10-14.

LARSEN, S.E., HØJSTRUP, J., and GIBSON, C., Fast response temperature sensors. NATO School on Instrumentation and Methods in Air Sea Interaction,Ustaoset, Norway, April.

LARSEN, S.E., MATHIASSEN, O., and BUSCH, N.E., Analysis of data from 3-dimensional hot-wire probes, using comparison with profile instrumentation for calibration. Dynamic measurements in unsteady flows. Dynamic Flow Conference 1978, Marseille, France, September 11-14.

LEBECH, B., FISCHER, P.A., MEIER, G., and RAINFORD, B.D., The phase diagram of the anomalous antiferromagnet CeSb, Danish Physical Society, Spring Meeting, Elsinore, June 15-16.

LEBECH, B. and BAK, P., Two dimensionally modulated magnetic structure of neodymium metal. Eleventh International Congress of Crystallography, Warsaw, Poland, August 3-12.

LEBECH, B. and BAK, P., Two dimensionally modulated magnetic structure of neodymium metal. International CNRS Colloquium on "La Physique des Terres Rare a l'Etat Metallique", St.-Pierre de Chartreuse, France, September 4-7.

LEBECH, B., FISCHER, P.A., MEIER, G., and RAINFORD, B.D., Phase diagram of the anomalous antiferromagnet CeSb. Deutsche Physikalische Gesellschaft, 42. Physikertagung, Berlin, October 3-7.

LINDGÅRD, P.-A. and RASTELLI, E., Comparison of spin wave theories for a planar ferromagnet. Danish Physical Society, Spring Meeting, Elsinore, June 15-16.

LISTER, J.D., ALS-NIELSEN, J., BIRGENEAU, R.J., DANA, S.S., DAVIDOV, D., GARCIA-GOLDING, F., KAPLAN, M., SAFINYA, C.R., and SCHAETZING, R., High resolution X-ray and light scattering studies of bilayer smectic A compounds. Seventh International Conference on Liquid Crystals, Bordeaux, France, July 3-7.

LYNOV, J.P., Energy properties of ion acoustic waves. Plasma og Gassutladningssymposiet, Gausdal, Norway, February 5-8.

LYNOV, J.P., Energy properties of ion acoustic waves. Danish Physical Society, Spring Meeting, Elsinore, June 15-16.

LYNOV, J.P., MICHELSEN, P., PÉCSELI, H.L., RASMUSSEN, J. JUUL, SAEKI, K., and TURIKOV, V.A., Observations of solitary structures in a magnetized plasma loaded waveguide. Chalmers Symposium on Solitons, Göteborg, Sweden, June 7-14.

MACKENZIE, G.A., Phonons in molecular crystals. Danish Physical Society. Winter School on Experimental Methods in Solid State Physics, Copenhagen, January 23-26.

MACKENZIE, G.A., The lattice dynamics of molecular crystals. International Summer School on Crystallographic Computing. Twente, Enschede, The Netherlands, July 28-August 1.

MACKENZIE, G.A., BURAS, B., and PAWLEY, G.S., Structural studies of molecular crystals at high pressure by neutron powder diffraction. European High Pressure Research Group, 16th Annual Conference, Reading, U.K., April 11-13.

MICHELSEN, P., Observation of solitons and electron holes in a collisionless plasma. Danish Physical Society, Spring Meeting Elsinore, June 15-16.

MICHELSEN, P., LYNOV, J.P., PÉCSELI, H.L., RASMUSSEN, J. JUUL, SAEKI, K., TURIKOV, V.A., Formation and interaction of electron solitary holes. 20th Annual Meeting of the American Physical Society, Division of Plasma Physics, Colorado, USA, October 30-November 3.

MIKKELSEN, T., Strong turbulence in a Q-machine plasma. Plasma og Gassutladningssymposiet, Gausdal, Norway, February 5-8.

MØLLENBACH, K. and KJEMS, J.K., Study of the order parameter near the Jahn-Teller transition in $TbVO_4$, $DyVO_4$ and $DyAsO_4$. Danish Physical Society, Spring Meeting, Elsinore, June 15-16.

MØLLER, H. BJERRUM, LANDER, G.H., and VOGT, O., Investigation of critical fluctuation near T_c in ferromagnetic UTe. Third International Actinide Conference, Grenoble, France, August 30-September 11.

MØLLER, H. BJERRUM and MACKINTOSH, A.R., Magnon lifetimes in terbium at low temperatures. International CNRS Colloquium on "La Physique des Terre Rares a l'Etat Metallique", St.-Pierre de Chartreuse, France, September 4-7.

NIELSEN, M., The α-β transition of O_2 layers and the commensurate-incommensurate transition of O_2 layers. Workshop Phase Transitions on Surfaces. Nordita/Risø National Laboratory, March 6-8.

NIELSEN, M., The phase transitions of physisorbed monolayers studied by neutron scattering. Workshop on Electronic Properties of One- and Two-Dimensional Conductors, Nordita, Copenhagen, June 6-14.

NIELSEN, M. and McTAUGUE, J.P., The dynamics of physisorbed layers studied by neutron scattering. International Conference on Vibrations in Adsorbed Layers, Jülich, F.R.G., June 12-14.

PECSELI, H.L., Observation of electron holes or unitons. Plasma- og Gasutladningssymposiet, Gausdal, Norway, February 5-8.

PECSELI, H.L., Nonlinear wave modulation. Danish Physical Society, Spring Meeting, Elsinore, June 15-16.

PECSELI, H.L., MICHELSEN, P., LYNOV, J.P., RASMUSSEN, J. JUUL, TURIKOV, V.A., Solitons in a strongly magnetized plasma loaded waveguide. 20th Annual Meeting of the American Physical Society, Division of Plasma Physics, Colorado Springs, Colorado, USA, October 30-November 3.

PETERSEN, E.L. and LARSEN, S.E., Stochastic model building for discrete time series applied on paleo-temperature series from the last 700 000 years. Nordic Symposium on Climate Changes and Related Problems, Copenhagen, April

PETERSON, E.W., BUSCH, N.E., JENSEN, N.O., HØJSTRUP, J., KRISTENSEN, L., and PETERSEN, E.L., The effect of local terrain irregulatities on the mean wind and turbulence characteristics near the ground. WMO symposium on Boundary Layer

Physics Applied to Specific Problems of Air Pollution, Norrköping, Sweden, June 19-23.

RASMUSSEN, J. JUUL, Finite amplitude electron plasma waves in a cylindrical waveguide. Danish Physical Society, Spring Meeting, Elsinore, June 15-16.

SCHOU, J., SØRENSEN, H., and LITTMARK, U., Energy reflection coefficients for 5-10 keV He ions incident on Au, Ag and Cu. Third International Conference on Plasma Surface Interactions in Controlled Fusion Devices, UKAEA Culham Laboratories, U.K. April 3-7.

STEINER, M. and KJEMS, J.K., Solitons in $CsNiF_3$: Their experimental evidence and the thermodyramics. Conference on Nonlinear Phenomena in Physics. Oxford, U.K., June 29.

STEINER, M. and KJEMS, J.K., Spin waves and solitons in $CsNiF_3$. Conference on Low Temperature Physics Lt-15. Grenoble, France, August 23-29.

STEINER, M. and KJEMS, J.K., Inelastic neutron scattering studies of solitons in $CsNiF_3$ in an external field. Fourth General Conference of the European Physical Society, York, U.K., September 25-29.

SØRENSEN, H. and SCHOU, J., On secondary electron emission from solid H_2 and D_2. Third International Conference on Plasma Surface Interactions in Controlled Fusion Devices, UKAEA Culham Laboratories, U.K., April 3-7.

SØRENSEN, H. and SCHOU, J., On secondary electron emission from solid H_2 and D_2. Danish Physical Society, Spring Meeting, Elsinore, June 15-16.

TURIKOV, V.A., Computer simulation of the formation of Langmuir solitons and holes in a cylindrical magnetized plasma column. Danish Physical Society, Spring Meeting, Elsinore, June 15-16.

YANG, D. and LINDGÅRD, P.-A., First principles calculation of the damping and the quasielastic mode in dhcp Pr. Danish Physical Society, Spring Meeting, Elsinore, June 15-16.

YANG, D. and LINDGÅRD, P.-A., Theory of the transition temperature and the magnitization in Pr_3Tl under change of volume. International CNRS Colloquium on "La Physique des Terres Rares a l'Etat Metallique", St -Pierre de Chartreuse, France, September 4-7.

5.4 Degrees, students, etc

Per-Anker Lindgård defended a dissertation entitled "Theory of anisotropic magnets: Magnetic properties of rare earth metals and compounds"((Risø Report No. 358) on June 9, 1978, at the University of Copenhagen.

The following were awarded the degree of lic.techn. (Ph.D.) for work carried out in the department:

Peter Aarosiin Hansen	(Solid State Physics)
Jens Juul Rasmussen	(Plasma Physics)

The following postgraduates carried out research (which will lead to the degrees of lic. techn. or lic. scient.) at the department:

Kurt Clausen	(Solid State Physics)
Sven-Erik Gryning	(Meteorology)
Jørgen Højstrup	(Meteorology)
Palle Buus Jensen	(Plasma Physics)
Jens-Peter Lynov	(Plasma Physics)
Knud Møllenbach	(Solid State Physics)
Jørgen Schou	(Plasma Physics)
Ib Troen	(Meteorology)

The following students from Technical University of Denmark and the University of Copenhagen worked on Master's thesis projects:

Finn E. Christensen	(Solid State Physics)
Mogens Gadeberg	(Plasma Physics)
Henrik Herlufsen	(Solid State Physics)
Olaf Mathiassen	(Meteorology)
Torben Mikkelsen	(Plasma Physics)

During February and September students from the Universities of Aarhus, Copenhagen and Odense participated in the following laboratory courses:

1) Neutron Scattering organized by:
   J.G. Houmann, K. Møllenbach, and
   K. Clausen.

2) Plasma Physics, organized by:
J.-P. Lynov, P. Michelsen, and H.L. Pécseli

Four students from the University of Copenhagen performed measurements at DR3 as part of their training.

Three foreign students sponsored by the IAESTE carried out practical work at the department as part of their general training.

6. STAFF OF THE PHYSICS DEPARTMENT

Head: Hans Bjerrum Møller

Office staff: Lone Astradsson, Karen Lundgård Hansen[+], Lis Hoffmann Nielsen[++], Gerda Stauning, Alice Thomsen, and temporary assistants.

The sections:
6.1 Solid State Physics
6.2 Plasma Physics
6.3 Meteorology
6.4 Liquid N_2 and He Plant

6.1 Solid State Physics

Scientific staff
Jens Als-Nielsen
Ove W. Dietrich[*]
Jens Gylden Houmann[*]
Jørgen Kjems
Bente Lebech
Per-Anker Lindgård
Hans Bjerrum Møller
Mourits Nielsen
Hans L. Skriver

Collaborators
Bronislav Buras[**]
Kim Carneiro[**]

Technical staff
Bjarne Breiting
Kaj Christensen
Bent Heiden
John Z. Jensen
Louis G. Jensen
Dorte Justesen[§]
Morits Lund
Steen Jørgensen
Werner Kofoed
Jens Linderholm
Jørgen Munck
Per Heighwood Nielsen[§]
Carsten Sørensen[§]

---

[*] On leave at Energy System Analysis, Risø
[**] University of Copenhagen
[§] Temporary assistant
[+] From August 21 to October 15
[++] From December 1

Consultants

Allan R. Mackintosh[+]

Postgraduates

Kurt Clausen
Knud Møllenbach
Karen Schou Pedersen[++]

Long-term visitors

G. Mackenzie	University of Edinburgh, Scotland
J. Schmidt	University of Delaware, Delaware, USA
D. Yang[*]	INPE, Los Campos, Brasil

Short-term visitors (two to twelve weeks)

E. Baharie	University of Edinburgh, Scotland
M. Dickens	AERE Harwell, U.K.
M.T. Hutchings	AERE Harwell, U.K.
B. Johansson	FOA, Stockholm, Sweden
A. Loidl	University of Mainz, Mainz, F.R.G.
J.D. Litster	Massachusetts Institute of Technology, Massachusetts, USA
K.A. McEwen	University of Salford, Salford, U.K.
A.D. McMahan	Lawrence Livermore Laboratory, California, USA
J.P. McTague	University of California, Los Angeles, California, USA
D. Mukamel	Weizman Institute of Science, Rehovat, Israel
H. Ott	ETH, Zurich, Switzerland
R. Pynn	Institute Max von Laue-Paul Langevin, Grenoble, France
T. Riste	IFA, Kjeller, Norway
J.J. Rhyne	National Bureau of Standards, Washington D.C. USA
M. Steiner	Hahn-Meitner Institute, Berlin
B. Szpunar	Academy of Mining and Metallurgy, Krakow, Poland

---

[*] Address after Feb. 1 1979

[+] University of Copenhagen

[++] From the Technical University of Denmark

6.2 Plasma Physics

Scientific staff

Verner Andersen
Che-Tyan Chang
Vagn O. Jensen
Otto Kofoed-Hansen*
Poul Michelsen
Per Nielsen
Hans Pécseli
Jens Juul Rasmussen++
Hans Sørensen

Technical staff

Paul Andersen
Bengt Hurup Hansen
Mogens Nielsen
Arne Nordskov
John Petersen
Børge Reher
Hans Skovgård

Consultant

Chan Mou Tchen+

Postgraduates

Palle Buus
Jens-Peter Lynov
Jørgen Schou

Long-term visitor

Valery A. Turikov	People's Friendship University, Moscow, USSR

Short-term visitors (two to twelve weeks)

S. Kuhn	University of Innsbruck, Innsbruck, Austria
R. Schrittwieser	University of Innsbruck, Innsbruck, Austria
H. Sugai	Nagoya University, Nagoya, Japan

---

* Also at Niels Bohr Institute, Copenhagen

\+ City University of New York, USA

++ From July 1.

6.3 Meteorology

Scientific staff	Technical staff
Carl Jørgen Christensen	Jørgen Christensen
Ole Christensen	Gunner Dalsgård
Sten Frandsen	Morten Frederiksen
Per Ekelund Hansen	Arent Hansen
Niels Otto Jensen	Finn Hansen
Leif Kristensen	Flemming Dyhr Hansen§
Søren E. Larsen	Jan Kildegaard Hansen§
Torben Mikkelsen	Gunnar Jensen
Erik Lundtang Petersen	Helle Lyons§
	Knud Sørensen

Consultant	Postgraduates
Chan Mou Tchen+	Sven-Erik Gryning
	Jørgen Højstrup
	Ib Troen

Long-term visitors

Kenneth L. Davidson	Naval Postgraduate School, Monterey, California, USA
John A. Dutton	Pennsylvania State University Pennsylvania, USA
Dennis W. Thomson	Pennsylvaina State University, Pennsylvania, USA

Short-term visitors (two to twelve weeks)

A.B. Fraser	Pennsylvania State University, Pennsylvania, USA
W.H. Mach	
J.M. Normann	
S.G. Perry	
K. Perry	
R. Peters	
K.H. Underwood	
E.W. Peterson	Oregon State University, Oregon, USA

---

§ Temporary assistant

+ City University of New York, USA

6.4 Liquid N_2 and He Plant

Technical staff

Ib Bonne

Bent Heiden

John Z. Jensen

Sales distributors:
Jul. Gjellerup, Sølvgade 87,
DK-1307 Copenhagen K, Denmark

Available on exchange from:
Risø Library, Risø National Laboratory,
P. O. Box 49, DK-4000 Roskilde, Denmark

ISBN 87-550-0578-0
ISSN 0418-6443